

**EFFECT OF FINE AND MOLDING WATER CONTENTS ON  
PULLOUT RESISTANCE OF BEARING REINFORCEMENT  
EMBEDDED IN COHESIVE-FRICTIONAL SOILS AND  
2D FINITE ELEMENT ANALYSIS OF BEARING  
REINFORCEMENT EARTH WALL WITH  
DIFFERENT BACKFILL MATERIALS**

**Gampanart Sukmak**



**A Thesis Submitted in Partial Fulfillment of the Requirements for the  
Degree of Doctor of Philosophy in Civil Engineering  
Suranaree University of Technology  
Academic Year 2015**

ผลกระทบจากปริมาณอนุภาคดินละเอียดและปริมาณความชื้นต่อกำลังต้านทาน  
แรงกดของเหล็กเสริมแบกทานในดินเสียคทานยัดเกาะและการวิเคราะห์  
ไฟไนท์อิลลิเมนต์สองมิติของกำแพงกันดินเสริมเหล็กแบกทาน  
ด้วยวัสดุดินถมต่างกัน



นายกัมปนาท สุขมาก

วิทยานิพนธ์นี้เป็นส่วนหนึ่งของการศึกษาตามหลักสูตรปริญญาวิศวกรรมศาสตรดุษฎีบัณฑิต  
สาขาวิชาวิศวกรรมโยธา  
มหาวิทยาลัยเทคโนโลยีสุรนารี  
ปีการศึกษา 2558

**EFFECT OF FINE AND MOLDING WATER CONTENTS  
ON PULLOUT RESISTANCE OF BEARING REINFORCEMENT  
EMBEDDED IN COHESIVE-FRICTIONAL SOILS AND 2D  
FINITE ELEMENT ANALYSIS OF BEARING REINFORCEMENT  
EARTH WALL WITH DIFFERENT BACKFILL MATERIALS**

Suranaree University of Technology has approved this thesis submitted in partial fulfillment of the requirements for the Degree of Doctor of Philosophy

Thesis Examining Committee

---

(Prof. Dr. Arul Arulrajah)

Chairperson

---

(Prof. Dr. Suksun Horpibulsuk)

Member (Thesis Advisor)

---

(Prof. Dr. Jie Han)

Member

---

(Assoc. Prof. Dr. Avirut Chinkulkitniwat)

Member

---

(Asst. Prof. Dr. Decho Phueakphum)

Member

---

(Asst. Prof. Dr. Rattaphol Pueboobpaphan)

Member

---

(Dr. Jirayut Suebsuk)

Member

---

(Prof. Dr. Sukit Limpijumnong)

Vice Rector for Academic Affairs  
and Innovation

---

(Assoc. Prof. Flt. Lt. Dr. Kontorn Chamniprasart)

Dean of Institute of Engineering

กัมปนาท สุขมาก : ผลกระทบจากปริมาณอนุภาคดินละเอียดและปริมาณความชื้น  
ต่อกำลังต้านทานแรงดึงของเหล็กเสริมแบกทานในดินเหนียวเหนียวและการวิเคราะห์  
ไฟไนต์เอลิเมนต์สองมิติของกำแพงกันดินเสริมเหล็กแบกทานด้วยวัสดุดินถมต่างกัน  
(EFFECT OF FINE AND MOLDING WATER CONTENTS ON PULLOUT  
RESISTANCE OF BEARING REINFORCEMENT EMBEDDED IN COHESIVE-  
FRICTIONAL SOILS AND 2D FINITE ELEMENT ANALYSIS OF BEARING  
REINFORCEMENT EARTH WALL WITH DIFFERENT BACKFILL MATERIALS)  
อาจารย์ที่ปรึกษา : ศาสตราจารย์ ดร.สุชนันต์ หอพิบูลสุข, 174 หน้า

วิทยานิพนธ์นี้ประกอบด้วยสามส่วนหลัก ส่วนแรกศึกษาอิทธิพลจากปริมาณอนุภาคดิน  
ละเอียดต่อกำลังรับแรงดึงของเหล็กเสริมแบกทานในดินเหนียวเหนียวที่มีปริมาณอนุภาคดิน  
ละเอียดเท่ากับร้อยละ 20 40 80 และ 98 โดยน้ำหนักแห้ง ซึ่งอนุภาคดินละเอียดมีขนาดน้อยกว่า  
0.075 มิลลิเมตร กำลังต้านทานแรงดึงรวมเป็นผลรวมจากกำลังจุดเสียดทานและกำลังจุดแบกทาน  
ซึ่งค่ากำลังจุดเสียดทานขึ้นอยู่กับค่ากำลังของดินและค่าแฟกเตอร์ปฏิสัมพันธ์ (interaction factor,  
 $\alpha$ ) โดยค่า  $\alpha$  มีความสัมพันธ์เชิงเส้นกับปริมาณอนุภาคดินละเอียด และค่ากำลังจุดแบกทานของ  
เหล็กเสริมกำลังตามขวางหนึ่งตัวคำนวณได้จากสมการกลไกการวิบัติเฉือนทะลุปรับปรุง  
(modified punching shear mechanism) ซึ่งขึ้นอยู่กับระนาบวิบัติเปลี่ยนรูป (transformation failure  
plane angle,  $\beta$ ) และปริมาณอนุภาคดินละเอียด สมการนี้ถูกพัฒนาโดย limit equilibrium analysis  
ซึ่งเป็นวิธีที่ง่ายสำหรับการตรวจสอบเสถียรภาพภายในของกำแพงกันดินเหล็กเสริมแบกทาน

งานวิจัยในส่วนที่สอง คือ การนำเสนออิทธิพลจากปริมาณความชื้น (ด้านแห้งและด้าน  
เปียกของปริมาณความชื้นเหมาะสม) ต่อกำลังรับแรงดึงของเหล็กเสริมแบกทานในดินลูกรัง  
(lateritic soil) ดินทดสอบถูกบดอัดที่ปริมาณความชื้นเริ่มต้นต่าง ๆ คือ -2.5 -1.5 0 +1.5 และ +2.5  
ของปริมาณความชื้นเหมาะสม (optimum water content,  $w_{owc}$ ) กำลังจุดเสียดทานคำนวณได้จากค่า  
กำลังของดินและค่าแฟกเตอร์ปฏิสัมพันธ์ (interaction factor,  $\alpha$ ) และค่ากำลังจุดแบกทานของ  
เหล็กเสริมกำลังตามขวางหนึ่งตัวขึ้นอยู่กับกำลังของดินทดสอบและรูปแบบการวิบัติ เมื่อดิน  
ทดสอบถูกบดอัดที่อัตราส่วนปริมาณความชื้นระหว่าง  $0.67 \leq w/w_{owc} \leq 1.0$  ค่า  $\beta$  มีค่าคงที่และ  
เท่ากับ  $\pi/2$  และสำหรับดินทดสอบถูกบดอัดที่อัตราส่วนปริมาณความชื้นระหว่าง  
 $1.0 \leq w/w_{owc} \leq 1.33$  ค่า  $\beta$  จะลดลงในฟังก์ชันโพลิโนเมียลกับการเพิ่มขึ้นของอัตราส่วนปริมาณ  
ความชื้น ( $w/w_{owc}$ )



งานวิจัยในส่วนสุดท้าย คือ การศึกษาพารามิเตอร์แบบจำลองต่อพฤติกรรมของกำแพงกันดินเหล็กเสริมแบกทานด้วยคุณสมบัติดินถมชนิดต่างกันด้วยโปรแกรม PLAXIS 2D โดยประกอบด้วยสองวัตถุประสงค์ วัตถุประสงค์แรกของการศึกษาคือ เพิ่มความรู้และความเข้าใจในการเปลี่ยนแปลงของ ความเค้นในดินใต้ฐานราก (bearing stresses) การทรุดตัว (settlements) การเคลื่อนตัวด้านข้างของกำแพง (horizontal wall facing deformation) และการเปลี่ยนแปลงแรงดันดินด้านข้าง (lateral earth pressures) เมื่อวัสดุดินถมต่างกัน วัตถุประสงค์ที่สองของการศึกษาเพื่อประเมินผลกระทบของ ค่าปฏิสัมพันธ์ระหว่างดินและเหล็กเสริมแบกทาน (soil-reinforcement interaction) ฐานราก (foundation) และค่าสติฟเนสของเหล็กเสริมแบกทาน (stiffness of reinforcement; EA) ต่อการเคลื่อนตัวด้านข้างของกำแพง วัสดุดินถมต่างที่ใช้ในการศึกษาประกอบด้วยดินถม 4 ประเภท มีคุณสมบัติต่างกันซึ่งถูกผสมระหว่างดินอนุภาคละเอียดประเภทดินเหนียว (silty clay) และดินทราย (sand) โดยที่ปริมาณดินอนุภาคละเอียดเท่ากับ 2 20 40 และ 80 เปอร์เซ็นต์โดยน้ำหนักแห้ง ค่าพารามิเตอร์ของแบบจำลองได้จากการทดสอบในห้องปฏิบัติการ และการคำนวณกลับจากการทดสอบแรงกดของเหล็กเสริมแบกทาน ซึ่งเป็นวิธีการอย่างง่ายสำหรับการจำลองเหล็กเสริมแบกทาน ความสัมพันธ์ระหว่างการเคลื่อนตัวด้านข้างสูงสุดของกำแพงกันดินเหล็กเสริมแบกทานและปริมาณอนุภาคดินละเอียด ถูกนำเสนอในฟังก์ชันโพลิโนเมียล โดยที่ค่าการเคลื่อนตัวด้านข้างสูงสุดเพิ่มขึ้น เมื่ออนุภาคดินละเอียดของดินถมเพิ่มขึ้น และพบว่ากำแพงกันดินมีการเคลื่อนตัวด้านข้างสูง เมื่อวัสดุดินถมมีอนุภาคดินละเอียดมีค่ามากกว่าร้อยละ 45 โดยน้ำหนักแห้ง จากการศึกษาพบว่า ตำแหน่งการเคลื่อนตัวด้านข้างสูงสุดจะสูงขึ้น เมื่อปริมาณอนุภาคดินละเอียดเพิ่มขึ้น วัตถุประสงค์ที่สอง จากการศึกษาค่าพารามิเตอร์ soil-reinforcement interaction, foundation และ stiffness of reinforcement พบว่าพารามิเตอร์เหล่านี้ มีผลต่อการเคลื่อนตัวด้านข้างของกำแพงกันดิน ซึ่งเป็นส่วนสำคัญสำหรับการออกแบบกำแพงกันดินเหล็กเสริมแบกทาน ซึ่งความรู้ที่ได้จากศึกษานี้เป็นแนวทางเบื้องต้นในการทำนายพฤติกรรมของกำแพงกันดินเสริมแบกทาน และสามารถนำไปประยุกต์ใช้สำหรับกำแพงกันดินเสริมแบกทานอื่นๆ ที่มีความสูงและลักษณะเหล็กเสริมแบกทานต่างๆ

GAMPANART SUKMAK : EFFECT OF FINE AND MOLDING WATER  
CONTENTS ON PULLOUT RESISTANCE OF BEARING  
REINFORCEMENT EMBEDDED IN COHESIVE-FRICTIONAL SOILS  
AND 2D FINITE ELEMENT ANALYSIS OF BEARING  
REINFORCEMENT EARTH WALL WITH DIFFERENT BACKFILL  
MATERIALS. THESIS ADVISOR : PROF. SUKSUN HORPIBULSUK,  
Ph.D., 174 PP.

FINE ANE WATER CONTENTS/BEARING REINFORCEMENT/PULLOUT  
REISITANCE/2D FINITE ELEMENT ANALYSIS

This thesis consists of six chapters with three main parts. First part presents effect of fine content on the pullout resistance mechanism of bearing reinforcement embedded in cohesive-frictional soils with different fine contents of 20, 40, 80, and 98% by dry weight. The total pullout resistance is the sum of the pullout friction and bearing resistances. The pullout friction resistance is approximated from soil shear strength and interaction factor,  $\alpha$ , which is linearly related to fine content. The bearing pullout resistance of a single isolated transverse member can be approximated from the modified punching shear mechanism where the failure plane angle,  $\beta$  is primarily dependent upon fine content. The developed equations are useful for the internal stability analysis of bearing reinforcement earth walls.

Second part presents effect of molding water content (on dry and wet sides of optimum water content) on the pullout resistance mechanism of bearing reinforcement embedded in a cohesive-frictional soil. The tested soil is compacted at five initial

compacted water contents (i.e. -2.5, -1.5, 0, +1.5, and +2.5 of OWC). The pullout friction resistance is approximated from the soil and shear strength and interaction factor,  $\alpha$ . The  $\beta$  values of the compacted soil at  $0.67 \leq w/w_{owc} \leq 1.0$  are essentially constant and equal to  $\pi/2$  (where  $w_{owc}$  is the optimum water content). For  $1.0 \leq w/w_{owc} \leq 1.33$ , the  $\beta$  value decreases polynomial with an increase in

Last part presents the numerical parametric study on behavior of the bearing reinforcement earth (BRE) walls with different backfill properties using PLAXIS 2D. This work is mainly to understand bearing stress, settlement, lateral earth pressure, and horizontal wall movement of BRE walls with different backfill materials and to evaluate the effects of various soil-structure interactions, foundations, and stiffness of reinforcements on horizontal wall deformations. The backfill materials consist of four types of soils, which are mixtures of silty clay and sand at different fine contents of 2, 20, 40, and 80% by weight. The model parameters for the simulation are obtained from the conventional laboratory tests and back-calculated from the laboratory pullout tests of the bearing reinforcement. The relationship between the maximum horizontal wall movement and the fine content can be expressed by a polynomial function. The maximum horizontal wall movement significantly increases as the fine content increases. The excessive movement is realized when fine content is greater than 45%. The knowledge gained from this study provides the preliminary guideline in predicting the behavior of BRE wall and can be applied to other BRE walls with different wall heights and features of bearing reinforcements.

School of Civil Engineering

Academic Year 2015

Student's Signature \_\_\_\_\_

Advisor's Signature \_\_\_\_\_

## **ACKNOWLEDGEMENTS**

Seven years ago, the author has entered the School of Civil Engineering, Suranaree University of Technology, to pursue my Bachelor's and Ph.D. degrees. It was my great opportunity to work under the supervision of Professor Dr. Suksun Horpibulsuk during Ph.D. Studies. The author would like to express his deepest sincere and gratitude to Professor Dr. Suksun Horpibulsuk for his guidance valuable advices, endless kindness, encouragement and enthusiasm throughout my studies. Even with his tight and hectic schedules, he always gave his time and support every time the author needed them. It has been a very pleasant experience to work under of guidance of Professor Dr. Suksun Horpibulsuk, who has highly disciplined life style, leadership character and philosophical thoughts.

Profound gratitude is expressed to Professor Dr. Jie Han, my coadvisor, for his valuable comments, suggestion and insights into mechanically stabilized earth (MSE) walls. The examining committee has also played a significant role in the completion of this thesis. I am grateful to Professor Dr. Arul Arulrajah for serving as a chair of the Ph.D. thesis examining committee. I would like to thank Associate Professor Dr. Avirut Chinkulkijniwat, Assistant Professor Dr. Rattaphol Pueboobpaphan, Assistant Professor Dr. Decho Phueakphum and Dr. Jirayut Suebsuk for serving as Ph.D. thesis examiner.

I wish to thank all the staff and faculty members of the School of Civil Engineering, Suranaree University of Technology, for the academic, administrative and technical support during my study. I would like to acknowledge Dr. Patimapon

Sukmak for valuable comments and discussions. I acknowledge Mr. Somjai Youbonchi, Mr. Sermsak Tiyasangthong, and Mr. Thaworn Takaikaew for their discussions and encouragement. I would like to thank Suranaree University of Technology for facilities, equipment and financial support. I also would like to acknowledge Thailand Research Fund (TRF) for financial support under the Ph.D. Royal Jubilee program Grant No. 0117/2554.

Finally, I would like to appreciate my family for their love and kind support on my graduate studies.

Gampanart Sukmak



# TABLE OF CONTENTS

	<b>Page</b>
ABSTRACT (THAI) .....	I
ABSTRACT (ENGLISH) .....	III
ACKNOWLEDGEMENTS .....	V
TABLE OF CONTENTS .....	VII
LIST OF TABLES .....	XV
LIST OF FIGURES .....	XVI
SYMBOLS AND ABBREVIATIONS .....	XXII
<b>CHAPTER</b>	
<b>I INTRODUCTION</b> .....	<b>1</b>
1.1 Statement of problem .....	1
1.2 Objective of the study .....	4
1.3 Structure of presentation .....	5
1.4 Scope and Limitation .....	6
1.5 References .....	7
<b>II THEORETICAL BACKGROUND AND LITERATURE</b>	
<b>REVIEW</b> .....	<b>10</b>
2.1 General .....	10
2.2 Component of Reinforced Soil Structure .....	12

## TABLE OF CONTENTS (Continued)

	<b>Page</b>
2.2.1 Facing system.....	12
2.2.2 Reinforcing material .....	13
2.2.2.1 Inextensible reinforcements .....	13
2.2.2.2 Extensible reinforcements.....	14
2.2.3 Soil placement.....	19
2.3 Advantages and Disadvantages of Reinforced Soil Structure Walls.....	19
2.4 Basic Principle of Mechanical Stabilization of Reinforced Soil Structure.....	20
2.4.1 External stability .....	20
2.4.2 Internal stability .....	21
2.5 Interaction Behavior between Backfill and Reinforcing Materials .....	23
2.5.1 Direct shear test.....	24
2.5.2 Pullout test .....	26
2.5.2.1 Frictional resistance .....	26
2.5.2.2 Bearing resistance .....	27
2.5.3 Interference factor coefficients .....	30
2.6 Literature reviews of direct shear and pullout tests .....	34
2.7 Pullout resistance of bearing reinforcement.....	36

## TABLE OF CONTENTS (Continued)

	Page
2.7.1 Pullout friction resistance .....	37
2.7.2 Pullout bearing mechanism of a single isolated transverse member ( $n = 1$ ) .....	39
2.7.3 Pullout resistance of the bearing reinforcement ( $n > 1$ ) .....	39
2.8 The behavior of bearing reinforcement earth (BRE) wall.....	43
2.8.1 Bearing stress .....	43
2.8.2 Settlement .....	46
2.8.3 Lateral wall movement .....	48
2.8.4 Coefficient of lateral earth pressure .....	48
2.8.5 Possible failure plane .....	49
2.9 Finite Element Modeling of Reinforced Earth Structure .....	53
2.9.1 Elasto-plastic model .....	53
2.9.1.1 Elasto-perfectly-plastic Mohr Coulomb model.....	53
2.9.2 Soil and reinforcement interface model .....	55
2.9.3 The influential parameters .....	56
2.10 References.....	60



## TABLE OF CONTENTS (Continued)

	<b>Page</b>
<b>III EFFECT OF FINE CONTENT ON THE PULLOUT</b>	
<b>RESISTANCE MECHANISM OF BEARING</b>	
<b>REINFORCEMENT EMBEDDED IN</b>	
<b>COHESIVE-FRICTIONAL SOILS.....</b>	<b>66</b>
3.1 Statement of problem.....	66
3.2 Laboratory investigation.....	67
3.2.1 Soil samples.....	67
3.2.2 Bearing Reinforcement.....	70
3.2.3 Methodology.....	70
3.3 Test results and discussion.....	74
3.3.1 Pullout friction resistance.....	74
3.3.2 Pullout bearing resistance of a single isolated transverse member (n=1).....	77
3.3.3 Pullout resistance of the bearing reinforcement (n>1).....	82
3.4 Conclusions.....	88
3.5 References.....	90

## TABLE OF CONTENTS (Continued)

	Page
<b>IV      PULLOUT RESISTANCE OF BEARING</b>	
<b>         REINFORCEMENT EMBEDDED IN MARGINAL</b>	
<b>         LATERITIC SOIL AT MOLDING</b>	
<b>         WATER CONTENTS.....</b>	<b>92</b>
4.1 Statement of problem .....	92
4.2 Laboratory investigation .....	93
4.2.1 Soil samples .....	97
4.2.2 Large scale direct shear tests.....	94
4.2.3 Bearing reinforcement .....	96
4.2.4 Pullout tests.....	97
4.3 Test results and discussion.....	97
4.3.1 Pullout friction resistance .....	97
4.3.2 Pullout bearing resistance of a single isolated transverse member (n=1) .....	100
4.3.3 Pullout resistance of the bearing reinforcement (n>1) .....	104
4.5 References .....	112

## TABLE OF CONTENTS (Continued)

	Page
<b>V      NUMERICAL PARAMETRIC STUDY ON BEHAVIOR OF BEARING REINFORCEMENT EARTH (BRE) WALLS WITH DIFFERENT BACKFILL MATERIAL PROPERTIES .....</b>	<b>115</b>
5.1 Statement of problem .....	115
5.2 Full-scale test earth wall for reference numerical model.....	117
5.2.1 Foundation and backfill .....	117
5.2.2 Construction and instrumentation of the test wall .....	118
5.3 Material constitutive models and parameters.....	120
5.3.1 Backfill and Foundation.....	122
5.3.1.1 Backfill.....	122
5.3.1.2 Foundation .....	124
5.3.2 Wall Facing and Reinforcement .....	125
5.3.2.1 Wall facing.....	125
5.3.2.2 Reinforcement.....	125
5.3.2.3 Soil-reinforcement interaction .....	127
5.3.3 Staged construction.....	128
5.4 Finite element analysis.....	129

## TABLE OF CONTENTS (Continued)

	Page
5.4.1 Soil-structure interaction ratio, $R_{inter}$ .....	129
5.4.2 Behavior of BRE wall with different types of soil .....	129
5.4.2.1 Bearing stress .....	132
5.4.2.2 Settlement .....	135
5.4.2.3 Horizontal wall movement.....	137
5.4.2.4 Lateral earth pressure.....	140
5.4.3 Parametric study on horizontal wall displacement .....	143
5.4.3.1 Influence of soil-structure interaction ratio, $R_{inter}$ .....	143
5.4.3.2 Influence of reinforcement stiffness, EA .....	144
5.4.3.3 Influence of foundation.....	146
5.4 Conclusions.....	147
5.5 References .....	150
<b>VI CONCLUSIONS AND RECOMMENDATIONS.....</b>	<b>155</b>
6.1 Summary and conclusions .....	155
6.1.1 Effect of fine content on the pullout resistance mechanism .....	155

## TABLE OF CONTENTS (Continued)

	<b>Page</b>
6.1.1.1 Pullout friction resistance .....	155
6.1.1.2 Pullout bearing mechanism.....	156
6.1.2 Effect of molding water content on the pullout resistance mechanism .....	157
6.1.2.1 Pullout friction resistance .....	157
6.1.2.2 Pullout bearing mechanism.....	157
6.1.3 Numerical parametric study on behavior of bearing reinforcement earth (BRE) walls with different backfill material properties.....	158
6.1.3.1 Behavior of BRE wall with different types of soil .....	158
6.1.3.2 Parametric study on horizontal wall displacement.....	159
6.2 Recommendations for future work .....	160
 APPENDIX	
APPENDIX A. List of publication .....	161
BIOGRAPHY .....	174

## LIST OF TABLES

Table	Page
2.1 Comparison of reinforced soil structure (FHWA-RD-89-043, 1990).....	18
2.2 Common type of reinforcement (Palmeira, 1987) .....	24
3.1 Index and engineering properties of tested soils.....	72
3.2 Predicted and measured pullout resistance of bearing reinforcement with 40x150 mm transverse member for $n = 1, 2, 3$ , and 4 and $F:S = 20:80$ .....	86
4.1 Physical and engineering properties of tested soils .....	96
3.2 Predicted and measured pullout resistance of bearing reinforcement with 40x150 mm transverse member for $n = 1, 2, 3$ , and 4 and $w_4/w_{owc} = 1.20$ .....	111
5.1 Reinforcement details for the test wall (Horpibulsuk and Niramitkornburee, 2010) .....	120
5.2 Model parameters for backfills and foundations .....	126
5.3 Model parameters for reinforcement and concrete facing .....	127

## LIST OF FIGURES

Figure	Page
1.1 Configuration of the bearing reinforcement of the test wall (Horpibulsuk and Niramitkronburee, 2010) .....	3
2.1 Conventional concrete structure wall (a), Reinforced soil structure wall (b) .....	13
2.2 Metallic strips used in a concrete-faced structure.....	15
2.3 Cross-section of different types of hexagonal wire mesh reinforcement .....	15
2.4 Configuration of the bearing reinforcement of the test wall (Horpibulsuk and Niramitkornburee, 2010) .....	16
2.5 Types of geogrids.....	17
2.6 Potential external failure mechanisms of MSE structures .....	22
2.7 Internal failure mechanisms of reinforced soil structure .....	22
2.8 Stress transfer mechanisms for soil reinforcement (FHWA-RD-89-043, 1990).....	23
2.9 Pullout resistance at 25 mm pullout displacement of Tensar SR80 geogrid (Abiera, 1991).....	32
2.10 Components of the pullout force against the geogrid displacement at the rigid front face (Alagiyawanna et al., 2001) .....	32
2.11 Modes of failure mechanism.....	33

## LIST OF FIGURES (Continued)

Figure	Page
2.12 Pullout test results of a longitudinal member under different normal stresses (Suksiripattanapong et al., 2013).....	38
2.13 Maximum pullout bearing resistance of a single isolated transverse member for all tested soils (Suksiripattanapong et al., 2013).....	41
2.14 Measured and predicted $P_{bn}/P_{b1}$ and $S/B$ relationship for 40x150 mm transverse members (Suksiripattanapong et al., 2013) .....	44
2.15 Relationship between bearing stresses and time under the wall (Horpibulsuk et al.,2011) .....	45
2.16 Bearing stress distribution after the completion of construction (Horpibulsuk et al.,2011) .....	46
2.17 Relationship between settlement and time (Horpibulsuk et al.,2011) .....	47
2.18 Final settlement profile at 47 days after the completion of construction (Horpibulsuk et al.,2011) .....	48
2.19 Measured lateral wall movement after the completion of construction (Horpibulsuk et al.,2011) .....	50
2.20 Coefficients of lateral earth pressure at maximum tension for the bearingreinforcements compared with those for other reinforcements.....	51



## LIST OF FIGURES (Continued)

Figure	Page
2.21 Coefficient of lateral earth pressure for the bearing reinforcement (AASHTO (1996) and Horpibulsuk et al., 2011) .....	51
2.22 Measured tensions in the bearing reinforcements (Horpibulsuk et al., 2011) .....	52
2.23 Interaction diagram for effect of reinforcement stiffness density (Rowe and Ho, 1997).....	58
2.24 Interaction diagram for effect of backfill soil friction angle (Rowe and Ho, 1997).....	59
2.25 Interaction diagram for effect of facing/soil interface friction angle (Rowe and Ho, 1997).....	60
3.1 Grain size distribution curves of the tested soils .....	72
3.2 Relationship between shear stress and fine content of all tested soil .....	73
3.3 Schematic diagram of pullout test apparatus (Horpibulsuk and Niramitkornburee, 2010) .....	73
3.4 Pullout test results of a longitudinal member under different normal stresses .....	73
3.5 Relationship between    and fine content for various applied normal stresses at peak and residual failures .....	72
3.6 Typical pullout test results of the bearing reinforcement in tested soils .....	79

## LIST OF FIGURES (Continued)

Figure	Page
3.7 Maximum pullout bearing resistance of a single isolated transverse member for all tested soils .....	80
3.8 Relationship between $\beta$ and fine content .....	81
3.9 Relationship between maximum pullout bearing resistance and applied normal stress .....	81
3.10 Measured and predicted and relationships for 40 x 150 mm transverse members .....	87
3.11 Transverse member interference .....	88
4.1 Compaction curve .....	94
4.2 Pullout test results of a longitudinal member under different normal stresses .....	99
4.3 Relationship between soil-soil and soil-longitudinal interfaces of all tested soils.....	100
4.4 Typical pullout test of the bearing reinforcement in tested soils .....	102
4.5 Maximum pullout bearing resistance of a single isolated transverse member for all tested soils .....	103
4.6 Relationship between $\beta$ and water content ratio .....	104
4.7 Measured and predicted $P_{bn}/P_{b1}$ and $S/B$ relationship for 40x150 mm transverse members .....	108
4.8 Effect of water content on $S_2/B$ .....	109

## LIST OF FIGURES (Continued)

Figure	Page
5.1 Schematic diagram of the test wall instrumentation .....	119
5.2 Construction sequence .....	120
5.3 Numerical model and mesh details for 2D FE model simulation of BRE wall .....	121
5.4 Grain size distributions .....	124
5.5 Finite element model for pullout tests .....	129
5.6 Simulated and measured pullout test results of the bearing reinforcement .....	131
5.7 Relationship between soil-structure interaction and fine content .....	132
5.8 Comparison between the simulated and measured settlements with construction time for different backfill .....	134
5.9 Measured and simulated bearing stresses and calculated overburden stresses for different backfill .....	135
5.10 Measured and simulated settlements with construction time for different backfill .....	136
5.11 Comparison between the measured and simulated horizontal wall movement for different soil embankments .....	138
5.12 Simulation horizontal movement of unreinforced zone at 4.5 m away from facing wall for different soil embankments .....	139

## LIST OF FIGURES (Continued)

Figure	Page
5.13 Relationship between maximum horizontal wall movement and fine content .....	140
5.14 Measured and simulated lateral earth pressure distributions for different backfill .....	142
5.15 Relationship between maximum horizontal displacement and soil-structure interaction ratio for different backfill .....	145
5.16 Relationship between maximum horizontal displacement and axial stiffness.....	145
5.17 Influence of Elasticity modulus of foundation.....	147



## SYMBOLS AND ABBREVIATIONS

$\sigma_{b\max}$	=	Maximum bearing stress
$D_{50}$	=	Average grain sizes
$R_{inter}$	=	Interface factor
$\sigma_n$	=	Normal stress
$A_t$	=	Total surface area of soil sliding
$f_{ds}$	=	Coefficient of direct shear resistance
$\phi_{ds}$	=	Friction angle of soil obtained from a direct shear test
$\delta$	=	Angle of skin friction
$\alpha_{ds}$	=	Fraction of grid surface area
$E_c$	=	Efficiency of grid reinforcement on cohesion
$E_\phi$	=	Efficiency of grid reinforcement on friction
$c_a$	=	Cohesion between soil and grid reinforcement
$c, c'$	=	Cohesion between soil and soil
$A_s$	=	Frictional area between soil and grid reinforcement
$\overline{\sigma_s}$	=	Average normal stress
$\overline{\sigma_b}$	=	Maximum bearing stress against a single transverse members
$n$	=	Number of transverse members
$d$	=	Diameter or width of a single transverse member

## SYMBOLS AND ABBREVIATIONS (Continued)

$N_c, N_q$	=	Bearing capacity factors
$\beta$	=	Angle of rotational failure zone
$k$	=	Horizontal earth pressure coefficient
$R$	=	Transverse member interference
$a, b, nr$	=	Constants
$P_f$	=	Maximum pullout friction resistance
$L$	=	Length of the longitudinal member
$D$	=	Diameter of the longitudinal member
$P_{bn}$	=	Maximum pullout bearing force
$\sigma_h$	=	Lateral earth pressure
$S_v$	=	Vertical spacing
$S_h$	=	Horizontal spacing
$T$	=	Axial tension in reinforcing wire
$E$	=	Modulus of elasticity of steel
$A$	=	Cross-sectional area of the reinforcing wire
$\varepsilon$	=	Axial strain in the reinforcing wires
$f$	=	Yield function
$g$	=	Plastic potential function

## SYMBOLS AND ABBREVIATIONS (Continued)

$D^e$	=	Elastic constitutive matrix
$G_{ref}$	=	Reference shear modulus
$G$	=	Shear modulus of soil
$G_i$	=	Shear of interface element
$\wedge$	=	Reinforcement stiffness factor
$J$	=	Reinforcement stiffness
$K_a$	=	Rankine's active earth pressure coefficient
$\gamma$	=	Unit weight of the soil
$H$	=	Wall height
$B$	=	Leg length of the transverse member
$F$	=	Interference factor
$a, b, c, d, e, f$	=	Constants
$\nu$	=	Elastic constitutive matrix
$G_{ref}$	=	Reference shear modulus
$G$	=	Shear modulus of soil

# **CHAPTER I**

## **INTRODUCTION**

### **1.1 Statement of problem**

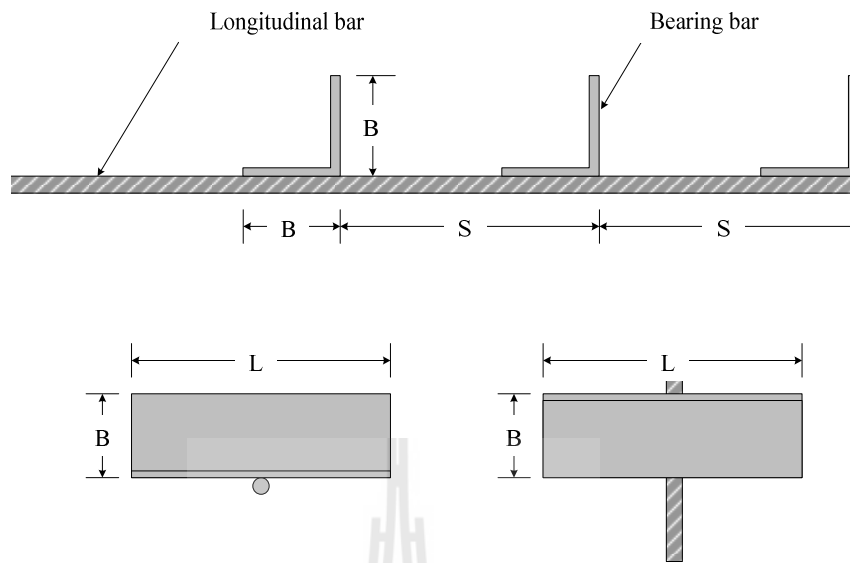
Mechanically stabilized earth (MSE) wall is generally used for retaining structures. The MSE wall was pioneered by Henri Vidal of France in the 1960s and was designated as “Reinforced Earth or Reinforced Soil Structure”. Over the past four decades, the usage of MSE structures in civil engineering applications has grown rapidly and widely worldwide, including Thailand, China, Australia and the United States of America. The construction cost of the mechanically stabilized earth (MSE) wall is mainly dependent upon the reinforcement type, backfill material type, and transportation of backfill which depend on the location between the borrow source and the construction site.

Metal strip reinforcement classified as inextensible reinforcement type has been widely used in Thailand because this reinforcement is conveniently transported to a factory for galvanization and subsequently to the construction site, and furthermore is simple and fast to install due to its strip shape. However, it is primarily imported from Africa, leading to high construction costs. Steel grid is the other inextensible reinforcement type, which has been widely researched (Bergado et al., 1996; Bergado et al., 1993; Chai, 1992; Tin et al., 2011) and applied to many MSE projects in Thailand. Even though the grid reinforcement exhibits higher pullout resistance, its installation is more difficult than that of the strip reinforcement.



Horpibulsuk and Niramitkronburee (2010) have recently developed a new cost-effective inextensible reinforcement type, termed as “Bearing reinforcement”. Figure 1.1 shows the typical feature of the bearing reinforcement, which is composed of a longitudinal member and transverse (bearing) member. The longitudinal member is a steel deformed bar (DB) and the transverse members are a set of equal angle steel. This reinforcement includes the advantages of both strip and grid reinforcements, i.e., simple and fast installation to the panel wall facing and high pullout resistance with less steel quantity. The transverse members are only installed in the passive zone (behind the maximum tension plane) as determined by the coherent gravity structure hypothesis for engineering and economic purposes. The earth stabilized by this reinforcement is designated as “Bearing Reinforcement Earth (BRE) wall” (Horpibulsuk et al., 2011b). The BRE wall system has been developed into one of the standard MSE walls for the Department of Highways in Thailand.

According to AASHTO (2002) and the Department of Highway, Thailand specification, the backfill for MSE wall is generally coarse-grained soils, which should contain no more than 15% fine passing a sieve No. 200 by weight and the Plasticity Index (PI) should be limited to 6. However, some guidelines for the construction of reinforced soil structures and slopes allow using cohesive-friction soils for embankment material (BS8006, 1995; Elias et al., 2001; NCMA, 2002). NCMA (2002) recommendations allow for up to 35% of fine-grained soil and PI is less more than 20. Furthermore, low quality backfills with up to 80% fine-grained soils have been used and accepted in full-scale tests (Bergado et al., 1992; Bergado et al., 1993; Keller, 1995).



**Figure 1.1** Configuration of the bearing reinforcement of the test wall  
(Horpibulsuk and Niramitkronburee, 2010).

When coarse-grained soils are not commonly available in construction site, transportation cost depends on the location between the borrow source and the construction site. Ou et al. (1982) reported that that fuel costs could constitute as much as 20% of the total transportation cost of high-quality soils. The use of locally available marginal soils as a backfill (e.g. low quality soils with more than 15% fine soil) can help reduce the cost of fill material by as much as 60% (Keller, 1995) and reduce the air pollution from the transportation.

Based on the field investigation and laboratory pullout tests (Horpibulsuk and Niramitkronburee, 2010; Horpibulsuk et al., 2011b; Suksiripattanapong et al., 2013), a design method for BRE walls founded on a firm ground was subsequently introduced. This method has been adopted to design several BRE walls under the supervision of Department of Highways in Thailand since 2008. Recently, Suksiripattanapong et al.

(2012) proposed a simplified method to model the bearing reinforcement, which converts its friction and bearing resistance to the equivalent friction resistance for 2D finite element analysis. So far, all above studies on bearing reinforcement are limited to high-quality coarse-grained soils. However, in some areas, high-quality soil is not available, leading to subsequently high haulage cost for imported materials. It would thus be cost-effective if marginal soils available locally or on-site can be used as a backfill material for MSE walls with an appropriate drainage system. Nevertheless, a variation of water content in the marginal soil, which was caused by seasonal precipitation, rainfall infiltration and variation of the ground water table can significantly affect a performance of the reinforced soil structure.

To apply these marginal soils in practice, the effect of fine and water contents on pullout resistance mechanism is an important aspect that needs to be addressed. In addition, the 2D finite element analysis of the Bearing Reinforcement Earth (BRE) wall is needed to be performed to obtain an useful information for further analysis.

## **1.2 Objective of the study**

- 1.2.1 To study the effect of fine content on the pullout resistance mechanism of bearing reinforcement embedded in cohesive-frictional soils.
- 1.2.2 To study the effect of initial water content on the pullout resistance mechanism of bearing reinforcement embedded in lateritic soil.
- 1.2.3 To model the behavior of the bearing reinforcement earth wall by 2D finite element analysis using Horpibulsuk et al. (2011b) data.

### 1.3 Structure of presentation

This thesis consists of six chapters and outlines of each chapter are presented as follows:

Chapter II presents the review of previous research on physical and engineering properties of cohesive-friction soil with various fine and water contents, the interaction between reinforcement and soils, the behavior of the reinforced walls and the numerical analysis of the reinforced wall.

Chapter III presents the study of effect of fine content on the pullout resistance mechanism of bearing reinforcement embedded in cohesive-frictional soils. The tested soils used in this study were a mixture of silty clay and sand at various ratios. The silty clay was collected from the Suranaree University of Technology campus, Nakhon Ratchasima, Thailand, at a depth of 3 m. This clay is high plasticity (CH) type classified by Unified Soil Classification System (USCS). The sand is classified as poorly graded sand (SP). The fine : sand ratios (F:S) were 20:80, 40:60, 80:20, and 98:2 by dry weight. The mode of failure and the transverse member interference of the bearing reinforcement are presented. Finally, the relationship between the failure plane angle,  $\beta$  and fine content is proposed and verified.

Chapter IV presents the effect of molding water content on the pullout resistance mechanism of bearing reinforcement embedded in lateritic soil. The locally available soil used in this study is a lateritic soil, which is collected from Nakhon Ratchasima, Thailand. The lateritic soil consists of 23% gravel, 51.2% sand, and 25.8% silty clay and is classified as GC according to the Unified Soil Classification System (USCS). The average grain size,  $D_{50}$  of lateritic soil is 1.17 mm. The tested soil was compacted at optimum (OWC), on dry side of OWC, and on wet side of

OWC, which have five initial compacted water contents (i.e. -2.5, -1.5, 0, +1.5, and +2.5 of OWC).

Chapter V presents the calibration of finite element models with material properties using laboratory large-scale pullout tests reported by Horpibulsuk and Niramitkornburee (2010) and Sukmak et al. (2015) and the full-scale BRE reported by Horpibulsuk et al. (2011a). The calibrated models are then adopted in this study to investigate the behavior and performance of BRE walls with different backfill material properties. The primary objective was to improve the understanding of bearing stress, settlement, lateral earth pressure, and horizontal wall movement of BRE walls with different backfill materials during and at the end of construction. The second objective of this study was to evaluate the effects of various soil-structure interactions, foundations, and stiffness of reinforcements on horizontal wall deformations.

#### **1.4 Scope and Limitation**

In the limitation of this research, it should be noted that due to very low hydraulic conductivity of cohesive-frictional soils (poor drainage), measuring the pullout resistance in term of drained condition is extremely time consuming. Consequently, the tested parameters in this paper were measured and analyzed in term of undrained condition pertinently to simulate short term performance of MSE wall in the field. For example, the reinforced soil structures were rapidly failed by earthquake loading imparted shear forces under undrained condition.

## 1.5 References

- AASHTO, 2002. **Standard Specifications for Highway Bridges, seventeenth ed.** American Association of State Highway and Transportation Officials, Washington, DC, USA.
- Bergado, D., Lo, K., Chai, J., Shivashankar, R., Alfaro, M., Anderson, L., 1992. **Pullout Tests Using Steel Grid Reinforcements with Low-Quality Backfill.** Journal of Geotechnical Engineering 118, 1047-1062.
- Bergado, D.T., Chai, J.C., Marui, H., 1996. **Prediction of pullout resistance and pullout force displacement relationship for inextensible grid reinforcements.** Soils and Foundations 36, 11-22.
- Bergado, D.T., Macatol, K.C., Amin, N.U., Alfaro, M.C., 1993. **Interaction of lateritic soil and steel grid reinforcement.** Can. Geotech. J 30, 376-384.
- BS8006, 1995. **British Standard.** Code of Practice for Strengthened/reinforced Soils and Other Fills, BSI.
- Chai, J.C., 1992. **Interaction between grid reinforcement and cohesive-frictional soil and performance of reinforced wall/embankment on soft ground.** D.Eng. dissertation, Asian Institute of Technology, Bangkok, Thailand.
- Elias, V., Christopher, B.R., Berg, R.R., 2001. **Mechanically Stabilized Earth Walls and Reinforced Soil Slopes-design and Construction Guidelines.** FHWA-NHI-00-043, Federal Highway Administration, Washington, DC, USA.
- Horpibulsuk, S., Niramitkornburee, A., 2010. **Pullout resistance of bearing reinforcement embedded in sand.** Soils Found 50, 215-226.
- Horpibulsuk, S., Niramitkornburee, A., 2010. **Pullout resistance of bearing reinforcement embedded in sand.** Soils and Foundations 50.

- Horpibulsuk, S., Suksiripattanapong, C., Niramitkornburee, A., Chinkulkijniwat, A., Tangsutthinon, T., 2011a. **Performance of an earth wall stabilized with bearing reinforcements**. Geotextiles and Geomembranes 29, 514-524.
- Horpibulsuk, S., Suksiripattanapong, C., Niramitkornburee, A., Chinkulkijniwat, A., Tangsutthinon, T., 2011b. **Performance of earth wall stabilized with bearing reinforcements**. Geotextiles and Geomembranes 29, 514-524.
- Keller, G.R., 1995. **Experiences with mechanically stabilized structures and native soil backfill**. Transportation Research Record 1474, 30-38.
- NCMA, 2002. **Design Manual for Segmental Retaining Walls**. second ed. National Concrete Masonry Association, Herndon, VA, USA.
- Ou, F.L., Cox, W., Collett, L., 1982. **Rock aggregate management planning for energy conservation: optimization methodology**. Transp. Res. Rec 872, 63-69.
- Sukmak, K., Sukmak, P., Horpibulsuk, S., Han, J., Shen, S.-L., Arulrajah, A., 2015. **Effect of fine content on the pullout resistance mechanism of bearing reinforcement embedded in cohesive-frictional soils**. Geotextiles and Geomembranes 43, 107-117.
- Suksiripattanapong, C., Chinkulkijniwat, A., Horpibulsuk, S., Rujikiatkamjorn, C., Tangsutthinon, T., 2012. **Numerical analysis of bearing reinforcement earth F(BRE) wall**. Geotextiles and Geomembranes 32, 28-37.
- Suksiripattanapong, C., Horpibulsuk, S., Chinkulkijniwat, A., Chai, J.C., 2013. **Pullout resistance of bearing reinforcement embedded in coarse-grained soils**. Geotextiles and Geomembranes 36, 44-54.

Tin, N., Bergado, D.T., Anderson, L.R., Voottipruex, P., 2011. **Factors affecting kinked steel grid reinforcement in MSE structures.** Geotextiles and Geomembranes 29,172-180.





## **CHAPTER II**

### **THEORETICAL BACKGROUND**

### **AND LITERATURE REVIEW**

#### **2.1 General**

In geotechnical engineering, one of the significant innovations is the use of synthetic materials after “Reinforced soil” was introduced by the French engineer H. Vidal in the late 1960s. The designation of “Reinforced Earth or Reinforced Soil Structure” was originally coined for this composite material which has subsequently been patented under that name in several countries. The reinforced soil structure is a construction which consists of a soil reinforced with some other material such as, for example, geogrids, geotextile, and metal strip. For the last four decades, the practice of reinforcing the soil with tensile inclusion has been widely implemented. These materials incorporated successfully in the design and construction of embankments, slopes, retaining walls, foundation soils and many other geotechnical projects.

Mechanical stabilized earth (MSE) structure is a composite construction. These MSE structure consists of three main components, namely facing, reinforcement, backfill material. The role of facing is constructional as it only prevents and protects surface erosion and affords the structure an aesthetic appearance.

Nowadays, several reinforcement types have been developed and, in comparison with conventional construction, they offer the advantages of simple

construction, low cost, and ability to tolerate large deformation without structural distress. The use of reinforcement will provide additional shear stress in the soil mass through the tensile force in the reinforcement, which will increase the strength of soil-reinforcement mass, and hence reduce the horizontal deformation, and thereby increasing the overall stability of the structure.

Design of reinforced soil structures requires the knowledge of either the mechanical behavior of reinforcement, or the behavior at the soil and reinforcement interface. The interaction behaviors of soil and reinforcement interface are more directly incorporated into design procedures for reinforced soil structure with shear and bearing (passive) resistances. The interaction behaviors were investigated by conducting direct shear or pullout tests. Both tests are widely used to study these interaction mechanisms. The evaluation of the friction and bearing resistances is an essential factor in the design of the reinforced soil structures.

For the direct shear test, the soil is forced to move on the surfaces of the reinforcement under a normal stress. The direct shear tests are performed to provide the design engineer with the friction angle and adhesion coefficient for the various interfaces within the design. The direct shear test is also used as a form of quality control to ensure product compliance to the value used in the design. The ASTM D-5321 standard direct shear test method is commonly used for determining the Bond Coefficient between soil and geosynthetic.

For pullout test, the reinforcement is pulled out from a soil mass subjected to a normal stress. If the soil particles are smaller than the reinforcement opening, efficiencies are high due to the soil particles could be able to penetrate through the reinforcement opening and to develop the passive bearing capacity resistance. The

ASTM D-6706 standard pullout test method is intended as a performance test to provide the design parameters. In all cases, pullout test resistances are less than the sum of the direct shear test resistances. This is due to the fact that the geosynthetic is taut in the pullout test and exhibits large deformation. This, in turn, causes the soil particle to reorient themselves into a reduced shear strength mode at the soil-reinforcement interfaces, resulting in lower pullout resistance.

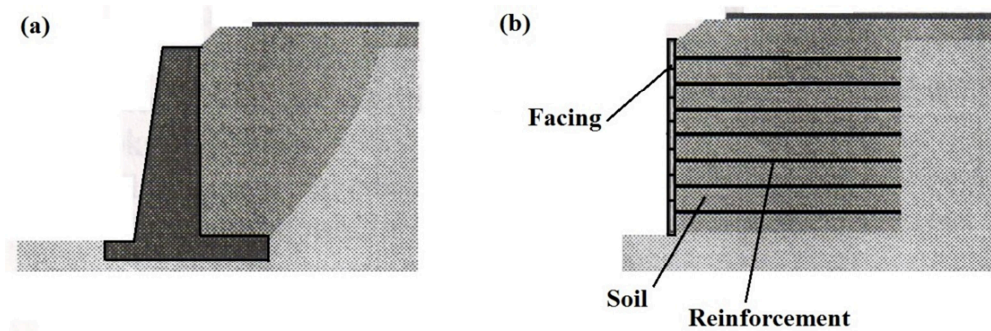
## **2.2 Component of reinforced soil structure**

Retaining structures are used not only for bridge abutments and wing walls but also for slope stabilization and to minimize right of way required for embankments. Reinforced soils walls and slope are cost-effective soil retaining structures which can tolerate much larger settlements than reinforced concreted walls. Extensive examples of reinforced soil application are presented in Bartos (1979); Ingold (1982); Raymond and Giroud (1993) and many other publications. Figure 2.1 shows schematically a conventional concrete structure and reinforced soil structure wall.

The reinforced soil structure wall is a composite construction. These MSE structure consists of three main components, namely facing, reinforcement, backfill material. Also described are the requirements for each component of the reinforcing system.

### **2.2.1 Facing system**

The type of facing elements used in the different reinforced soil structures control their aesthetics since they are the only visible parts of the completed structure. The role of facing is constructional as it only prevents and protects surface erosion. Major facing types are segmental precast concrete panels, cast in place concrete, metallic facings, and gabion facings.



**Figure 2.1** (a) Conventional concrete structure wall

(b) Reinforced soil structure wall.

### 2.2.2 Reinforcing material

The information on the reinforcement materials is needed for the design (i.e., geometric characteristics, strength and stiffness properties, and soil reinforcement interaction properties). By considering reinforcement extensibility, these reinforcing materials can be classified into two typical types; inextensible and extensible reinforcements.

#### 2.2.2.1 Inextensible reinforcements

The deformation of the reinforcement at failure is much less than the deformability of the soil. This type of reinforcements is normally assumed to be rigid, which can be made of metallic reinforcing materials e.g. metallic strips, metallic grids, hexagonal wire meshes, etc.

- **Metallic strips**

In most reinforced earth structures, metallic strips e.g. stainless, galvanize or coated steel strips are used as reinforcements in backfills (see Figure 2.2). Their dimensions vary with application and structure, but breadth and thickness are usually within the range of 5 to 100 mm, and 3 to 5 mm, respectively.

- **Metallic grids**

Typically, metallic grids consist of two member components: transverse member and longitudinal member. In field application, transverse members will be arranged parallel to the face or free edge of structures. The main purpose of the arrangement is to retain the transverse members in position. The longitudinal members are high modulus of elasticity and not susceptible to creep. Metallic grids can be formed from steel in the form of plain or galvanized weld mesh.

- **Hexagonal wire meshes**

There are two types of hexagonal wire meshes used as reinforcement: a) zinc-coated hexagonal wire meshes and b) PVC-coated hexagonal wire meshes (see Figure 2.3). There are two cell dimensions available for the former: a) 600mm x 80 mm, and b) 80 mm x 100 mm, and its steel core wire are 3.0 mm in diameter. The latter has additional 3.8 mm-diameter PVC coating as an outer surface for extra protection and each cell has dimensions of 80 mm x 100 mm while its steel core wire is 2.7 mm in dimensions.

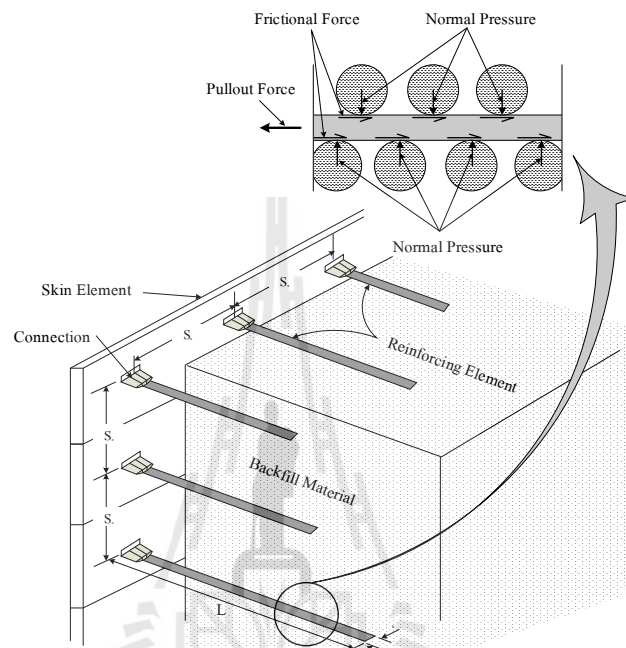
- **Bearing reinforcement**

Figure 2.4 shows the typical configuration of the bearing reinforcement, which is composed of a longitudinal member and transverse (bearing) members. The longitudinal member is a steel deformed bar and the transverse members are a set of steel equal angles.

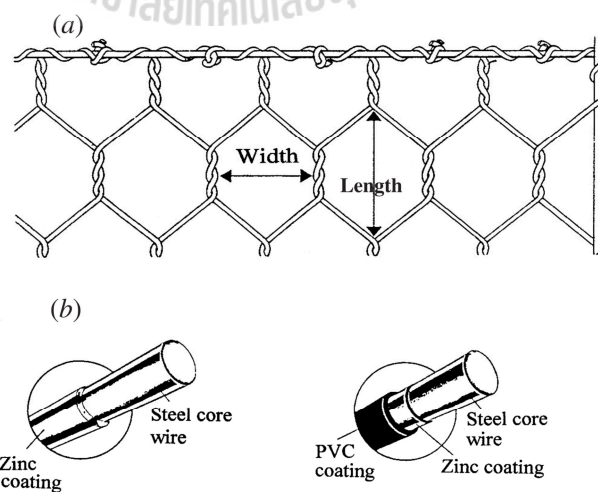
#### **2.2.2.2 Extensible reinforcements**

The deformation of the reinforcement at failure is comparable to or greater than the deformability of the soil. In general, the extensible reinforcement materials have lower strength and more extensible than the inextensible

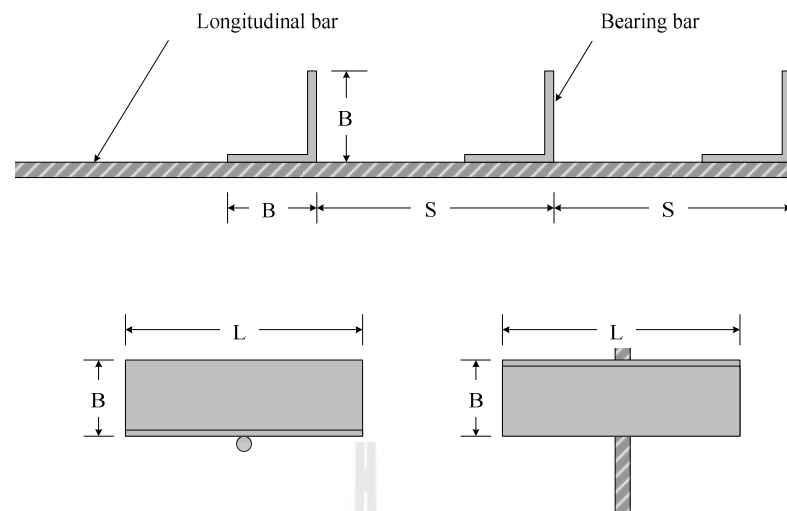
counterparts, which can be made by polymeric materials consisting of polypropylene, polyethylene, or polyester polymers e.g. geotextiles, geogrids, and geocomposites (consisting of geotextile and geogrid).



**Figure 2.2** Metallic strips used in a concrete-faced structure.



**Figure 2.3** Cross-section of different types of hexagonal wire mesh reinforcement.



**Figure 2.4** Configuration of the bearing reinforcement of the test wall  
(Horpibulsuk and Niramitkornburee, 2010).

- **Geotextiles**

There are two main types of conventional geotextile: a) woven geotextile and b) non-woven geotextile. The former is composed of two perpendicular sets of parallel linear elements systematically interlaced to form a planar structures, while the latter is formed from filaments or fibers randomly arranged and bonded together to form a planer structure, which can be achieved by mechanical, thermal or chemical means.

- **Geogrids**

Geogrid is normally composed of connected parallel sets of tensile ribs with apertures sufficient to allow strike-through of surrounding soil, stone, or other geotechnical materials. It is originated by adopting polymer materials (e.g. polypropylene and polyethylene. Such woven-type geogrids are generally coated with some chemical substances (e.g. PVC, latex, bitumen) for dimensional stability,

providing protection for the ribs during installation, and preventing them from biochemical degradation.

Generally, geogrid can be classified into two types: a) uniaxial and b) biaxial. Figure 2.5(a) and 2.5(b) illustrate these two types of such geogrids. Uniaxial geogrids are normally stronger than biaxial geogrids. Geogrid reinforcement material can be used in all main reinforced soil applications although it is not strong as heavier woven geotextile products. A particular feature of geogrid reinforcement is that its excellent bond, developed through the interlock between the geogrid and the soil, mobilize bearing stresses.

Reinforced soil structures can be described by the type of reinforcement, geometry, the stress transfer mechanism, the extensibility of the reinforcement material, and the method of soil placement as shown in Table 2.1.



a) Uniaxial



b) Biaxial

**Figure 2.5** Types of geogrids



**Table 2.1** Comparison of reinforced soil structure (FHWA-RD-89-043, 1990).

	REINFORCEMENT TYPE		SOIL GEOMETRY			RECOMMENDED SOIL TYPE <sup>1</sup>				STRESS TRANSFER MECHANISM		REINFORCEMENT MATERIAL		EXTENSIBILITY		PROPRIETY SYSTEM / PRODUCT NAMES
			30°	60°	90°	Clay	Silt	Sand	Gravel	Surface Friction	Passive Resistance	Metal	Non-Metal	Extensible	Inextensible	
						.002	.02	.2	2mm							
IMPORTED EMBANKMENT TYPE APPLICATION	STRIP	Smooth	—							•		•		—	•	Reinforced Earth
		Ribbed	—							•		•		—	•	Reinforced Earth Paraweb
	GRID		—								•	•			•	VSL, MSE, CAS, RSE, and Welded Wire Wall
														•		Maccaferri Gabion
													•	—		Tensor, Mirafi, Tenax, Reinforced Earth Grid, Conwed
	SHEET		—							•			•	—		Geotextiles
	BENT ROD		—								•	•			•	Anchored Earth
IN SITU GROUND IMPROVEMENT APPLICATION	FIBER		—							•		•	•	—		
	FLEXIBLE, SMALL DIAMETER NAILS		—							•		•			•	
	RIGID, LARGE DIAMETER PILES		—								•	•	•		•	

<sup>1</sup>Based on stress transfer between soil reinforcement.  
Other Criteria may preclude use of soils for specific applications.

### **2.2.3 Soil placement**

The soil used as backfill material should be coarse-grained soil (granular soil), characterized by high frictional properties, stable soil properties with time and with change in water/moisture content, and to provide free-drainage backfill. This is mainly due to the extensive use of granular soil as backfill in MSE structures and embankments. Thus, many researches have been focused on the evaluation of the interaction properties of the reinforcement in coarse-grained soil. However, several researches have used the fine-grained soils as the backfill (Bergado et al., 1992; Bergado et al., 1993; Keller, 1995). The lack of coarse-grained soil and the availability of fine-grained soil in Thailand, as well as, in some other area of the world, have initiated the growing interest in the use of the local or available soil in the construction of the reinforced soil structures. The use of local soil (lower quality soil) in MSE wall could significantly reduce the cost of construction.

## **2.3 Advantages and disadvantages of reinforced soil structure walls**

One of the greatest advantages of the reinforced soil structure is their flexibility and capability to absorb deformations due to poor subsoil conditions in the foundations when compared to rigid concrete structure. The relatively small quantities of manufactured materials have resulted in a cost reduction of construction due to rapid construction. Moreover, the precast concrete facing elements of these structures can be made with various shapes for the aesthetic considerations.

Generally disadvantages, the reinforced soil structures generally require a relatively large space behind the wall face in order to obtain enough wall width for internal and external stability.

## **2.4 Basic principle of mechanical stabilization of reinforced soil structure**

The role of the reinforced soil structure is to support slopes which otherwise would fail under self-weight and external loads. A limit equilibrium analysis allows the engineer to check the overall stability of the structure. Two type of stability must be considered (i.e. external and internal stability). For external stability, the MSE slope must satisfy the same external design criteria as a conventional retaining wall. For internal stability, the length of reinforcement is sufficient to prevent its slippage under the action of its own weight and externally applied forces. In addition, the reinforcement must be sized and spaced so that it does not fail in tension under the stresses that are applied.

### **2.4.1 External stability**

The principle of conventional reinforced soil structure walls can easily be explained on example of a heavy rigid block which similarly considers to the reinforced concrete cantilever and gravity retaining walls. External failure of these structures is generally assumed to be four potential failure mechanisms:

- 1) Sliding of the reinforced soil block over the foundation soil.
- 2) Overturning of the reinforced soil block.
- 3) Bearing capacity failure of the foundation soil.

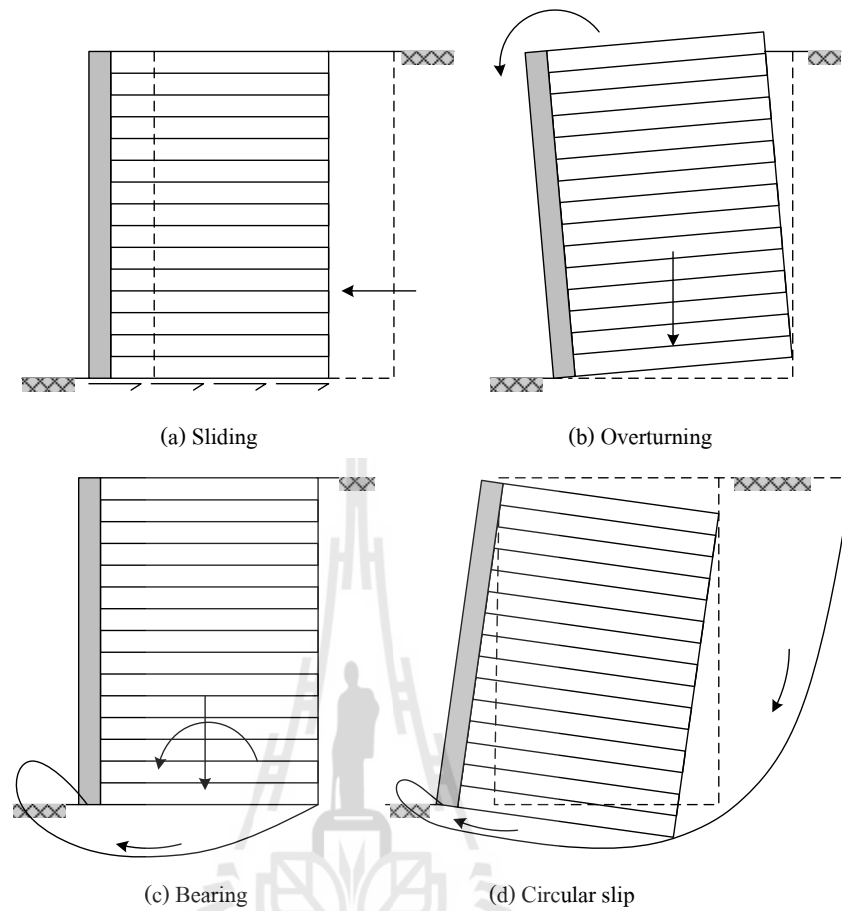
- 4) Deep seated stability failure (rotational slip-surface or slip along a plan of weakness).

These external failures of the reinforced soil structures are shown in Figure 2.6. Factors of safety of external stability are based on classical analysis of reinforced concrete and gravity wall. The reduced values for factor of safety for external failure are lower than those used for classical unreinforced retaining structure in order to the flexibility and satisfactory field performance of the reinforced soil structure. For example, the factor of safety for overall bearing capacity is 2 lower than the conventional value of about 3, which is used for more rigid structures.

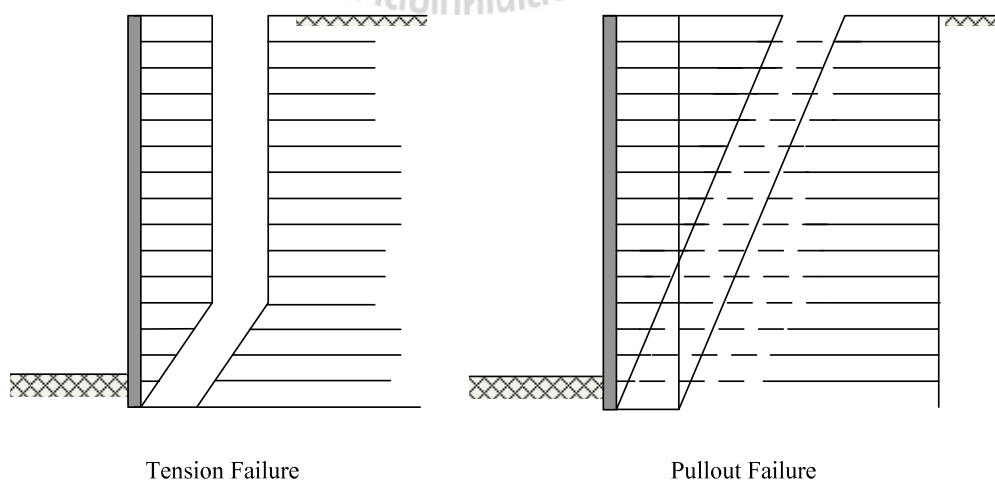
#### **2.4.2 Internal stability**

The internal failure of a mechanically stabilized soil structure can be categorized into two different ways, the tensile failure and the pullout failure (Figure 2.7):

- 1) Tensile failure is caused by rupture of reinforcement. Tension failure occurs when the tension developed in the reinforcement exceed its tensile strength, leading to large movements and possible collapse of the reinforced soil structure.
- 2) Slippage failure is caused by the tensile forces on the reinforcement become larger than the pullout resistance. Thus, the reinforcements are pulled out from the soil mass. This mode of failure is called failure by pullout.



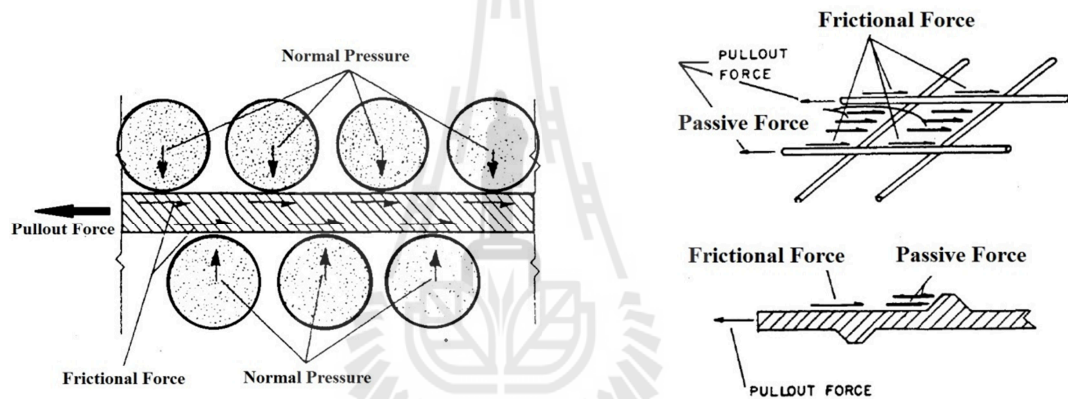
**Figure 2.6** Potential external failure mechanisms of MSE structures.



**Figure 2.7** Internal failure mechanisms of reinforced soil structure.

## 2.5 Interaction behavior between backfill and reinforcing materials

Interaction between soil and reinforcement is of major importance to reinforced soil structure design. It depends on the nature and mechanical characteristic of the soil and reinforcement. The degree of the interaction and the failure mechanism are developed in a function of the type of reinforcement. Stresses are transferred between soil and reinforcement by two main mechanisms: friction and passive (bearing) resistances as shown in Figure 2.8.










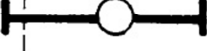
**Figure 2.8** Stress transfer mechanisms for soil reinforcement  
(FHWA-RD-89-043, 1990).

Friction resistance develops at locations where there is a relative shear displacement and corresponding shear stress between soil and reinforcement surface. The contribution of this resistance will depend on the roughness of the surface, and normal stress.

Passive or bearing resistance occurs through the development of bearing stress on transverse reinforcement surfaces normal to the direction of soil reinforcement relative movement.

In Table 2.2 some typical reinforcements are shown with the main mechanism involved between reinforcement and the surrounding soil.

**Table 2.2** Common type of reinforcement (Palmeira, 1987).

reinforcement	type	mechanism	
		frictional	bearing
plain metal strip			
ribbed metal strip			
geotextile			
geogrid			

Current laboratory techniques to determine the soil-reinforcement interface include interface shear tests (ASTM D5321, 2009) and pullout test (ASTM D6706, 2013) on soil-reinforcement specimens. Several studies can be found in the literature on the direct shear and pullout testing of soil-reinforcement interfaces (Bergado et al., 1996; Bergado et al., 1993; Frost and Han, 1999; Goodhue et al., 2001; Koerner, 2005)

### 2.5.1 Direct shear test

For the direct shear test, the soil is forced to move on the surfaces of the reinforcement under a normal stress. Jewell et al. (1984) reported that direct shear

resistance between soil and grid reinforcement generally consists of three components. The first component is the shear resistance between soil to soil shearing resistances at the opening of grid reinforcement. The second component is the shearing resistances between soil and the surface area of grid reinforcement. Final component is the resistance from soil bearing surface of grid reinforcement, which is too difficult to assess. Thus, the direct shear resistance between soil and grid reinforcement can normally be expressed in terms of only two shearing resistance contribution; one is the shearing resistance between soil and soil at the apertures of the grid reinforcement and, other is the shearing resistance between soil and surface area of the grid reinforcement:

$$F_s = \sigma_n A_t f_{ds} \tan \phi_{ds} \quad (2.1)$$

$$f_{ds} \tan \phi_{ds} = \alpha_{ds} \tan \delta + (1 - \alpha_{ds}) \tan \phi_{ds} \quad (2.2)$$

Where  $\sigma_n$  is normal stress at the shear plane,

$A_t$  is total surface area of soil sliding,

$f_{ds}$  is coefficient of direct shear resistance,

$\phi_{ds}$  is friction angle of soil obtained from a direct shear test,

$\delta$  is angle of skin friction, and

$\alpha_{ds}$  is fraction of grid surface area providing the direct shear resistance.

If  $\alpha_{ds}$  is equal to zero, it will be the case of soil shearing over soil and then  $f_{ds}$  will be equal to one; but if  $\alpha_{ds}$  is equal to one, it will be the case of soil shearing over the surface area of grid reinforcement and the  $f_{ds}$  will be equal to  $\tan \delta / \tan \phi_{ds}$ .



### 2.5.2 Pullout test

Pullout resistance of grid reinforcement embedded in backfill soils basically consists of two resistance contributions; the former is frictional resistance and the latter is passive or bearing resistance, which is stated herein in the following sections:

#### 2.5.2.1 Frictional resistance

Bergado et al. (1993) concluded that the mobilization process of frictional resistance from a pullout force is similar to the friction resistance of an axially loaded pile, which just needs a small relative displacement to be mobilized. Frictional resistance induced from a pullout force can be expressed in the form of the skin friction between the longitudinal member of grid reinforcement (having same direction of the pullout force) and backfill soil. Frictional resistance is denoted as  $P_f$ . For grid reinforcements, the frictional resistance can be expressed simply in the following equation:

$$P_f = A_s \overline{\sigma_s} \tan \delta \quad (2.3)$$

where  $A_s$  is frictional area between soil and grid reinforcement,

$\overline{\sigma_s}$  is average normal stress being equal to  $0.75 \overline{\sigma_s}$  for inextensible grid reinforcement (Anderson and Nielsen, 1984), and

$\delta$  is skin friction angle between soil and grid reinforcement.

In case of geogrid reinforcements, the shape of longitudinal and transverse ribs is flat; therefore, the frictional resistance can be mobilized along not only the surface area of the longitudinal ribs, but also the surface area of the

transverse ones. The pullout resistance of steel grid and geogrid samples, about 10 % of pullout resistance of the steel grid reinforcement was governed by the frictional resistance that mobilized at a small pullout displacement (Bergado et al., 1993). In contrast, about 90 % of pullout resistance of the geogrid reinforcements (i.e. Tensar SR80) was governed by the frictional resistance, and the test results of two geogrid samples—one with transverse ribs and the other without and transverse ribs are shown in Figure 2.9. The obtained results of pullout resistance were assumed to be equal to the frictional resistance mobilized along the surface area of the longitudinal ribs.

For highly extensible geogrid reinforcements, the contribution of longitudinal ribs to the pullout force is more significant than that of the transverse ribs during the deformation stage because large elongation occurring in the geogrids restricts the mobilization of the full effect of the transverse ribs as reported by Alagiyawanna et al. (2001). They performed pullout tests on highly extensible geogrid samples with different spacing arrangements of the longitudinal and transverse ribs. The friction resistance mobilized along the longitudinal rib surface governs the pullout resistance,  $F_p$ , not the bearing resistance against the front of the transverse ribs (see Figure 2.10).

#### 2.5.2.2 Bearing resistance

The bearing resistance is induced only on the area of grid transverse members perpendicular to the pullout force and denoted as  $P_b$ . For grid reinforcements, bearing resistance can be expressed simply in the following equation:

$$P_b = \bar{\sigma}_b nd \quad (2.4)$$

Where  $\overline{\sigma}_b$  is maximum bearing stress against a single transverse members,

$n$  is number of transverse members, and

$d$  is diameter or thickness of a single transverse member being normal to the maximum bearing stress.

The maximum bearing stress of a single transverse member can be estimated by applying three different failure mechanisms; the first is general shear failure mode or known as bearing capacity failure mode (Perterson and Anderson, 1980), the second is punching shear failure mode (Jewell et al., 1984), and the last is modified punching shear failure mode (Chai, 1992). The first failure mode tends to occur possibly for inextensible grid reinforcements, while the second and the last are likely to occur for extensible grid reinforcements. Such three failure mechanisms are illustrated in Figure 2.11a, 2.11b, and 2.11c.

**a) Bearing capacity failure mode**

Bearing capacity equation was proposed by Terzaghi. This equation is based on inextensible grid reinforcements, and Terzaghi's bearing capacity equation of a shallow foundation. The equation can thus be expressed as follows:

$$\overline{\sigma}_b = cN_c + \sigma_n N_q \quad (2.5)$$

$$N_c = \cot \phi (N_q - 1) \quad (2.6)$$

$$N_q = \exp(\pi \tan \phi) \tan^2 \left( \frac{\pi}{2} + \frac{\phi}{2} \right) \quad (2.7)$$

Where  $\sigma_b$  is maximum bearing stress of a single transverse member,

$c$  is cohesion based on effective stress,

$\phi$  is effective friction angle of backfill soil, and

$N_c, N_q$  are bearing capacity factors.

### b) Punching shear failure mode

This failure mode is based on extensible grid.

According to (Jewell et al., 1984), the maximum bearing stress,  $\bar{\sigma}_b$  can be calculated as follows:

$$\bar{\sigma}_b = \sigma_n N_q \quad (2.8)$$

$$N_q = \exp \left\{ \left( \frac{\pi}{2} + \phi \right) \tan \phi \right\} \left( \frac{\pi}{4} + \frac{\phi}{2} \right) \quad (2.9)$$

Where  $\sigma_n$  is applied normal stress and

$N_q$  is bearing capacity factor

If the soil behavior is perfectly plastic and the problem satisfies the above equation, the solution is the exact solution. From several test results, they revealed that the bearing capacity and punching shear failure modes provided the apparent upper and lower bounds for the actual pullout test results (Palmeira and Milligan, 1990). In other words, neither of such failure modes might represent pullout failure mechanisms well.

**c) Modified punching failure mode**

This failure mode is based on extensible grid reinforcements as well. However, Chai, 1992 proposed the modified  $N_c$  and  $N_q$  for Eq. 2.5 as follows:

$$N_c = \frac{1}{\sin \phi} \exp^{(2\beta \tan \phi)} \tan \left( \frac{\pi}{4} + \frac{\phi}{2} \right) - \cot \phi \quad (2.10)$$

$$N_q = \left[ \frac{1+k}{2} + \frac{1-k}{2} \sin(2\beta - \phi) \right] \frac{1}{\cos \phi} \exp^{(2\beta \tan \phi)} \tan \left( \frac{\pi}{4} + \frac{\phi}{2} \right) \quad (2.11)$$

Where  $\beta$  is angle of rotational failure zone and

$k$  is horizontal earth pressure coefficient.

**2.5.3 Interference factor coefficients**

The transverse member interference,  $R$ , of the bearing member has a strong influence on pullout resistance. Generally, the larger this ratio, the higher the pullout passive bearing resistance for an individual bearing member (Bergado and Chai, 1994). Introduced as a bearing resistance ratio,  $R$  is a function of transverse member spacing ratio,  $S/D$  as follows:

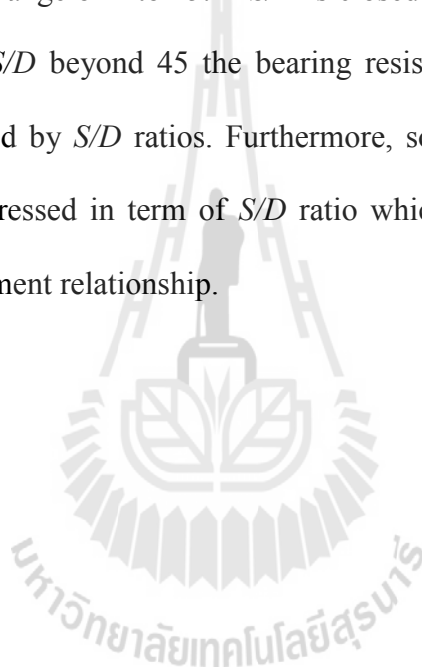
$$R = a + b(S/D)^{nr} \quad (2.12)$$

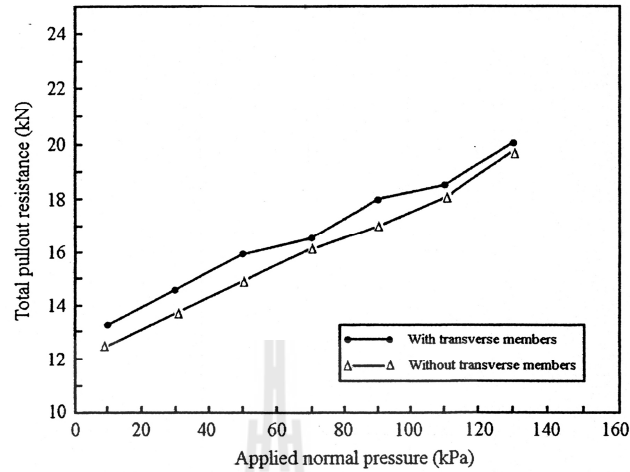
Where  $a$ ,  $b$  and  $nr$  are constants.

Bergado et al. (1996) found that the bearing resistance ratio,  $R$ , corresponds to  $S/D$  ratios. The  $S/D$  ratios influence the bearing resistance of individual member in range of 1 to 45. If  $S/D$  is closed to one, the grid behaves like a

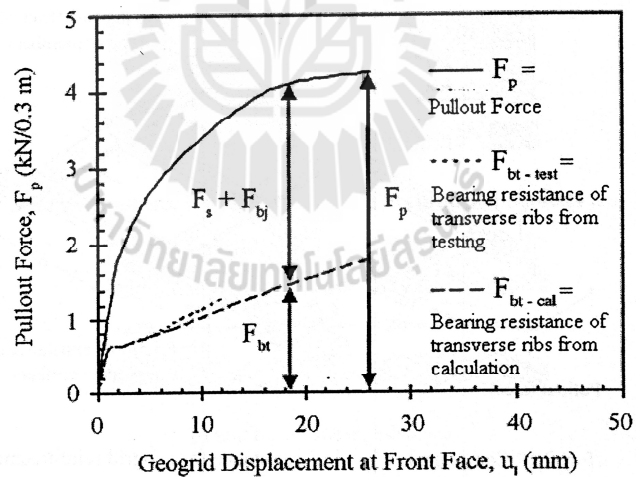
rough sheet and for  $S/D$  beyond 45 the bearing resistance of individual transverse member is not affected by  $S/D$  ratios. Furthermore, some constant parameters have been defined and expressed in term of  $S/D$  ratio which is needed for prediction of pullout force/displacement relationship.

Bergado et al. (1996) found that the bearing resistance ratio,  $R$ , corresponds to  $S/D$  ratios. The  $S/D$  ratios influence the bearing resistance of individual member in range of 1 to 45. If  $S/D$  is closed to one, the grid behaves like a rough sheet and for  $S/D$  beyond 45 the bearing resistance of individual transverse member is not affected by  $S/D$  ratios. Furthermore, some constant parameters have been defined and expressed in term of  $S/D$  ratio which is needed for prediction of pullout force/displacement relationship.

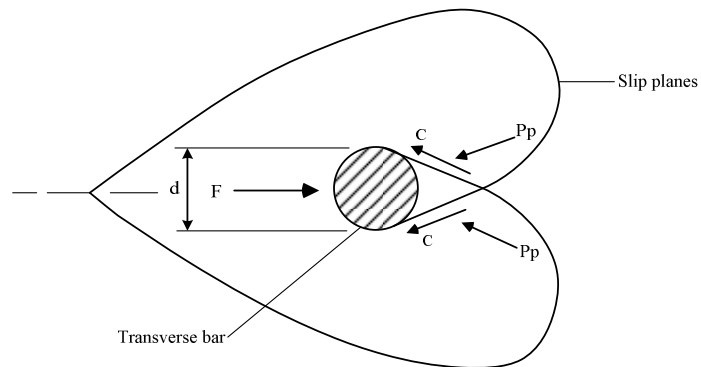




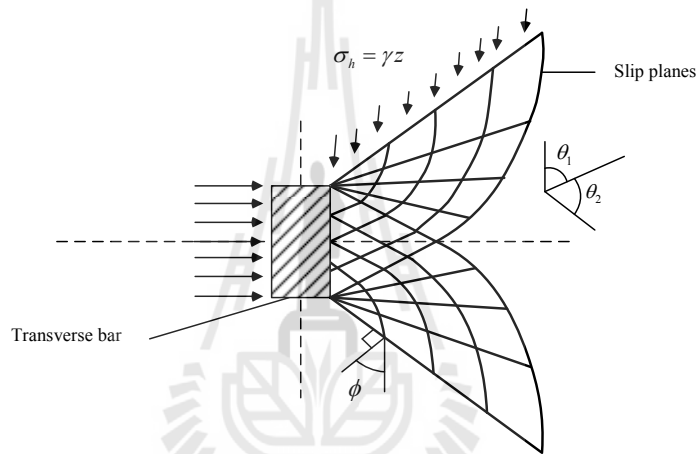
**Figure 2.9** Pullout resistance at 25 mm pullout displacement of Tensar SR80 geogrid (Abiera, 1991).



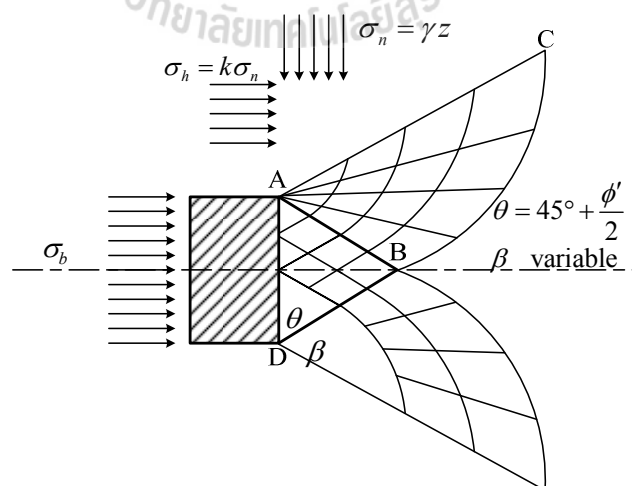
**Figure 2.10** Components of the pullout force against the geogrid displacement at the rigid front face (Alagiyawanna et al., 2001).



(a) General shear failure mode (Peterson and Anderson, 1980)



(b) Punching shear failure mode (Jewell et al., 1984)



(c) Modified punching failure mode (Bergado et al., 1996)

**Figure 2.11** Modes of failure mechanism.



## 2.6 Literature reviews of direct shear and pullout tests

Several researchers have carried out the direct shear and the pullout tests of reinforcement in soils (Bergado et al., 1992; Koutsourais et al., 1998; Liu et al., 1996). These tests were originally carried out for the purpose of clarifying the mechanism and evaluating of the reinforced soil structures. The method of preparing the soils specimens, reinforcement materials, and the size of apparatus were among the factors investigated. The test conditions are very important for the determination of the design and analysis parameters of the reinforced soil structures. The interaction between soil and reinforcement is frequently evaluated and analyzed in terms of apparent interface friction factor, which were obtained from the direct shear and pullout tests (Ingold, 1983; Juran et al., 1991; Rowe et al., 1985)

Alfaro et al. (1995) reported that in the direct shear test, the interface frictional resistance is a function of the soil to reinforcement and the soil to soil shear resistance, whereas in the pullout tests, the frictional resistance is a function of surface roughness, geosynthetic extensibility.

Koutsourais et al., (1998) compared the results of pullout and direct shear tests of geosynthetic reinforcement in marginal cohesive soil, in term of apparent interface friction angle,  $\delta$ . The tested results were concluded that the pullout test provided approximately 13% to 17% soil interaction values higher than direct shear test at low confining pressures and provided essentially the same soil interaction values at higher confining pressures. The total pullout resistance of geotextile is contributed only by the frictional resistance, which was evaluated by Mohr-Coulomb yield criterion. This resistance depends on engineering properties of soil, roughness surface of the reinforcement, and confining pressure.

Liu et al. (1996) investigated the performance of polymeric geogrids in compacted lateritic soils and complemented the analysis done by Bergado et al. (1992). They concluded that the test results accordance with the results of Bergado et al. (1992), i.e., the bearing capacity failure and the punching failure modes appeared to be an upper bound and lower bound envelop for the pullout capacities for grid reinforcements.

Tatlisoz et al. (1998) studied the interaction between geosynthetic and soil-tire chip mixtures. The coefficient of interaction,  $c_i$ , for different geosynthetic types and different soil contents was evaluated. The  $c_i$  results ranged from 0.3 to 1.5. They concluded that the  $c_i$  value greater than unity ( $c_i > 1$ ), the efficient bond between soil and reinforcement is greater than shear strength of the soil. In addition, if the  $c_i$  value is less than 0.5 ( $c_i < 0.5$ ) indicates weak bonding between soil and geosynthetic of breakage of geosynthetic layer.

Ochiai et al. (1996) and Holtz (1977) investigated the shear stress distribution along the length of geosynthetics using pullout tests. The deformation along the length of geosynthetic was measured using LVDTs. The studies concluded that the shear stress is maximum at the face of the geosynthetic and gradually decreases along its length.

Elias et al. (2001) examined that the pullout resistance factor,  $F^*$  (friction and bearing interaction factor) and  $\alpha$  (scale correction factor). In order to determine  $\alpha$  factor, the pullout tests were investigated under different length of geosynthetic with vary confining pressures. The recommended value of  $\alpha$  for design parameter was recommended in the range of 0.6 to 0.8.

Liu et al. (2009) studied the interface shear strength of geogrids and geotextile embedded in sand and gravel using direct shear apparatus. The test results indicated that the shear strength of soil-geotextile interface was 0.7 and 0.85 of the soil shear strength for Ottawa sand and gravel, respectively. In addition, there results showed that the soil-geogrid interface was generally higher than that of soil-geotextile.

Hamid and Miller (2009) carried out a series of modified direct shear tests in which the matric suction of the soil specimen was controlled in order to study the shear strength behavior of an unsaturated low-plasticity fine-grained soil. Their results showed that the matric suction contributed to the peak shear strength of unsaturated interfaces but did not significantly affect their post-peak shear strength. However, the variation of confining pressure affected both peak and post-peak shear strength values.

Mitchell et al. (1990) conducted the direct shear tests to study the effect of dry and wet interface on the frictional resistance of smooth HDPE membranes compacted clay interface. The results showed that when the clay was compacted at dry condition, the shear resistance at HDPE-clay interface was about 95.8 kPa. Moreover, the interface shear resistance reduced to 43.1 kPa when the clay was nearly compacted at saturation state.

## **2.7 Pullout resistance of bearing reinforcement**

Horpibulsuk and Niramitkronburee (2010) have recently developed a new cost-effective inextensible reinforcement type, termed as "Bearing reinforcement", which is composed of a longitudinal member and transverse (bearing) member. The longitudinal member is a deformed steel bar (DSB) and the transverse members are a

set of equal angle steel. The earth stabilized by this reinforcement is designated as “Bearing Reinforcement Earth (BRE) wall” (Horpibulsuk et al., 2011). The BRE wall system has been developed into one of the standard MSE walls for the Department of Highways in Thailand.

Performance of the BRE wall on a firm ground was first investigated on the campus of Suranaree University of Technology (SUT) through a research project sponsored by the Thailand Research Fund (TRF) in 2009. Based on the field investigation and laboratory pullout tests (Horpibulsuk and Niramitkronburee, 2010; Horpibulsuk et al., 2011), a design method for BRE walls founded on a firm ground was subsequently introduced. This method has been adopted to design several BRE walls under the supervision of Department of Highways in Thailand since 2008.

Recently, Suksiripattanapong et al. (2012) proposed a simplified method to model the bearing reinforcement, which converts its friction and bearing resistance to the equivalent friction resistance for finite element analysis. So far, all the studies on bearing reinforcement are limited to high-quality coarse-grained soils (<15% fine content), as specified by the Department of Highways in Thailand.

### 2.7.1 Pullout friction resistance

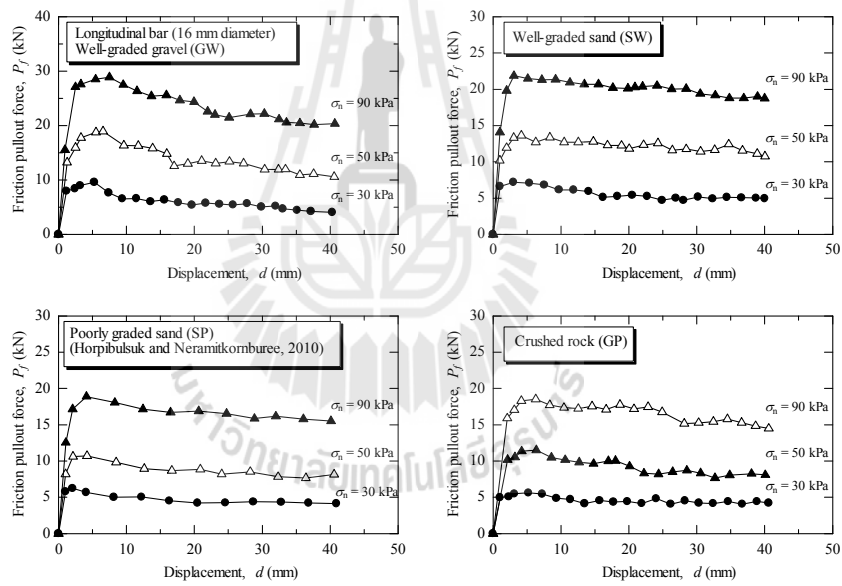
Figure 2.12 shows the pullout friction force and displacement relationship of a longitudinal member with a diameter of 16 mm and length of 2.6 m for well-graded gravel (GW), well-graded sand (SW), poorly-graded sand (SP) and crushed rock (GP). Maximum pullout friction resistance,  $P_f$  of the longitudinal member can be calculated from

$$P_f = \pi DL\sigma_n \tan \delta \quad (2.13)$$

Where  $D$  and  $L$  are diameter and length of the longitudinal member, respectively,

$\sigma_n$  is normal stress and  $\delta$  is the skin friction angle.

For a particular soil, the maximum pullout friction force,  $P_{f,\max}$  increases with the increase in normal stresses,  $\sigma_n$ . The displacement at peak failure is insignificantly affected by the normal stress; it is approximately 3 to 5 mm for all the applied normal stresses and tested soils. The well-graded gravel (GW) gives the highest pullout friction force because it has the highest friction angle.



**Figure 2.12** Pullout test results of a longitudinal member under different normal stresses (Suksiripattanapong et al., 2013).

### 2.7.2 Pullout Bearing Mechanism of a Single Isolated Transverse Member ( $n = 1$ )

Figure 2.13 shows comparison of maximum pullout bearing resistance of a single isolated transverse member. It is found that the maximum pullout bearing resistance can be determined from the plasticity solutions. The maximum bearing stress,  $\sigma_{b\max}$ , of a single transverse member in coarse-grained soil can be predicted by modified punching shear failure mechanism.

$$\sigma_{b\max} = N_q \sigma_n \quad (2.14)$$

$$N_q = \frac{1}{\cos \phi} \exp[\pi \tan \phi] \tan\left(\frac{\pi}{4} + \frac{\phi}{2}\right) \quad (2.15)$$

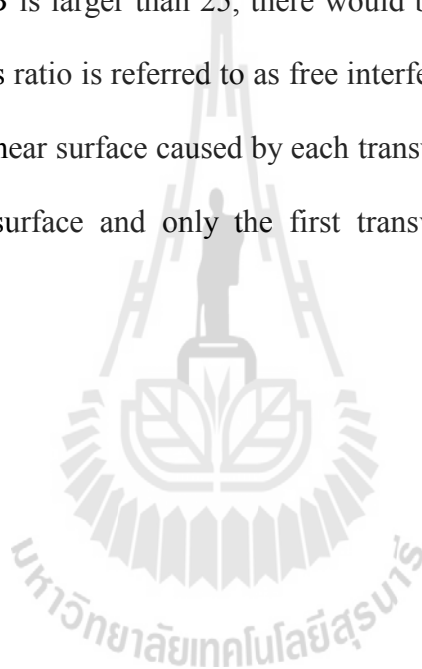
Figure 2.13 indicated that for the well-graded gravel (GW) and the crushed rock (GP), with large average grain size, the maximum bearing stress at low normal stress of approximately 30 kPa was close to the predicted by the general shear mechanism. However, the measured maximum bearing stress at high normal stress of 90 kPa was very close to that predicted by the modified punching shear mechanism (Suksiripattanapong et al., 2013).

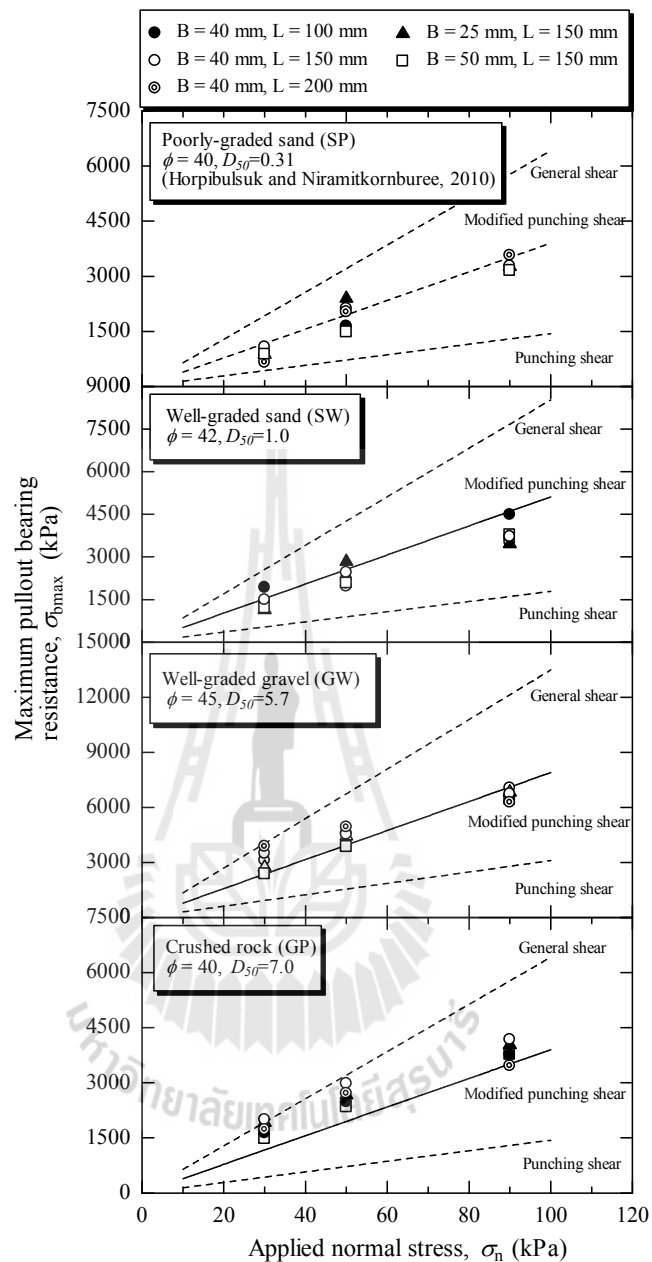
### 2.7.3 Pullout Resistance of the Bearing Reinforcement ( $n > 1$ )

In practice, the bearing reinforcement consists of several transverse members placed at regular intervals. During the pullout of the bearing reinforcement, the transverse members interfere with each other. A dimensionless parameter, transverse member spacing ratio,  $S/B$  is introduced herein to investigate the influence of spacing,  $S$ , and dimension ( $B$  and  $L$ ) of transverse members on the pullout bearing

characteristics. Generally, the larger the  $S/B$ , the higher the pullout bearing resistance up to a certain maximum value, due to less interference among transverse members.

Figure 2.14 shows the typical relationship between maximum pullout bearing force,  $P_{bn}$  and transverse member spacing ratio,  $S/B$  for 40x150 mm transverse members ( $n = 2$  to 4) under different applied normal stresses compared with maximum pullout bearing force of a single isolated transverse member ( $n = 1$ ),  $P_{b1}$ . It is found that when  $S/B$  is larger than 25, there would be no more transverse member interference. Thus, this ratio is referred to as free interference spacing ratio. When  $S/B$  is less than 3.75, the shear surface caused by each transverse member joins together to form a rough shear surface and only the first transverse member causes bearing resistance.





**Figure 2.13** Maximum pullout bearing resistance of a single isolated transverse member for all tested soils (Suksiripattanapong et al., 2013).

In this case, all the transverse members would act like a rough block. As such, the maximum pullout bearing resistance is determined from the sum of the friction on the block sides and the bearing capacity of the first transverse member. Since the bearing capacity is more dominant, the pullout bearing resistance is close to



that of a single isolated transverse member. This  $S/B$  ratio is thus defined as a rough block spacing ratio. From this finding, the failure mechanism of the bearing reinforcement is classified into three zones, depending upon  $S/B$  ratio as shown in Figure 2.16. Zone 1 is referred to as block failure when  $S/B \leq 3.75$ . Zone 2 is regarded as member interference failure when  $3.75 < S/B < 25$ . Zone 3 ( $S/B \geq 25$ ) is individual failure where soil in front of each transverse member fails individually.

The level of transverse member interference can be expressed by the interference factor,  $IF$ . It is defined as the ratio of the average maximum pullout bearing force of the bearing reinforcement with  $n$  transverse members to that of a single isolated transverse member.

$$IF = \frac{P_{bn}}{nP_{b1}} \quad (2.16)$$

The higher the level of transverse member interference (the lower the  $S/B$ ), the lower the  $P_{bn}$ , and hence the lower the  $R$ . Based on the analysis of the test data, it is found that the interference factor is mainly dependent upon  $S/B$ , and  $n$ , irrespective of  $L$  and applied normal stress. The following equation for interference factor is hence:

$$F = a + b \ln\left(\frac{S}{B}\right) \quad (2.17)$$

These two constants,  $a$  and  $b$  can be obtained with the two physical conditions: 1) when  $S/B$  equals 3.75, the interference factor equals  $1/n$  since  $P_{bn}$  and  $P_{b1}$  are the same, and 2) when  $S/B$  equals 25, the interference factor equals unity. These two conditions establish the lower and upper values of  $R$  at corresponding

values of  $S/B = 3.75$  and  $25$ , respectively. From these two conditions, the constants  $a$  and  $b$  can be determined by the following equations:

$$b = 0.527 \left[ 1 - \frac{1}{n} \right] \quad (2.18)$$

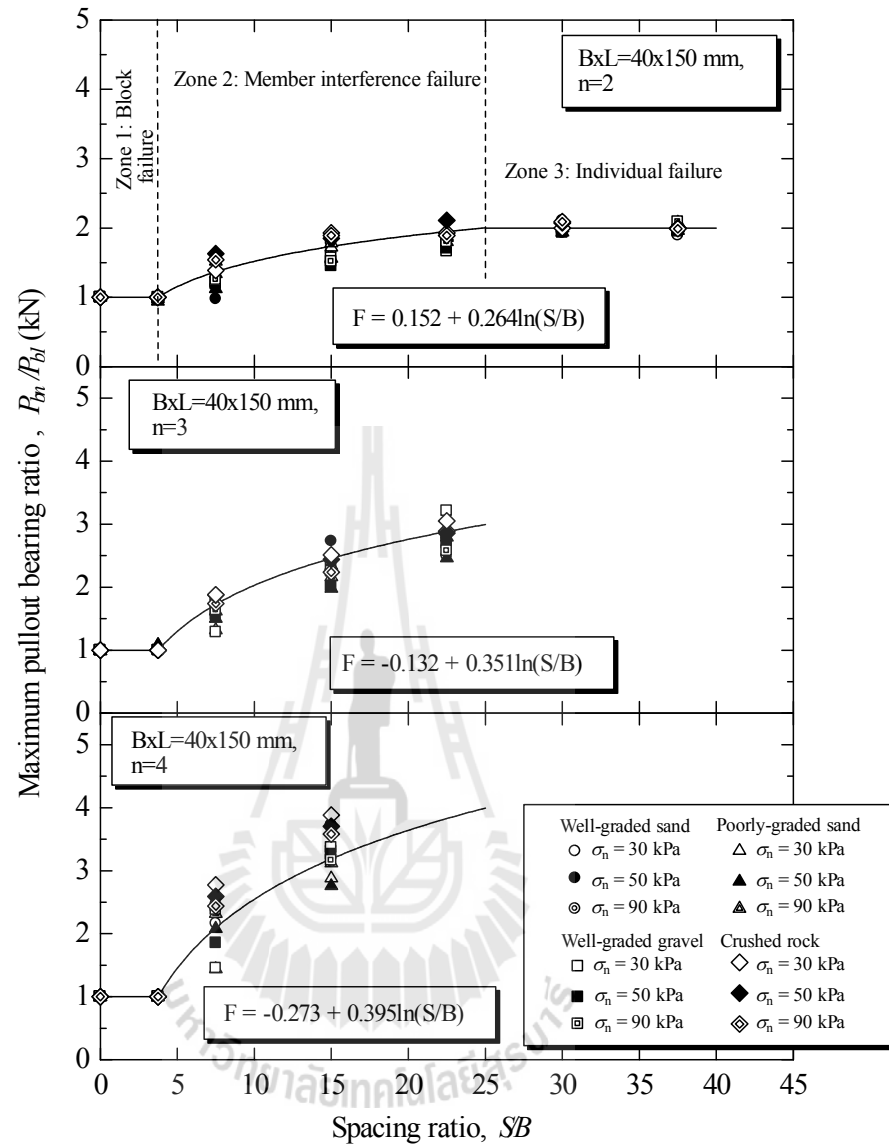
$$a = 1 - 3.219b \quad (2.19)$$

As such,  $a$  and  $b$  values are  $0.152$  and  $0.264$ ,  $-0.132$  and  $0.351$ , and  $-0.273$  and  $0.395$  for  $n = 2, 3$ , and  $4$ , respectively. Using these  $a$  and  $b$  values for different  $n$ , the maximum pullout bearing resistance can be predicted as shown by the solid lines in Figure 2.14. The laboratory  $P_{b1}$  values ( $P_{b1} = 6.4, 12.7$ , and  $19.7$  kN for  $n = 2, 3$ , and  $4$ , respectively) are used for this prediction.

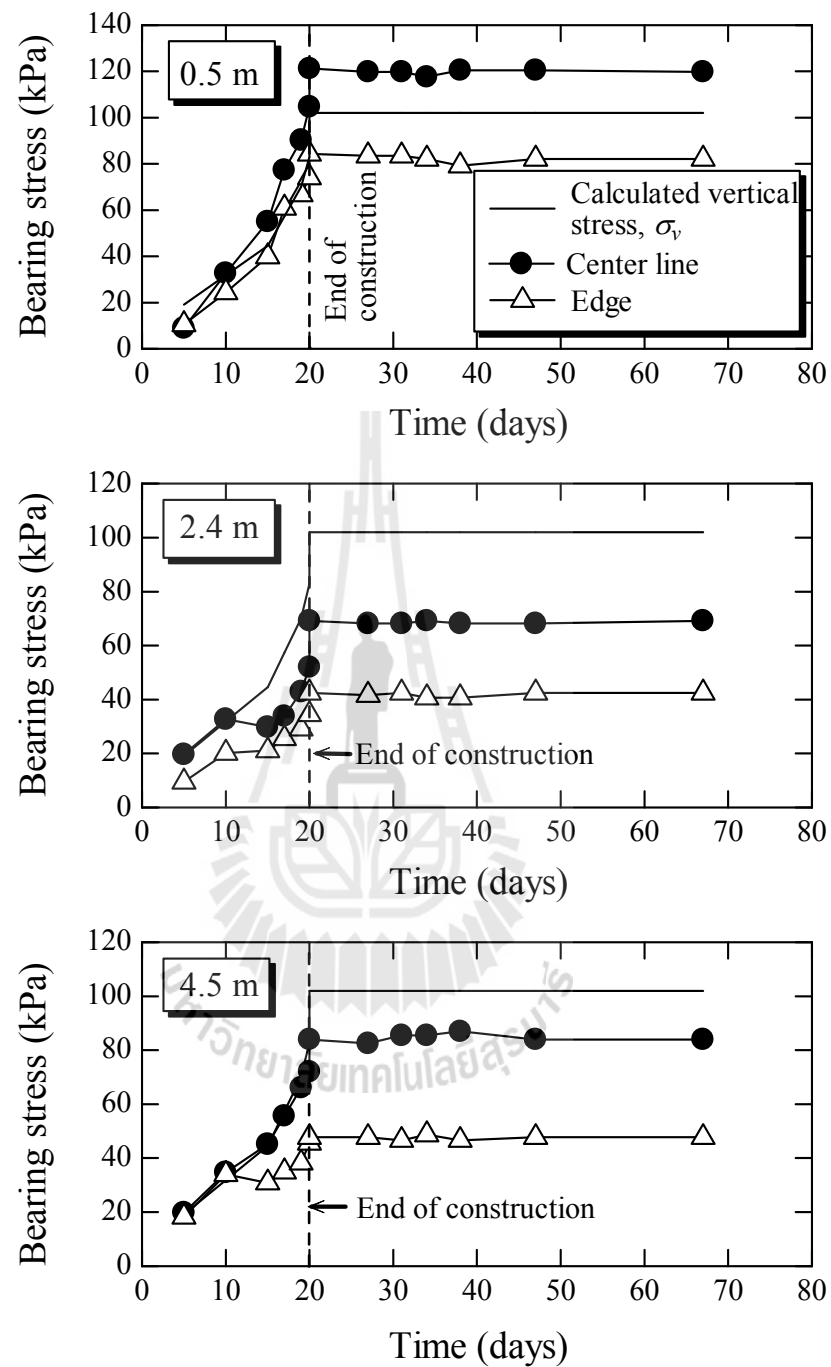
## 2.8 The behavior of bearing reinforcement earth (BRE) Wall

### 2.8.1 Bearing stress

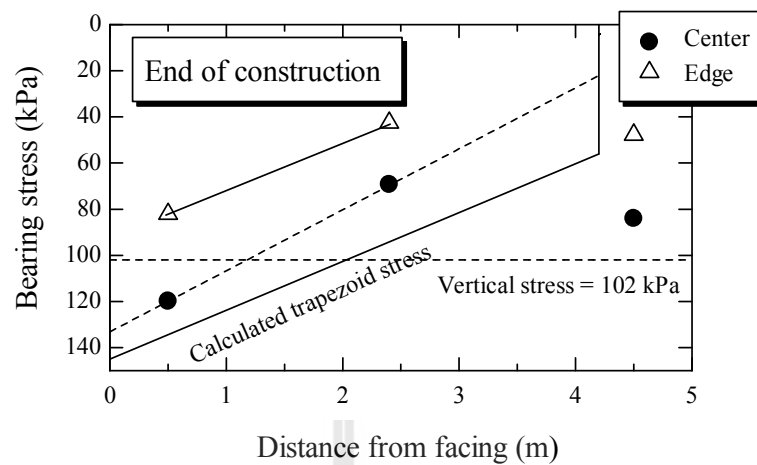
Figure 2.15 shows the increase in the bearing stress with construction time at the center and edge (3.45 m from the center) in the middle zone of the wall compared with the calculated vertical stress. The bearing stresses were measured both in reinforced (0.5 and 2.4 m from wall facing) and unreinforced (4.5 m from facing) zones. Within the reinforced zone, the bearing stress distributions in both the center and the edge are approximately trapezoid shape, which is typical of rigid foundation (*vide* Figure 2.16).



**Figure 2.14** Measured and predicted  $P_{bn}/P_{b1}$  and  $S/B$  relationship for 40x150 mm transverse members (Suksiripattanapong et al., 2013).



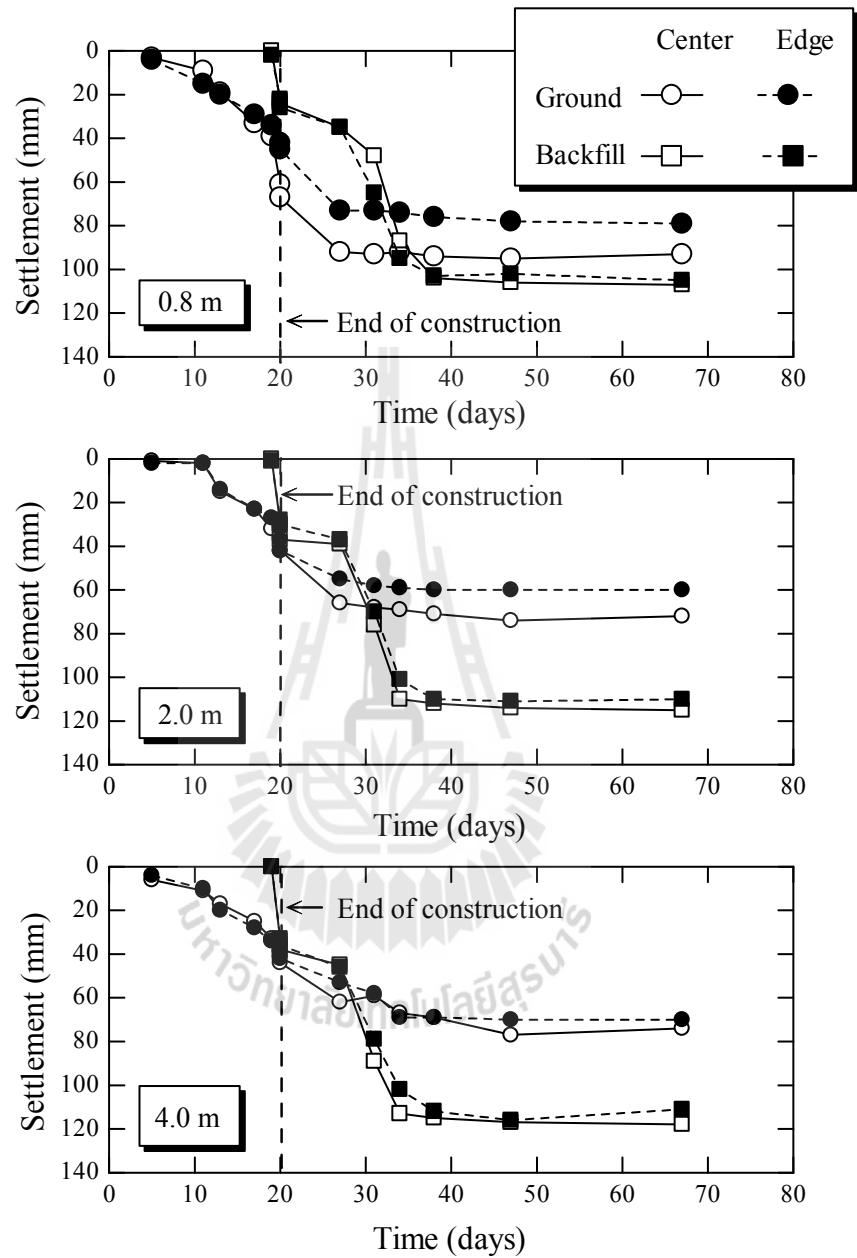
**Figure 2.15** Relationship between bearing stresses and time under the wall (Horpibulsuk et al., 2011).



**Figure 2.16** Bearing stress distribution after the completion of construction (Horpibulsuk et al., 2011).

### 2.8.2 Settlement

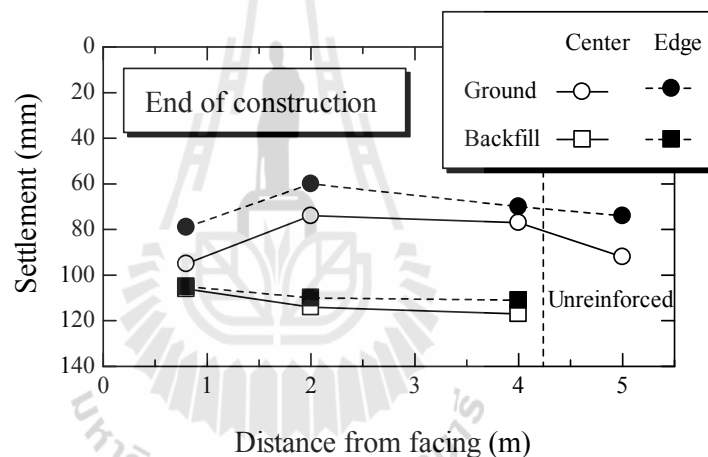
The measured settlements (in the ground and the reinforced backfill) at the center and edge in the middle zone of the test wall are illustrated in Figures 2.17. The wall settles very fast during construction. After the completion of construction, the rate of settlement decreases and the final settlement is attained at about 10 days after the completion of construction. More than 70% final settlement occurs at the end of construction. This is because the wall was founded on the relatively dry and hard stratum that the immediate settlement is dominant. In the reinforced zone, the ground settlements at the center of the BRE wall decrease from front (95 mm) to back (77 mm) (*vide* Figure 2.18). The large settlement at the front is possibly caused by the eccentric load and the weight of the segmental panels (*vide* Figure 2.18).



**Figure 2.17** Relationship between settlement and time (Horpibulsuk et al., 2011).

### 2.8.3 Lateral wall movement

The lateral movement of the wall face after the completion of construction was measured from the digital inclinometer located near the wall face. The initial readings on the inclinometer were taken corresponding to zero movement after the completion of construction. The lateral movement was monitored from the end of construction until 47 days. The lateral movement is very small with the maximum (at the top) of only less than 9 mm at 47 days after the completion of construction as shown in Figure 2.19.



**Figure 2.18** Final settlement profile at 47 days after the completion of construction (Horpibulsuk et al., 2011).

### 2.8.4 Coefficient of lateral earth pressure

The coefficients of lateral earth pressure for any backfill load were the ratios of the lateral earth pressure,  $\sigma_h$ , to the vertical pressure,  $\sigma_v$ . The lateral earth pressures at the maximum tension in reinforcement were determined from the strain gauges on the reinforcement and the lateral earth pressures at wall facing panels were

measured from earth pressure gauges attached to the wall facing panels. The  $K$  for the maximum tension in reinforcement is used for designing the internal stability of the earth wall (pullout and rupture failure criteria) whereas the  $K$  at the wall facing panels is used for designing the tie points and facing panels.

Figure 2.20 shows the relationship between the wall depth and the coefficients of lateral earth pressure at the maximum tension in the reinforcements after the completion of construction, compared with those for the other reinforcements (Christopher et al., 1990 and Bergado et al., 1999). Figure 2.20 shows the relationship between  $K$  and depth at the wall face and at maximum tension compared with that recommended by AASHTO (1996). AASHTO (1996) recommends that at the maximum tension, the lateral earth pressure,  $\sigma_h$ , at each reinforcement level of an earth wall with inextensible reinforcements shall be calculated using  $K = K_0$  at the top of the wall and decreases linearly to  $K = K_a$  at 6 m depth. Below a 6 m depth,  $K = K_a$  shall be used. It is found from Figure 2.21 that the measured  $K$  for the maximum tension in the bearing reinforcements is in agreement with this recommendation.

### 2.8.5 Possible failure plane

The initial reading on strain gage was taken from zero tension. Subsequent readings were then taken as that wall was constructed and past construction. From the strains calculate, the tensions in the wire can be computed as:



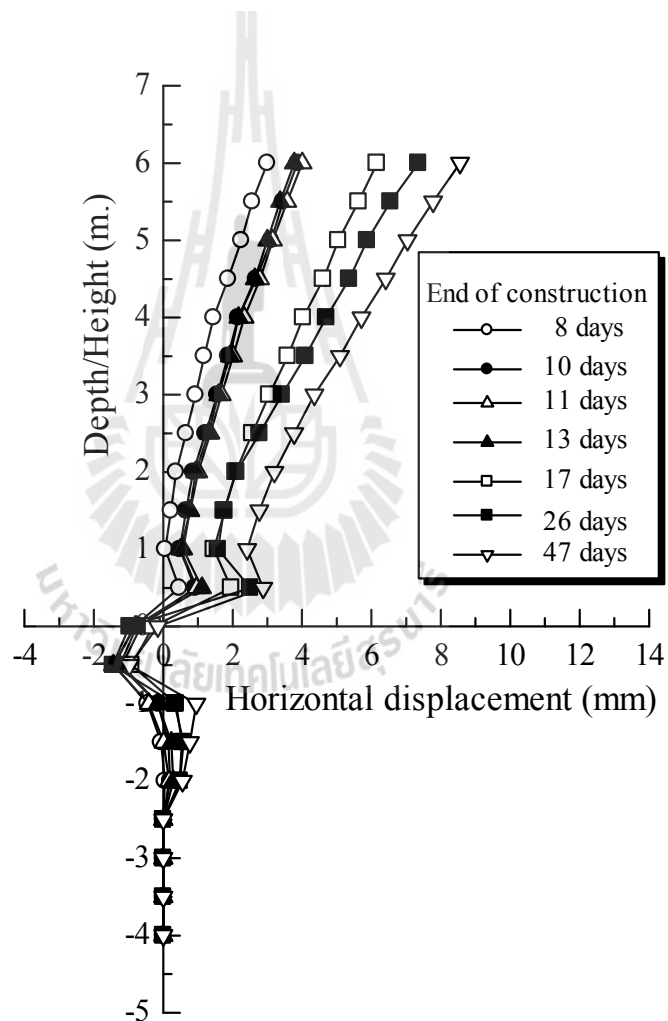
$$T = EA\varepsilon \quad (2.20)$$

Where  $T$  is axial tension in reinforcing wire,

$E$  is modulus of elasticity of steel,

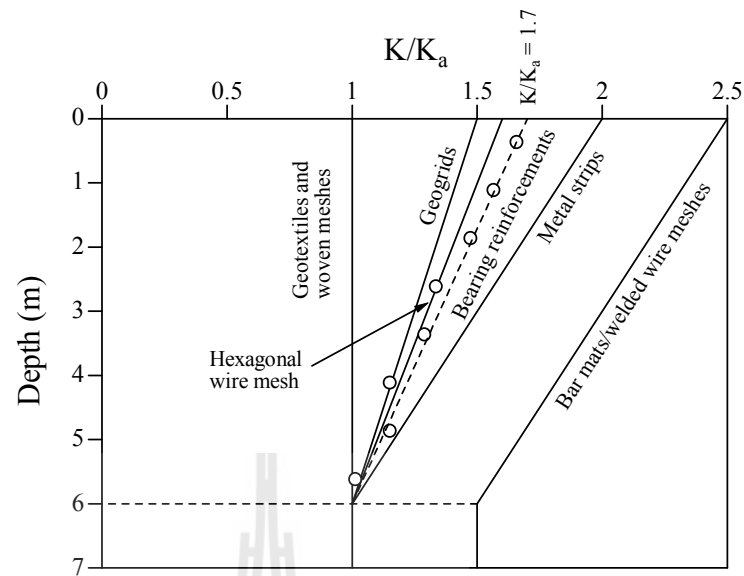
$A$  is cross-sectional area of the reinforcing wire, and

$\varepsilon$  is axial strain in the reinforcing wires.

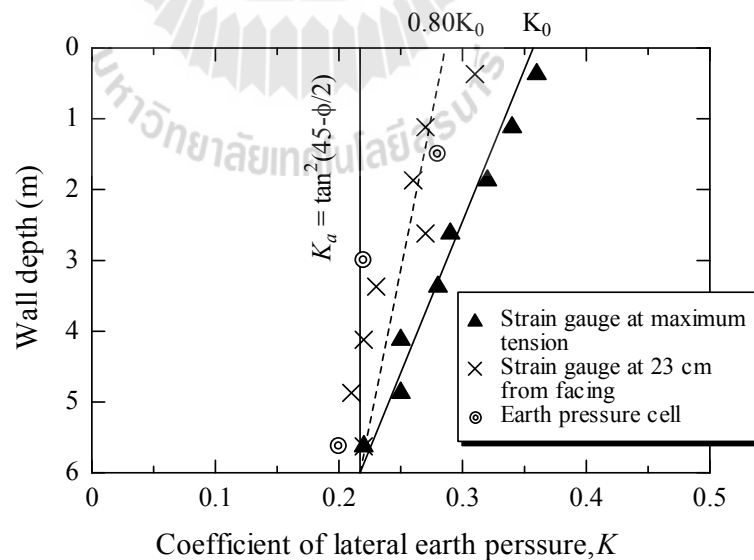


**Figure 2.19** Measured lateral wall movement after the completion of construction.

(Horpibulsuk et al., 2011).

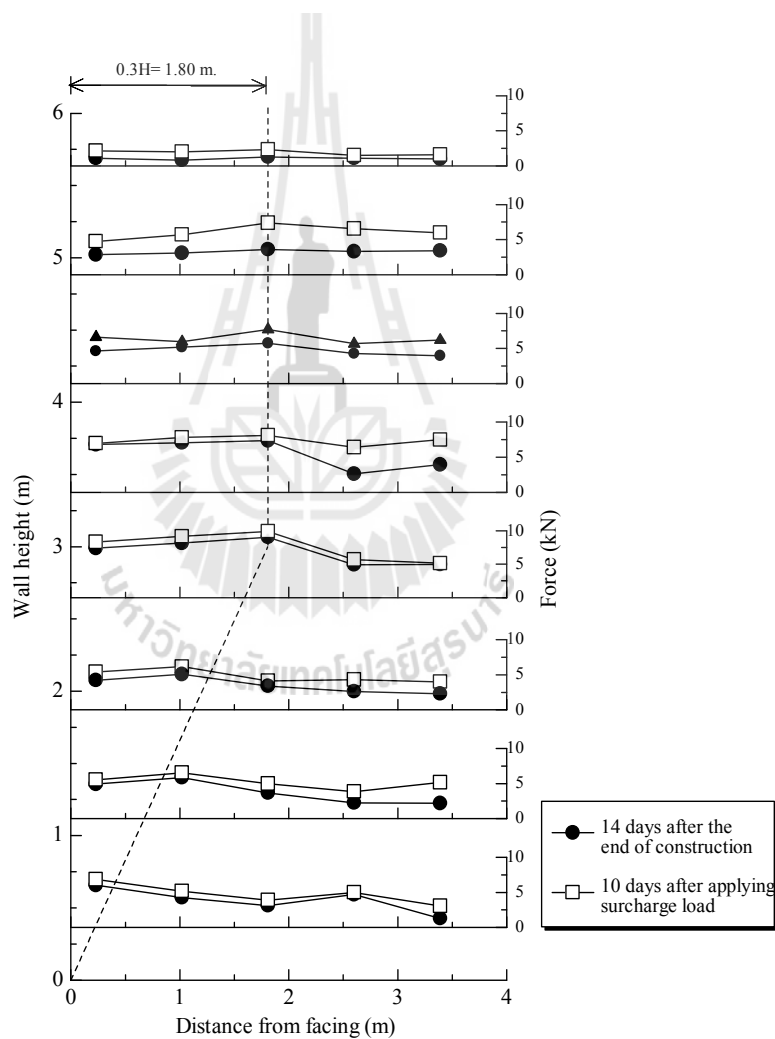


**Figure 2.20** Coefficients of lateral earth pressure at maximum tension for the bearing reinforcements.(Christopher et al., 1990, Bergado et al., 1999 and Horpibulsuk et al., 2011).



**Figure 2.21** Coefficient of lateral earth pressure for the bearing reinforcement.  
(AASHTO (1996)and Horpibulsuk et al., 2011)

Figure 2.22 illustrates the reinforcement tension measured at 14 days after the completion of construction and 10 days after additional surcharge load. The maximum tension line (possible failure plane) of the bearing reinforcement corresponds to the bilinear type of maximum tension line (coherent gravity structure hypothesis) as expected for metal strip and steel grids (AASHTO, 1996, 2002; and Anderson et al., 1987, Bergado et al., 1998; and Chai, 1992).



**Figure 2.22** Measured tensions in the bearing reinforcements  
(Horpibulsuk et al., 2011).

## 2.9 Finite Element Modeling of Reinforced Earth Structure

The behavior of reinforced earth structure on soft ground, and its influence factors have been analyzed using finite element method (FEM) by several researchers (Chai, 1992; Hird and Kwok, 1989; Long, 1996; Rowe and Ho, 1997). There are two general approaches to the finite element analysis of reinforced soil system, namely: discrete material and composite material. Although the discrete approach needs more computer time, it is preferable because the properties and responses of soil/reinforcement interaction properties are key factors that control its performance. Hence, the discrete approach is used in this research, and is discussed in detail in the following sections.

### 2.9.1 Elasto-plastic model

The elasto-plastic model is characterized by: the yield function, the flow rule, and the hardening law. The strain due to any increment of stress can be divided into two components: elastic strain and plastic strain. For conditions where the stress state is in yield locus, an increment stress can only cause elastic strain. If the stress conditions correspond to a point on the yield surface and if the material is stable, the increment of stress produces elastic and plastic strain. There are several elastoplastic models for soils as discussed below.

#### 2.9.1.1 Elasto-perfectly-plastic Mohr Coulomb model

The relationship between effective stress rate and strain rate for elastoplasticity (Smith and Griffith, 1988) are given as follows:

$$\dot{\sigma}' = \left[ D^e - \frac{\alpha}{d} D^e \frac{\partial g}{\partial \sigma'} \frac{\partial f^T}{\partial g} D^e \right] \dot{\epsilon} \quad (2.21)$$

$$d = \frac{\partial f^T}{\partial \sigma'} D^e \frac{\partial g}{\partial \sigma'} \quad (2.22)$$

Where  $f$  is yield function,  $g$  is plastic potential function,

$\sigma'$  is effective stress tensor,

$\varepsilon$  is strain tensor, and

$D^e$  is elastic constitutive matrix.

The term  $\alpha$  is used as a switch. If material behavior is elastic which, the value of  $\alpha$  is zero. For plastic behavior,  $\alpha$  is unity.

The yield function for Mohr Coulomb model is defined as three yield functions, which are formulated in terms of principal stress (Smith and Griffith, 1988) as follows:

$$f_1 = \frac{1}{2}|\sigma_2 - \sigma_3| + \frac{1}{2}|\sigma_2 + \sigma_3|\sin \phi - c \cos \phi \geq 0 \quad (2.23)$$

$$f_2 = \frac{1}{2}|\sigma_3 - \sigma_1| + \frac{1}{2}|\sigma_3 + \sigma_1|\sin \phi - c \cos \phi \geq 0 \quad (2.24)$$

$$f_3 = \frac{1}{2}|\sigma_1 - \sigma_2| + \frac{1}{2}|\sigma_1 + \sigma_2|\sin \phi - c \cos \phi \geq 0 \quad (2.25)$$

Where  $\phi$  is friction angle of soil,

$c$  is cohesion intercept.

The plastic potential functions are defined as follows:

$$g_1 = \frac{1}{2}|\sigma_2 - \sigma_3| + \frac{1}{2}|\sigma_2 + \sigma_3|\sin \phi \quad (2.26)$$

$$g_2 = \frac{1}{2}|\sigma_3 - \sigma_1| + \frac{1}{2}|\sigma_3 + \sigma_1|\sin \phi \quad (2.27)$$

$$g_3 = \frac{1}{2}|\sigma_1 - \sigma_2| + \frac{1}{2}|\sigma_1 + \sigma_2|\sin \varphi \quad (2.28)$$

where  $\varphi$  is the dilation angle.

In order to model the influence of stress level on the material stiffness, a simple power law for the shear modulus is introduced (Vermeer and Brinkgreve, 1995):

$$G = G_{ref} \left( \frac{P^*}{P_{ref}} \right)^m \quad (2.29)$$

Where  $P^* = -\frac{1}{3}(\sigma_1 + \sigma_2 + \sigma_3) + c \cot \phi$ ,

$G_{ref}$  is reference shear modulus, corresponding to  $P^* = P_{ref}$ ,  $P_{ref}$  is reference pressure model parameters for and  $m$  is power number.

Thus, the Mohr Coulomb model required a total of given parameters which are  $G_{ref}$ ,  $P_{ref}$ ,  $m$ ,  $\nu$ ,  $\phi$ ,  $c$ ,  $\varphi$ , which are familiar to most geotechnical engineers.

### 2.9.2 Soil and reinforcement interface model

In PLAXIS program, the stress-strain behavior at soil-interface is simulated by elastic, perfectly-plastic interface model. The model parameters at soil-structure interface can be generated from that soil using the interface coefficient,  $R_{inter}$ , defined as the ratio of the shear strength of the interface to the corresponding shear strength of the soil (Vermeer and Brinkgreve, 1995) as follows:

$$\tan \delta = R_{inter} \tan \phi \quad (2.30)$$

$$c_i = R_{inter} c \quad (2.31)$$

$$G_i = R_{inter}^2 G \quad (2.32)$$

Where  $G$  is shear modulus of soil that contacts with reinforcement,

$G_i$  is shear of interface element,

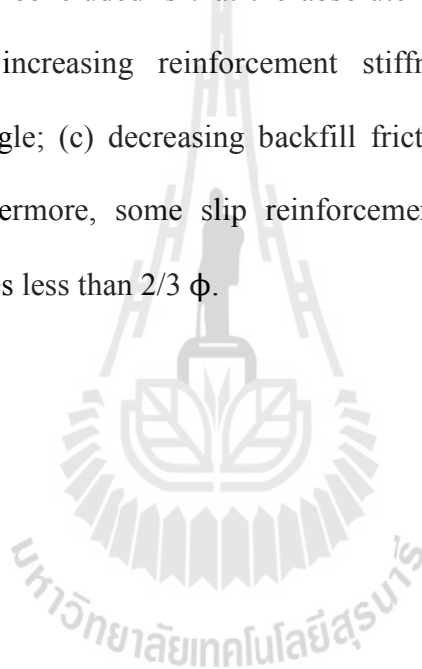
$\phi$  is angular of friction of soil contacted with reinforcement, and

$\delta$  is angular of friction of interface element.

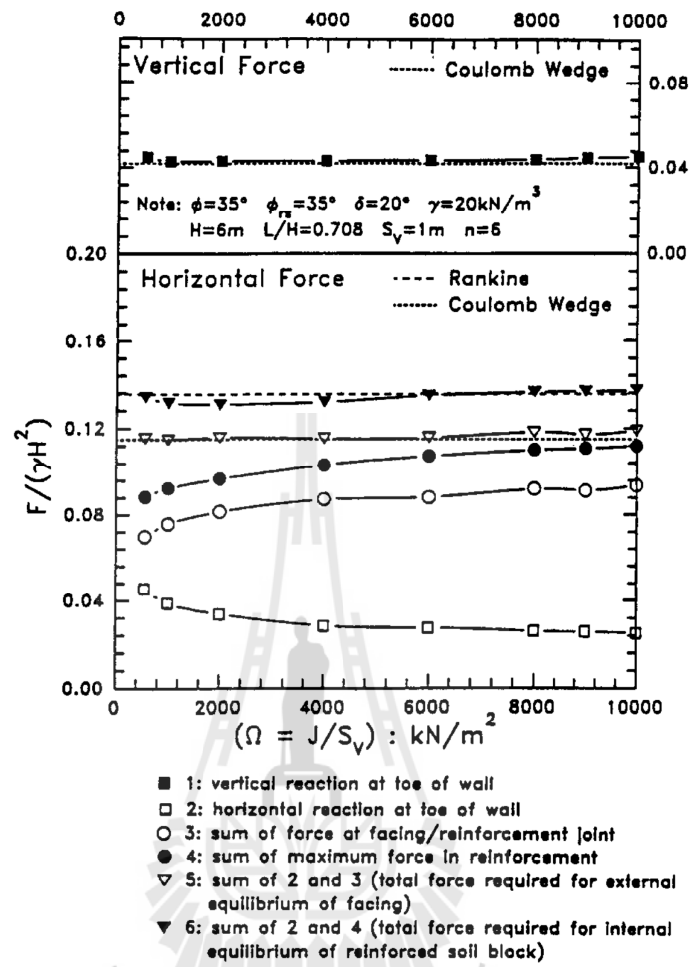
### 2.9.3 The influential parameters

There are many parameters that affect the behavior of reinforced wall such as interaction between reinforcement and soil, angular friction of backfill soil and stiffness of the reinforcement, etc. Alfaro (1996) has studied the effect of the stiffness of the reinforcement to the behavior of reinforced soil wall using FEM. Two embankments were constructed in the campus of the Asian Institute of Technology. The reinforcement were steel grid (Bergado et al., 1991) and Tenax geogrid (Bergado et al., 1994). Back analysis and parametric study were done. The conclusion was that the increase in stiffness or rigidity of reinforced soil system leads to smaller lateral movements of soil foundation and provides higher settlement at or the near the toe. On the other hand, lower reinforced soil system stiffness results in lower settlement at the toe with its maximum value located away from the toe to the interior portion. The role of reinforcement extensibility to tensions in the reinforcement is that the stiff reinforcements exhibit high tensions under working conditions.

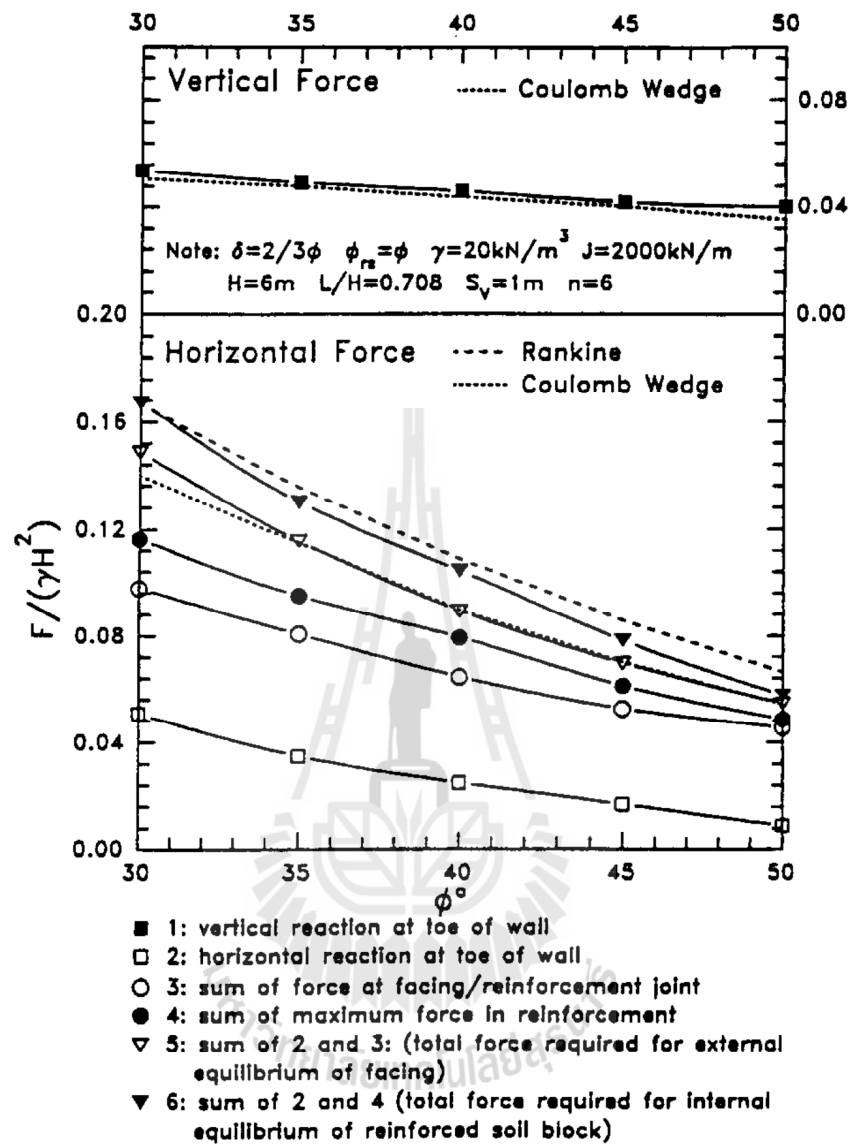
Rowe and Ho (1997) have studied the influential parameters based on finite element analysis of the continuous wall on rigid foundation with full facing panel and hinge toe. Granular backfill was used in the analysis. The effect of the influential parameters on the horizontal and the vertical forces developed within the reinforced soil system are shown in Figure 2.23, 2.24 and 2.25. The influential parameters consist of reinforcement stiffness, backfill friction angle and facing/soil interface friction. It is concluded that the absolute maximum reinforcement force increases with: (a) increasing reinforcement stiffness density; (b) decreasing facing/soil friction angle; (c) decreasing backfill friction angle; and (d) decreasing facing rigidity. Furthermore, some slip reinforcement-soil interface occurred for interface friction angles less than  $\frac{2}{3} \phi$ .



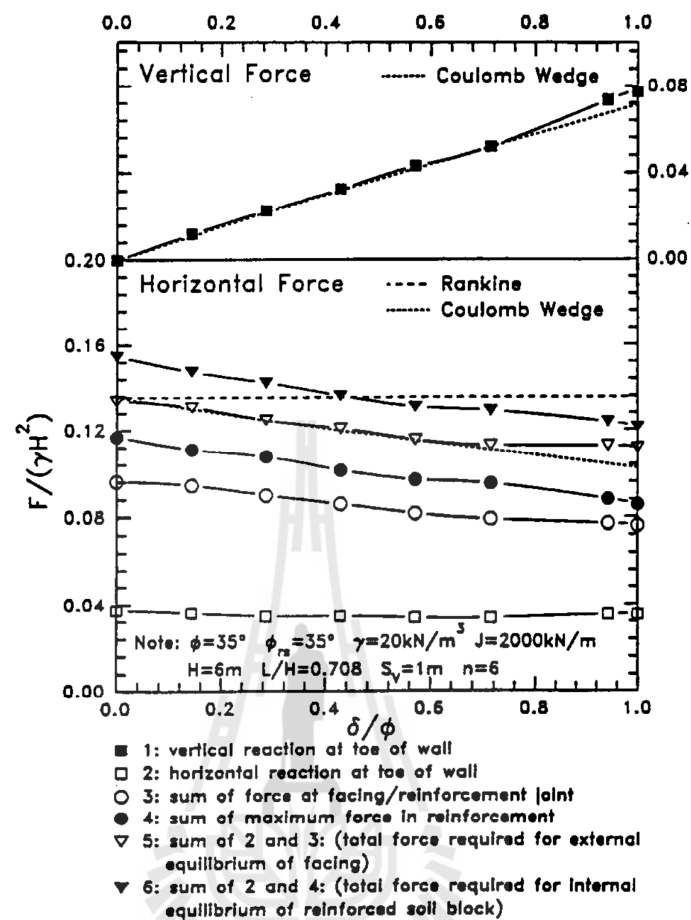




**Figure 2.23** Interaction diagram for effect of reinforcement stiffness density.  
 (Rowe and Ho, 1997).



**Figure 2.24** Interaction diagram for effect of backfill soil friction angle  
 (Rowe and Ho, 1997).



**Figure 2.25** Interaction diagram for effect of facing/soil interface friction angle (Rowe and Ho, 1997).

## 2.10 References

AASHTO, 1996. **Standard Specifications for Highway and Bridge, 1th edition.**

**Washington D.C.** American Association of State Highway and Transportation Officials.

Abiera, H.O., 1991. **Mechanically stabilized earth using TENSAR, bamboo and steel grid reinforcements with lateritic soil as backfill.** M. Eng Thesis GT-90-21, Asian Institute of Technology, Bangkok, Thailand. .

- Alagiyawanna, A.M.N., Sugimoto, M., Toyota, H., 2001. **Influence of longitudinal and transverse member on geogrid pullout behavior during deformation.** Geotextiles and Geomembranes 19, 483-507.
- Alfaro, M.C., 1996. **Reinforced soil wall-embankment system on soft foundation using inextensible and extensible grid reinforcements.** Ph.D Dissertation, Saga University, Japan.
- Alfaro, M.C., Miura, N., Bergado, D., 1995. **Soil-geogrid reinforcement interaction by pullout and direc shear tests.** Geotech. Test. J 18, 157-167.
- ASTM D5321, 2009. **The Shear Strength of Soil-Geosynthetic and Geosynthetic-Geosynthetic interfaces by Direct Shear.** ASTM International, W. Conshohocken. PA, USA 04.13.
- ASTM D6706, 2013. **Standard Test Method for Measuring Geosynthetic Pullout Resistance in Soil.** Annual book of ASTM standards 04.13.
- Bartos, M.J., 1979. **101 uses for earth reinforcement.** Civli Engineering, ASCE, January, 51-57.
- Bergado, D., Lo, K., Chai, J., Shivashankar, R., Alfaro, M., Anderson, L., 1992. **Pullout Tests Using Steel Grid Reinforcements with Low-Quality Backfill.** Journal of Geotechnical Engineering 118, 1047-1062.
- Bergado, D.T., Chai, J.C., Marui, H., 1996. **Prediction of pullout resistance and pullout force displacement relationship for inectensible grid reinforcements.** Soils and Founddations 36, 11-22.
- Bergado, D.T., Long, P.V., Loke, K.H., Werner, G., 1994. **Performance of reinforced embankment on soft Bangkok clay with high-strength geotextile reinforcement.** Geotextiles and Geomembranes 13, 403-420.

- Bergado, D.T., Macatol, K.C., Amin, N.U., Alraro, M.C., 1993. **Interaction of lateritic soil and steel grid reinforcement.** Can. Geotech. J 30, 376-384.
- Bergado, D.T., Sampaco, C.L., Shivashankar, R., Alfaro, M.C., Anderson, L.R., Balasubramaniam, A.S., 1991. **Performance of welded wire wall with poor quality backfills on soft clay.** ASCE Geotechnical Engineering Congress, Boulder, Colorado, U.S.A. , 909-922.
- Chai, J.C., 1992. **Interaction between grid reinforcement and cohesive-frictional soil and performance of reinforced wall/embankment on soft ground.** D.Eng. dissertation, Asian Institute of Technology, Bangkok, Thailand.
- Elias, V., Christopher, B.R., Berg, R.R., 2001. **Mechanically Stabilized Earth Walls and Reinforced Soil Slopes-design and Construction Guidelines.** FHWA-NHI-00-043, Federal Highway Administration, Washington, DC, USA.
- FHWA-RD-89-043, 1990. **Reinforced Soil Structures Volume I. Design and Construction Guidelines.** U.S. Department of Transportation Federal Highway Administration, 20.
- Frost, J.D., Han, J., 1999. **Behavior of interfaces between fiber-reinforcement polymers and sands.** ASCE Journal of Geotechnical and Geoenvironment Engineering 125, 633-640.
- Goodhue, M.J., Edil, T.B., Benson, C.H., 2001. **Interaction of foundry sands with geosynthetics.** ASCE Journal of Geotechnical and Geoenvironment Engineering 127, 353-362.
- Hamid, T.B., Miller, G.A., 2009. **Shear strength of unsaturated soil interface.** Can. Geotech. J. 46, 595-606.

- Hird, C.D., Kwok, C., M., 1989. **FE studies of interface behavior in reinforced embankments on soft ground.** Computers and Geotechnics 8, 111-131.
- Holtz, R.D., 1977. **Laboratory Studies of Reinforced Earth Using a Woven Polyester Fabric.** C.R. Coll. Int. Sols Textiles. Paris, 149-154.
- Horpibulsuk, S., Niramitkronburee, A., 2010. **Pullout resistance of bearing reinforcement embedded in sand.** Soils and Foundations 50.
- Horpibulsuk, S., Suksiripattanapong, C., Niramitkronburee, A., Chinkulkijniwat, A., Tangsutthinon, T., 2011. **Performance of earth wall stabilized with bearing reinforcements.** Geotextiles and Geomembranes 29, 514-524.
- Ingold, T.S., 1982. **Reinforced Earth.** Thomas Telford.
- Ingold, T.S., 1983. **Laboratory Pull-out Testing of Grid Reinforcements in Sand.** Geotechnical Testing Journal, GTJODJ 6, 101-111.
- Jewell, R.A., Milligan, G.W.E., Sarsby, R.W., Dubois, D., 1984. **Interaction between soil and geogrids.** Proceedings of the symposium on Polymer Grid Reinforcement in Civil Engineering, Thomas Telford Limited, London, UK, 11-17.
- Juran, I., Farrag, K.H., L., R., 1991. **Short and Long Term Performance of Polymeric Geogrids.** Geosynthetics International 91.
- Keller, G.R., 1995. **Experiences with mechanically stabilized structures and native soil backfill.** Transportation Research Record 1474, 30-38.
- Koerner, R.M., 2005. **Designing with Geosynthetics.** fifth ed., Pearson Prentice Hall, Upper Saddle River, NJ, USA.
- Koutsourais, M., Sandri, D., Swan, R., 1998. **Soil Interaction Characteristics of Geotextiles and Geogrids.** Geosynthetics 98, 739-744.

- Liu, C.N., Ho, Y.H., Huang, J.W., 2009. **Large scale direct shear tests of soil/PET-yarn geogrid interfaces.** *Geotextiles and Geomembranes* 27, 19-30.
- Liu, S.S., Liu, C.L., Liu, J.C., Kuo, S.H., 1996. **Short Term Pull-out Tests of Geogrid in a Compacted Lateritic Soil.** *Journal of Geotechnical Engineering, ASCE Journal of Geotechnical and Geoenvironment Engineering* 543-559.
- Long, P.V., 1996. **Behavior of geotextile-reinforced embankment on soft ground.** Doctoral Dissertation No. GT 96-1, Asian Institute of Technology, Bangkok, Thailand.
- Mitchell, J.K., Seed, R.B., Seed, H.B., 1990. **Kettleman Hills waste landfill slope failure. I: Liner-system properties.** *J. Geotech. Engrg.* 116, 647-668.
- Ochiai, H., Otani, J., Hayashic, S., T., H., 1996. **The Pull-out Resistance of Geogrids in Reinforced Soil.** *Geotextiles and Geomembranes* 14, 19-42.
- Palmeira, E.M., 1987. **The Study of Soil-Reinforcement Interaction by Mean of Large Scale Laboratory Tests.** A Thesis Submitted for the Degree of Doctor of Philosophy at the University of Oxford.
- Palmeira, E.M., Milligan, G.W.E., 1990. **Scale and other factors affecting the results of pull-out tests of grids buried in sand.** *Geotechnique* V39, N3, Sept 1989, P511–524. *International Journal of Rock Mechanics and Mining Sciences & Geomechanics Abstracts* 27, A103.
- Perterson, E.M., Anderson, L.R., 1980. **Pullout resistance of welded wire mats embedded in soil.** Research Report Submitted to Hilfiker Co, from the Civil and Environmental Engineering Department, Utah State University, USA.

- Raymond, G.P., Giroud, J.P., 1993. **Geosynthetics Case Histories**. Richmond: ISS MFE Tech. Com. & Bitech Publ.
- Rowe, R.K., Ho, S.K., 1997. **Continuous panel reinforced soil walls on rigid foundation**. Journal of Geotechnical and Geoenvironmental Engineering, ASCE 35.
- Rowe, R.K., Ho, S.K., Fisher, D.G., 1985. **Determination of Soil-Geotextile Interface Strength Properties**. Canadian Symposium on Geotextiles and Geomembranes 2, 25-34.
- Smith, I.M., Griffith, D.V., 1988. **Programming the Finite Element Method**. Second Edition, John Will and Sons, Chichester, U. K. .
- Suksiripattanapong, C., Chinkulkijniwat, A., Horpibulsuk, S., Rujikiatkamjorn, C., Tangsutthinon, T., 2012. **Numerical analysis of bearing reinforcement earth (BRE) wall**. Geotextiles and Geomembranes 32, 28-37.
- Suksiripattanapong, C., Horpibulsuk, S., Chinkulkijniwat, A., Chai, J.C., 2013. **Pullout resistance of bearing reinforcement embedded in coarse-grained soils**. Geotextiles and Geomembranes 36, 44-54.
- Tatlisoz, N., Edil, T.B., Benson, C.H., 1998. **Interaction between reinforcing geosynthetics and soil-tire chip mixtures**. Journal of Geotechnical and Geoenvironmental Engineering 124.
- Vermeer, P.A., Brinkgreve, R.B.J., 1995. **Finite Element Code for Soil and Rock Analysis**. A. A. Balkema, Rotterdam, Netherland.



# **CHAPTER III**

## **EFFECT OF FINE CONTENT**

### **ON THE PULLOUT RESISTANCE MECHANISM**

### **OF BEARING REINFORCEMENT EMBEDDED IN**

### **COHESIVE-FRICTIONAL SOILS**

#### **3.1 Statement of problem**

The maximum bearing stress,  $\sigma_{b\max}$ , of a single transverse member for the bearing reinforcement embedded in a cohesionless soils can be predicted satisfactorily based on the modified punching shear mechanism (Horpibulsuk and Niramitkronburee, 2010; Suksiripattanapong et al., 2013). The proposed equation was applicable to a particular compacted coarse-grained soil. However, in some areas, high-quality coarse-grained soil is not available, leading to subsequently high haulage cost for imported materials. It would thus be cost-effective if marginal soils available locally or on-site can be used as a backfill material for MSE walls with an appropriate drainage system. To apply these marginal soils in practice, the effect of fine content on pullout resistance mechanism is an important aspect that needs to be addressed.

This paper aims to investigate the pullout resistance mechanism of bearing reinforcement embedded in cohesive-frictional soils at various fine contents. The laboratory pullout tests on the bearing reinforcement embedded in various cohesive-frictional soils were performed by using a large-scale pullout apparatus

(Horpibulsuk and Niramitkronburee, 2010; Suksiripattanapong et al., 2013) under undrained condition to simulate the short-term situation (Chai, 1992; Bergado et al., 1993 and 1996). The pullout resistance equation for the bearing reinforcement in term of normal stress, dimension and spacing of transverse members, and fine content is also proposed. The outcome of this study is fundamental and useful for the internal stability analysis of the BRE wall using marginal soils as a backfill.

## 3.2 Laboratory investigation

### 3.2.1 Soil samples

The tested soils used in this study were a mixture of silty clay and sand at various ratios, which have different fine contents. The silty clay was collected from the Suranaree University of Technology campus, Nakhon Ratchasima, Thailand, at a depth of 3 m. Its specific gravity is 2.70. The liquid and plastic limits are approximately 54% and 28%, respectively. The silty clay consists of 45% silt, 53% clay, and 2% sand and is classified as a high plasticity clay (CH) according to the Unified Soil Classification System (USCS). The sand is classified as poorly graded sand (SP) with 2% fine content. The average grain size,  $D_{50}$  of sand is 0.30 mm and the specific gravity is 2.78. The compaction characteristics under the standard Proctor energy (ASTM D698-91, 1995) are optimum water content,  $OWC = 23\%$  and maximum dry unit weight,  $\gamma_{d,max} = 14.7 \text{ kN/m}^3$  for silty clay and  $OWC = 6.5\%$  and  $\gamma_{d,max} = 17.0 \text{ kN/m}^3$  for sand. This sand with a small  $D_{50}$  was used in this study to avoid the interlocking effect between transverse members and soil particles (Suksiripattanapong et al., 2013).

The silty clay and sand were mixed to attain the tested soils with fine content greater than 20%. The fine: sand ratios (F:S) were 20:80, 40:60, 80:20, and 98:2 by dry weight. Fine is defined as the particles passing No. 200 US sieve size. The grain size distribution curves of the samples are shown in Figure 3.1. The compaction characteristics and the gradation of the silty clay (F:S = 98:2), sand (F:S = 2:98) and mixed soils (F:S = 20:80, 40:60, 80:20) are summarized in Table 3.1. The  $\gamma_{d,max}$  and OWC values vary from 14.7 to 23.0 kN / m<sup>3</sup> and 12.2 to 23.0%, respectively.  $\gamma_{d,max}$  increased and OWC decreased as the fine content decreased due to the reduction in water holding capacity (Horpibulsuk et al., 2008 and 2009).

Total strength parameters of the tested soils were obtained from a large direct shear device with a dimension of 305 mm x 305 mm x 240 mm depth. In the direct shear tests, the upper half was fixed to the frame of the apparatus while the bottom half could move relative to the top half with the assistance of an actuator controlled by an electric motor. The shearing of the soil specimen occurred along the horizontal failure plane. The test soil thickness in the upper half was 100 mm, which was more than the minimum soil thickness of 50 mm recommended by ASTM D5321 (2008) to ensure the transfer of the normal stress onto the shearing plane. The vertical loading was applied on the rigid plate by a hydraulic jack supported by the rigid reaction frame. The vertical loading and its vertical displacement were measured during the test. The horizontal movement of the bottom half and the shear force exerted during shearing were also recorded. The vertical and horizontal displacements were recorded by two Linear Variable Displacement Transducers (LVDT).

The soil samples were prepared at the optimum water content (obtained from laboratory compaction tests) and transferred to the large direct shear

box. Before the compaction of the samples in the shear box, the shear box was assembled by keeping the two alignment pins in place to ensure that the upper and lower halves were aligned properly. The soil compaction was undertaken in three layers by a vibratory compactor until the maximum dry unit weight was attained. The applied normal stresses were 30, 50 and 90 kPa, respectively. The test commenced with no time allowed for the sample to consolidate during the applied normal stress and shearing. Before shearing, the vertical alignment pins were removed and a shear gap was allowed by opening the gap between the two halves to 0.64 mm using the four gap screws. The shear force was then applied at a constant shearing rate of 1 mm/min till the sample was sheared to 40 mm. The cohesive-frictional soils were compacted at the optimum water content, at which the degree of saturation was between 78 and 87%. Therefore, consolidation and drainage are not an issue for this kind of soil. For an unsaturated soil, total strength parameters are more appropriate to describe the soil behavior than undrained or drained parameters.

The direct shear test was conducted in this study to simulate the shear condition of the soil in short-term condition (during construction and at the end of construction of BRE wall) and to obtain the total strength parameters. The two main parameters: cohesion and internal friction angle for each soil were determined to illustrate the effect of fine content. Figure 3.2 shows the relationship between shear strength and fine content for the tested soils. The shear strength decreased with an increase in fine content. For F:S of 98:2, the shear strength values ranged from 48-52 kPa for all the applied normal stresses. In other words, the effect of normal stress on the shear strength was insignificant as the fine content increased. Shear strength parameters for each tested soil are also summarized in Table 1. The cohesion

increased and the internal friction angle decreased as the fine content increased. The highest cohesion and the lowest friction angle were found at F:S of 98:2 and equal to 43 kPa and 5.5 degrees, respectively. As additional fine particles are introduced into the coarse-grained soils, fine particles fill the void spaces between the coarse particles and dominate the coarse-grained behavior (Arulrajah et al., 2014 and (Wang et al., 2009). The decrease in the friction angles of tested soils with increasing fine content has also been reported by Al-Shayea (2001), Tiwari and Marui (2005), and Wang et al. (2009). Al-Shayea (2001) explained that this reduction in the friction angle is due to the increased lubrication of the clay paste, which causes the slippage and sliding of coarse grains.

### **3.2.2 Bearing Reinforcement**

The longitudinal member is a deformed steel bar (DSB) and the transverse members are a set of steel equal angles. Pullout tests on the bearing reinforcement with different dimensions, spacing and numbers of transverse members embedded in the tested soils were conducted under different applied normal stresses of 30, 50 and 90 kPa. The diameter of the longitudinal member was 16 mm and the leg lengths,  $B$  of the tested transverse members (steel equal angles) were 28, 30 and 50 mm, which are generally used for BRE walls. The lengths of the tested transverse members,  $L$  were 100 and 150 mm. The spacing between the transverse members,  $S$ , varied from 100 to 1200 mm, depending upon the number of transverse members. In this study, the number of transverse members,  $n$ , was 1 to 4.

### **3.2.3 Methodology**

Pullout tests were conducted in the laboratory using a rigid pullout box as shown in Figure 3.3. It was fabricated with rolled steel plates, angles, channels, and

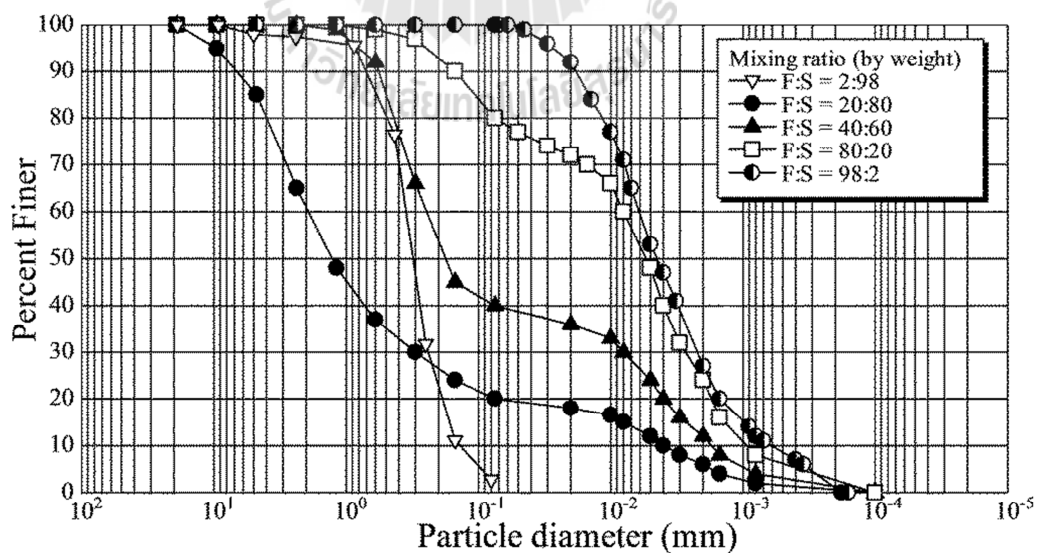
H-sections welded or bolted together to give inside dimensions of 2.60 m in length, 0.60 m in width and 0.8 m in height. The details and sketch of the pullout apparatus can be found in Horpibulsuk and Niramitkornburee (2010). The front wall contains the upper and lower parts with a slot in between for the reinforcement specimen. Friction between the tested soils and the side walls of the pullout apparatus was minimized by the use of a lubricated rubber member and smooth plates as recommended by Alforo et al. (1995), ASTM D6706-01 (2013), and Horpibulsuk and Niramitkornburee (2010). The sleeve was installed inside the slot opening of the pullout box to isolate the bearing reinforcement near the front wall. The sleeve reduces the horizontal stresses on the front face near the slot during the pullout and minimizes the arching effect over the bearing reinforcement. The compacted soil thickness above and below the reinforcement was 300 mm. The soil compaction for each portion (above and below the reinforcement) was undertaken in two layers (150 mm thickness) by a vibratory compactor until the maximum dry unit weight was attained.

Normal stress was applied to the upper layer of soil above the bearing reinforcement with a pressurized air bag. Before installation of the air bag, a 30 mm thick layer of fine sand was placed on the top of the compacted soil and covered with a 4 mm thick steel plate. This procedure was adopted to simulate a uniformly distributed normal stress on the top of the backfill. The pullout force was applied by a 200 kN capacity electro-hydraulic controlled jack and the pullout displacement in front of the pullout apparatus was monitored by a linear variable differential transformer (LVDT). The pullout force was applied at a rate of 1 mm/min.

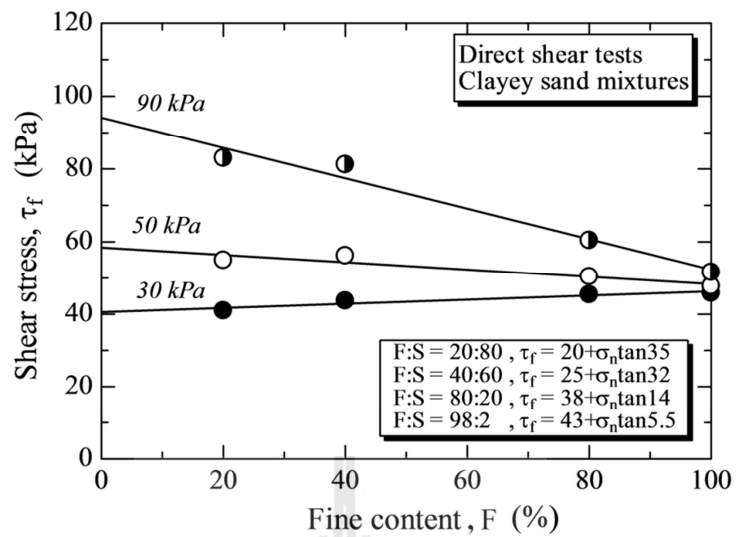
The maximum applied pullout displacement at the end of a test was 40 mm. The applied normal stresses were 30, 50, and 90 kPa, respectively.

**Table 3.1** Index and engineering properties of tested soils.

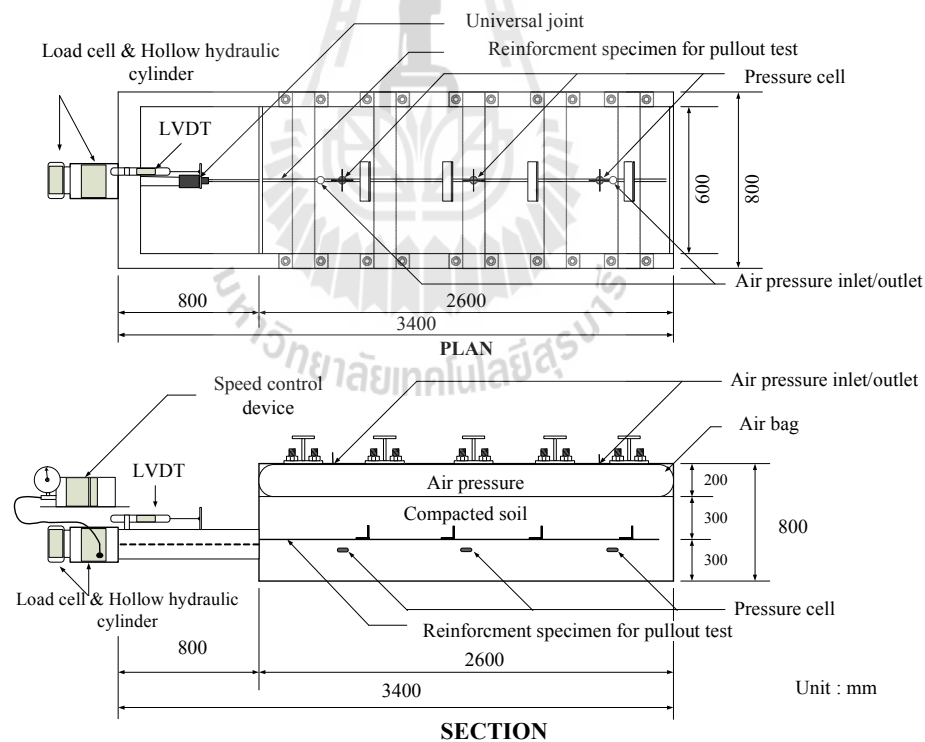
Parameters	Fine: sand ratios				
Mixing ratio (Fines content : Sand )	2:98	20:80	40:60	80:20	98:2
Specific gravity	2.78	2.75	2.72	2.71	2.70
Optimum water content (OWC) (%)	6.5	12.2	14.8	20.2	23.0
Maximum dry unit weight ( $\text{kN/m}^3$ )	23.0	20.1	18.9	16.1	14.70
Percent passing No.200 (%)	2	20	40	80	98
USCS classification	SP	SC	SC	CH	CH
Internal friction angle (degrees)	40	35	32	14	5.5
Cohesion (kPa)	0	20	25	38	43



**Figure 3.1** Grain size distribution curves of the tested soils.



**Figure 3.2** Relationship between shear stress and fine content of all tested soil.



**Figure 3.3** Schematic diagram of pullout test apparatus

(Horpibulsuk and Niramitkornburee, 2010).



### 3.3 TEST RESULTS AND DISCUSSION

#### 3.3.1 Pullout friction resistance

The pullout friction resistance of bearing reinforcement (without any transverse member) is obtained from the skin friction between the tested soils and the longitudinal bar with a diameter of 16 mm and a length of 2.6 m. The maximum and residual pullout friction forces ( $P_{f,max}$  and  $P_{f,residual}$ ) were determined using Eq. (3.1).

The friction pullout resistance,  $P_f$ , is expressed in the form:

$$P_f = A\alpha(c + \sigma_n \tan \phi) \quad (3.1)$$

Where  $A$  is the total surface area of the reinforcement,

$\alpha$  is the interaction factor,

$c$  and  $\phi$  are the soil strength parameters and,

$\sigma_n$  is the applied normal stress.

Figure 3.4 shows the results of the pullout friction tests on a longitudinal member for all tested soils. The friction force increased with the pullout displacement until  $P_{f,max}$  was reached and then leveled off at  $P_{f,residual}$ . The displacements corresponding to  $P_{f,max}$  ranged from 3-5 mm for all the tested soils and applied normal stresses. The values of  $P_{f,max}$  and  $P_{f,residual}$  increased with an increase of the normal stress, depending upon the fine content. The higher the fine content, the lower the values of  $P_{f,max}$  and  $P_{f,residual}$ . The difference between  $P_{f,max}$  and  $P_{f,residual}$  was dependent upon the normal stress and fine content. The larger difference was found at a lower normal stress, especially for a lower fine content due to significant

interlocking between soil and reinforcement. The smallest difference was found for the fine to sand ratio F:S of 98:2 (silty clay) where the punching shear failure governed. Previous research (Horpibulsuk and Niramitkronburee, 2010; Suksiripattanapong et al., 2013) showed that the  $\alpha$  values of various coarse-grained soils were greater than 1.0. Different  $\alpha$  values were found for the tested cohesive-frictional soils; i.e., the  $\alpha$  values were less than unity and decreased with the fine content.

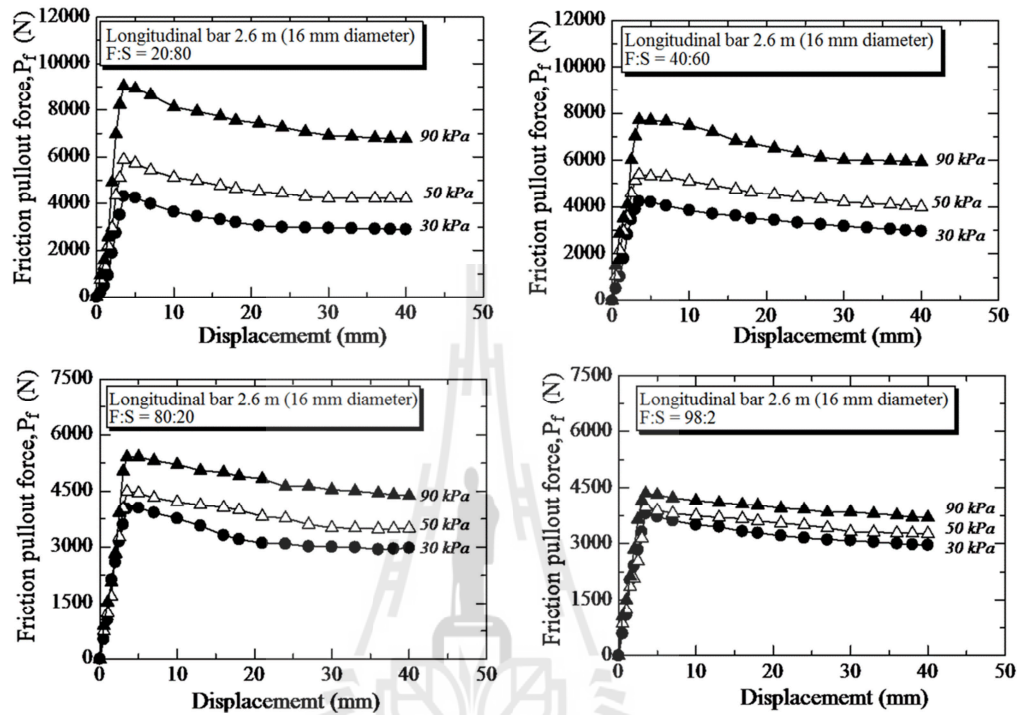
Figure 3.5 shows the relationship of  $\alpha_p$  or  $\alpha_r$  with the fine content at three different applied normal stresses. On this figure,  $\alpha_p$  and  $\alpha_r$  are the interaction factors at peak and residual failure states, respectively. The  $\alpha_p$  and  $\alpha_r$  values are independent of normal stress and tend to decrease with an increase in fine content due to reduction of the interlocking effect. The  $\alpha_p$  and  $\alpha_r$  are expressed in term of  $F$  (percentage of fines) by a linear function as follows:

$$\alpha_p = -0.002F + 0.859 \quad \text{for } 20 < F < 98\% \quad (3.2)$$

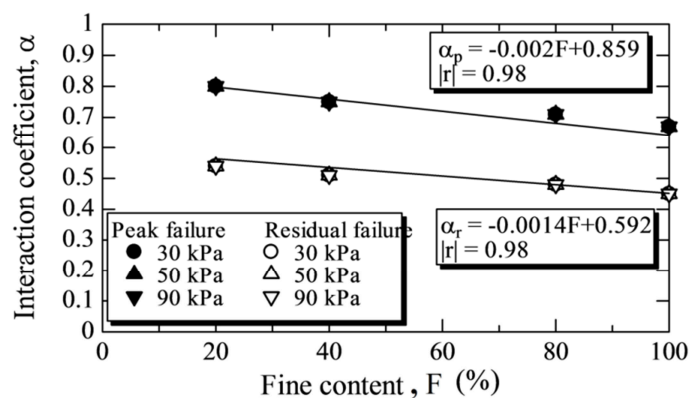
$$\alpha_r = -0.0014F + 0.592 \quad \text{for } 20 < F < 98\% \quad (3.3)$$

The above test results are similar to those found in the previous investigations for different reinforcements (Bakeer et al., 1998; Cazzuffu et al., 1993; Lallejo and Mawby, 2000; Tanchaisawat et al., 2010). The interaction factor between 0.5 and 1.0 indicates a good bond between soil and reinforcement. The poor bonds correspond to  $\alpha < 0.5$  (Tatlisoiz et al., 1998). The  $\alpha_p$  values were greater than 0.65 at

all fine contents. The good bond is due to the higher roughness of the steel bar (Horpibulsuk and Niramitkornburee, 2010).



**Figure 3.4** Pullout test results of a longitudinal member under different normal stresses.



**Figure 3.5** Relationship between  $\alpha$  and fine content for various applied normal stresses at peak and residual failures.

### 3.3.2 Pullout bearing resistance of a single isolated transverse member

( $n = 1$ )

The typical total pullout force and displacement curves for the bearing reinforcements with a 2.6 m longitudinal member and a 40 x 150 ( $B \times L$ ) mm transverse members in all tested soils are shown in Figure 3.6. The total pullout force increased with an increase in the applied normal stress for all tested soils. Initially, the pullout force sharply increased with the displacement and then gradually increased until the failure at a large displacement of approximately 40 mm, which was the end of the test, and the pullout resistance of these tests tends to constant value. The initial sharp increase was attributed to the friction pullout resistance, which fully mobilized at a small displacement (about 3 mm). The pullout bearing resistance of a single isolated transverse member,  $P_{b1}$ , was obtained from the difference between the total pullout resistance and the pullout friction resistance. The development in the bearing pullout resistance was comparatively lower for  $F > 80\%$ .

Figure 3.7 shows the measured maximum bearing resistance of a single isolated transverse member ( $P_{b1}/BL$ ), as compared with the calculated values by the proposed equations from Eqs. (2.8) to (2.13). Using  $k = 1.0$  as suggested by Bergado et al. (1996), the maximum bearing stresses for various dimensions ( $B \times L$ ) and F:S ratios are predicted satisfactorily by the modified punching shear solution where the  $\beta$  value decreased with increasing fine content. In other words, the failure mechanism approached the punching shear failure when the fine content increased. However, even for the cohesive soil (F:S = 98:2), the measured pullout bearing stress was higher than the calculated one by considering the punching shear failure

mechanism. The relationship between  $\beta$  and the fine content is shown in Figure 3.8 and is represented by a polynomial function in the form:

$$\beta_{(rad)} = \left[ -0.00002F^2 + 0.0002F + 0.505 \right] \pi \quad (3.4)$$

The  $\beta$  value ranged between  $\pi/2$  and  $\pi/2.92$  and can be taken as  $\pi/2$  for  $F < 45\%$ . The  $\beta$  value decreased significantly with the fine content when  $F > 45\%$ . It is implied from this study that the modified punching shear solution (Eq. 2.12 to 2.13) is a generalized expression for different failure modes. For example, when the  $\beta$  values are equal to  $\pi/1.65$  and  $\pi/3$ , Eq. (2.12 to 2.13) approaches the general shear (upper boundary) and punching shear (lower boundary), respectively. To extend Eq. (2.12 to 2.13) to other cohesive-frictional soils, the pullout test results on grids embedded in lateritic soil with  $F = 17.9\%$  (Bergado et al., 1993) and weathered clay with  $F = 82.9\%$  (Bergado et al., 1996) were taken and analyzed as shown in Figure 3.8. It is shown that the pullout resistances are predicted satisfactorily with the  $\beta$  values of  $\pi/2$  and  $\pi/2.25$  for lateritic soil and weathered clay, respectively. These  $\beta$  values and their corresponding  $F$  when plotted in Figure 3.9 are in the same trend with the relationship proposed in this study. This shows that Eq. (3.4) may be applicable to other cohesive-frictional soils.

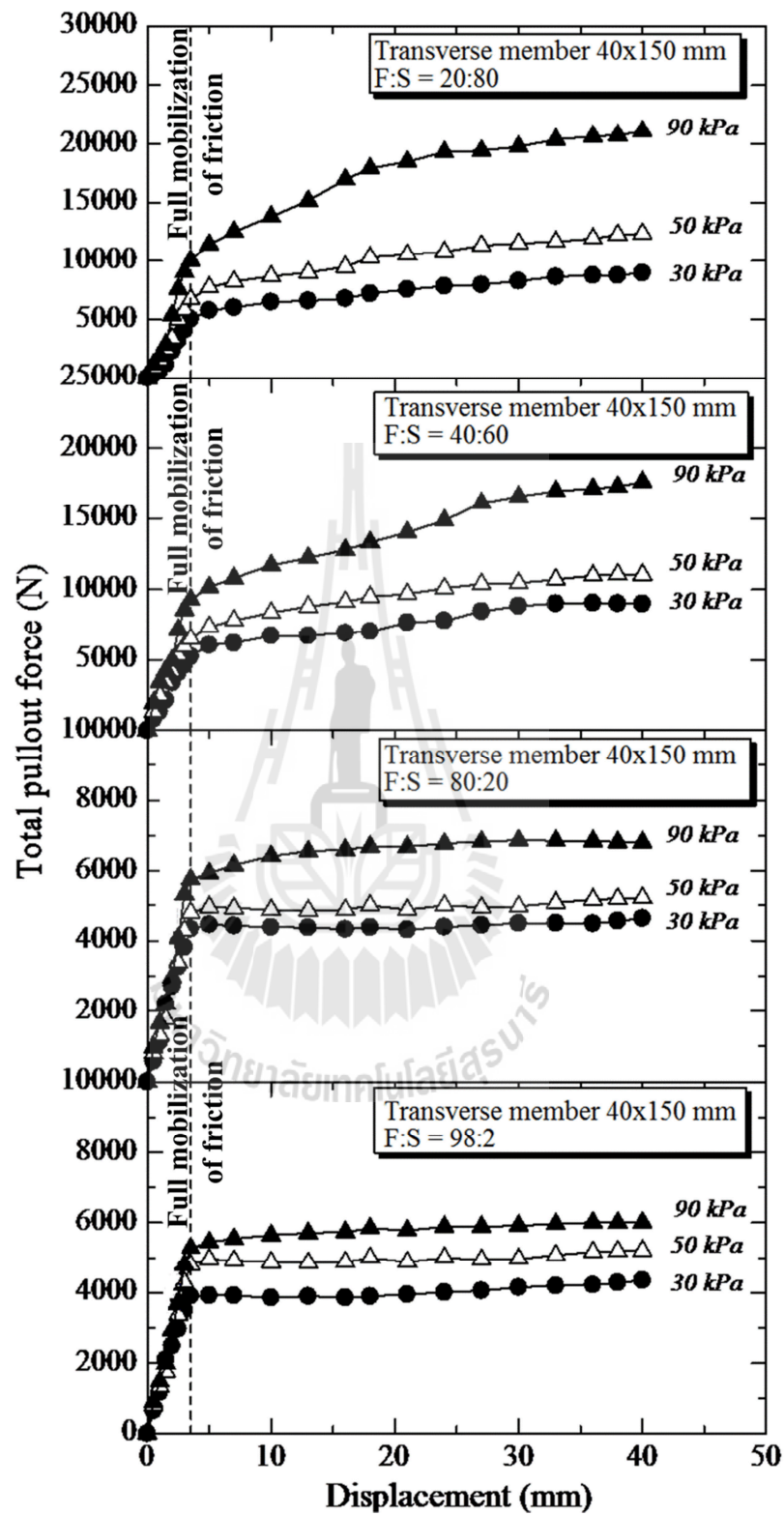


Figure 3.6 Typical pullout test results of the bearing reinforcement in tested soils.

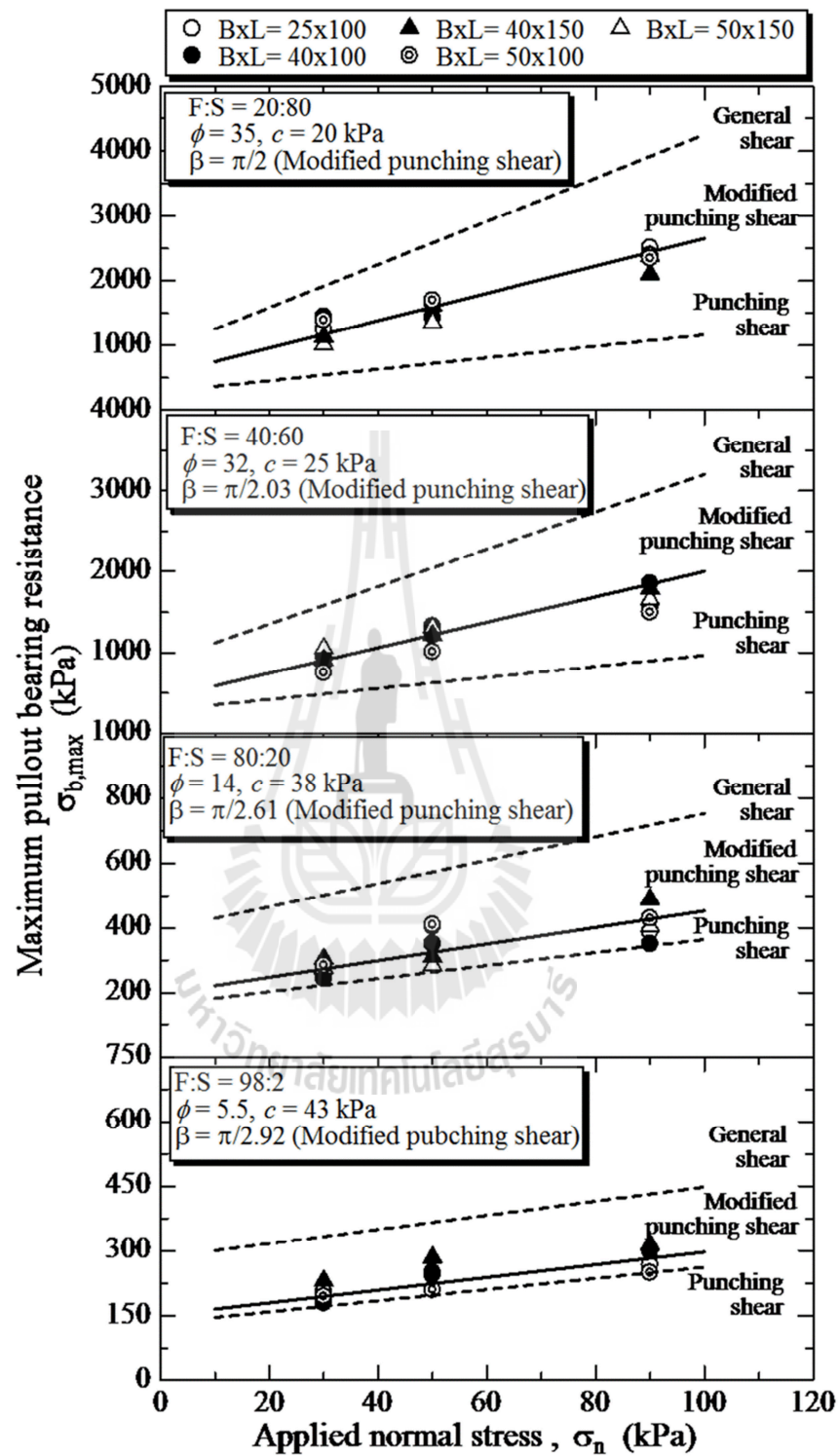


Figure 3.7 Maximum pullout bearing resistance of a single isolated transverse member for all tested soils.

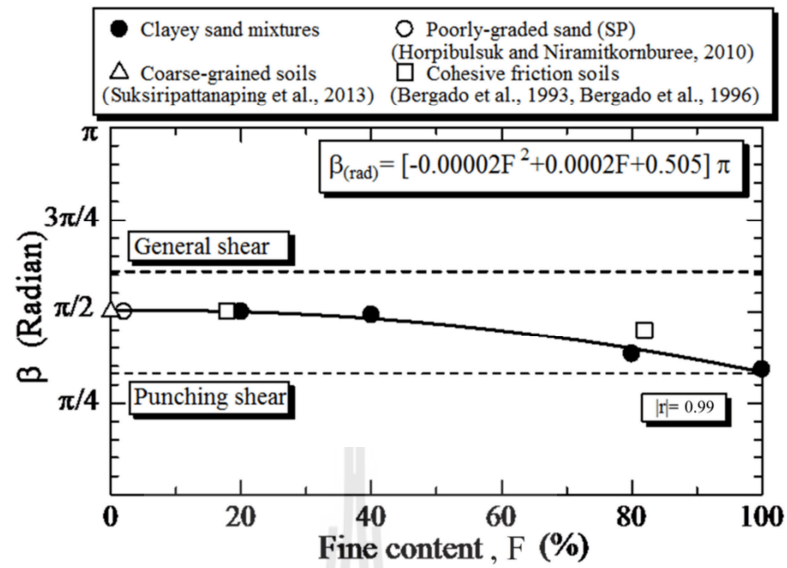


Figure 3.8 Relationship between  $\beta$  and fine content.

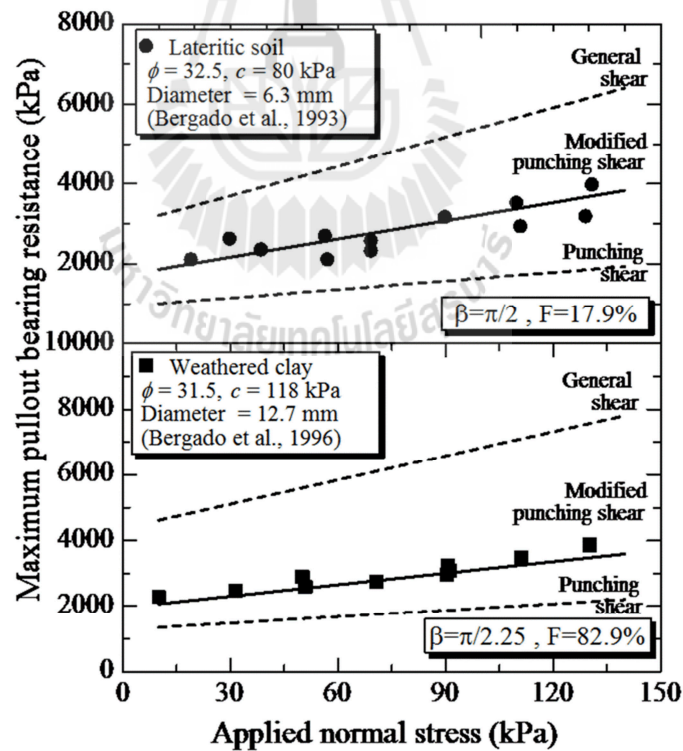


Figure 3.9 Relationship between maximum pullout bearing resistance and applied normal stress.



### 3.3.3 Pullout resistance of the bearing reinforcement ( $n > 1$ )

In practice, the actual bearing reinforcement has several transverse members placed at regular intervals (Figure 2.4). During the pullout of the bearing reinforcement from soil, the transverse members may interfere with each other. A dimensionless parameter, transverse member spacing ratio,  $S/B$ , has been introduced to express the influence of center-to-center spacing,  $S$ , and leg length ( $B$ ) of transverse members on the pullout resistance. This parameter was originally proposed by Bergado et al. (1996) and was subsequently used to investigate the transverse member interference by Horpibulsuk and Niramitkronburee (2010) and Suksiripattanapong et al. (2012).

Figure 3.10 shows a typical relationship between the maximum pullout bearing force ratio and  $S/B$  for 40 x 150 mm transverse members ( $n = 2$  to 4) under different applied normal stresses. The maximum pullout bearing force ratio is defined as a ratio of the maximum pullout bearing force of  $n$  transverse members,  $P_{bn}$ , to the maximum pullout bearing force of a individual transverse member,  $P_{b1}$ . It is found that the  $P_{bn}/P_{b1}$  ratio is controlled by the  $S/B$  value, which is in agreement with that reported by Horpibulsuk and Niramitkronburee (2010) and Suksiripattanapong et al. (2012).

Palmeira (2004) suggested two mechanisms for the transverse member interference during pullout. One is the increase in the magnitude of stresses and the rotation of principal stresses ahead of the members due to the mobilization of soil passive resistance. The other mechanism takes place behind each transverse member where a low stress region is formed and results in the softened region. The possible pullout mechanism for the bearing reinforcement is proposed and shown in Figure

3.11. The possible failure mechanism for a transverse member is based on the modified punching shear failure mechanism. The failure mechanism of the bearing reinforcement is classified into three zones, depending upon the  $S/B$  value. Zone 3 (Figure 3.10 and Figure 3.11a) is individual failure ( $S/B > S_2/B$ ) where the soil in front of each transverse member fails individually. The soil strength near the transverse member approaches a peak state during pullout and finally the soil fails individually. Zone 1 (Figure 3.11b) is referred to as block failure ( $S/B < S_1/B$ ), in which the shear surface caused by each transverse member joins together and forms a rough shear surface. Only the first transverse member provides bearing resistance. Zone 2 (Figure 3.11c) is regarded as the member interference failure ( $S_1/B < S/B < S_2/B$ ), where the soil failure occurs in the softened region.

It was reported that the  $S_1/B$  and  $S_2/B$  values for bearing reinforcement embedded in coarse-grained soils are independent of soil characteristics (well-graded or poorly graded) and friction angle (Suksiripattanaong et al., 2012). However, a different result was obtained for the tested cohesive-frictional soils, i.e., the  $S_2/B$  value was controlled by the fine content, which is similar to that in the previous study on grid reinforcements (Bergado et al., 1996; Palmeira and Milligan, 1990).

Figure 3.10 shows that the  $S_1/B$  value is essentially the same (i.e., 3.75) for different fine contents. This value is the same as that reported by Horpibulsuk and Niramitkornburee (2010) and Suksiripattanaong et al., (2013) for coarse-grained soils. However, the  $S_2/B$  value decreased with increasing fine content (decreasing shear strength). In other words, the fine content affected the softened region and the failure plane,  $\beta$ , of the ahead transverse members.

The ratio between  $P_{bn}$  to  $nP_{b1}$  is defined as the interference factor,  $IF$ . Based on the analysis of the present test data and previous works (Suksiripattanapong et al., 2013), the interference factor is mainly dependent upon  $S/B$  and  $n$  for a particular soil, but irrespective of applied normal stress:

$$IF = \frac{P_{bn}}{nP_{b1}} = a + b \ln\left(\frac{S}{B}\right) \quad (3.4)$$

Where  $a$  and  $b$  are constants, depending upon  $n$  and fine content.

These two constants can be obtained under two physical conditions: (1) when  $S/B$  equals 3.75,  $IF$  equals  $1/n$  because  $P_{bn}$  and  $P_{b1}$  are essentially the same, and (2) when  $S/B$  equals  $S_2/B$ ,  $IF$  equals unity. These two conditions define the lower and upper values of  $IF$  at the corresponding values of  $S/B = S_1/B$  and  $S_2/B$ , respectively. From these two conditions, the constants  $a$  and  $b$  can be determined by the following equations:

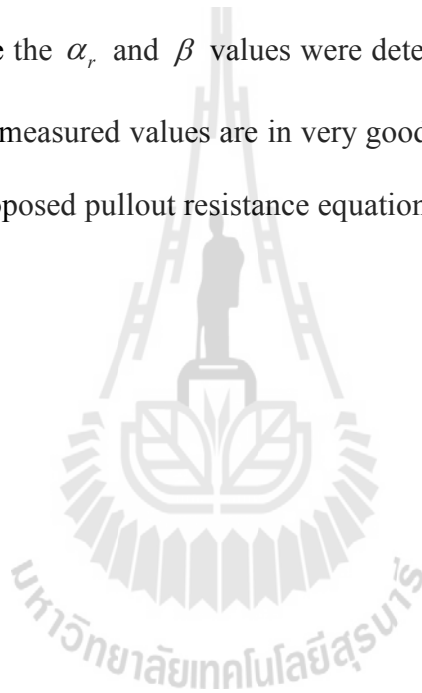
$$b = \frac{\left[1 - \frac{1}{n}\right]}{\left[\ln\left(\frac{S_2}{B}\right) - \ln\left(\frac{S_1}{B}\right)\right]} = \frac{\left[1 - \frac{1}{n}\right]}{\left[\ln\left(\frac{S_2}{B}\right) - 1.322\right]} \quad (3.5)$$

$$a = 1 - b \ln\left(\frac{S_2}{B}\right) \quad (3.6)$$

Based on the analysis of this study and other recent works (Horpibulsuk and Niramitkornburee, 2010; and Suksiripattanapong et al. (2012), it is found that the  $S_2/B$  value decreases linearly with an increase in fine content as shown in Figure 3.12 and presented in the form:

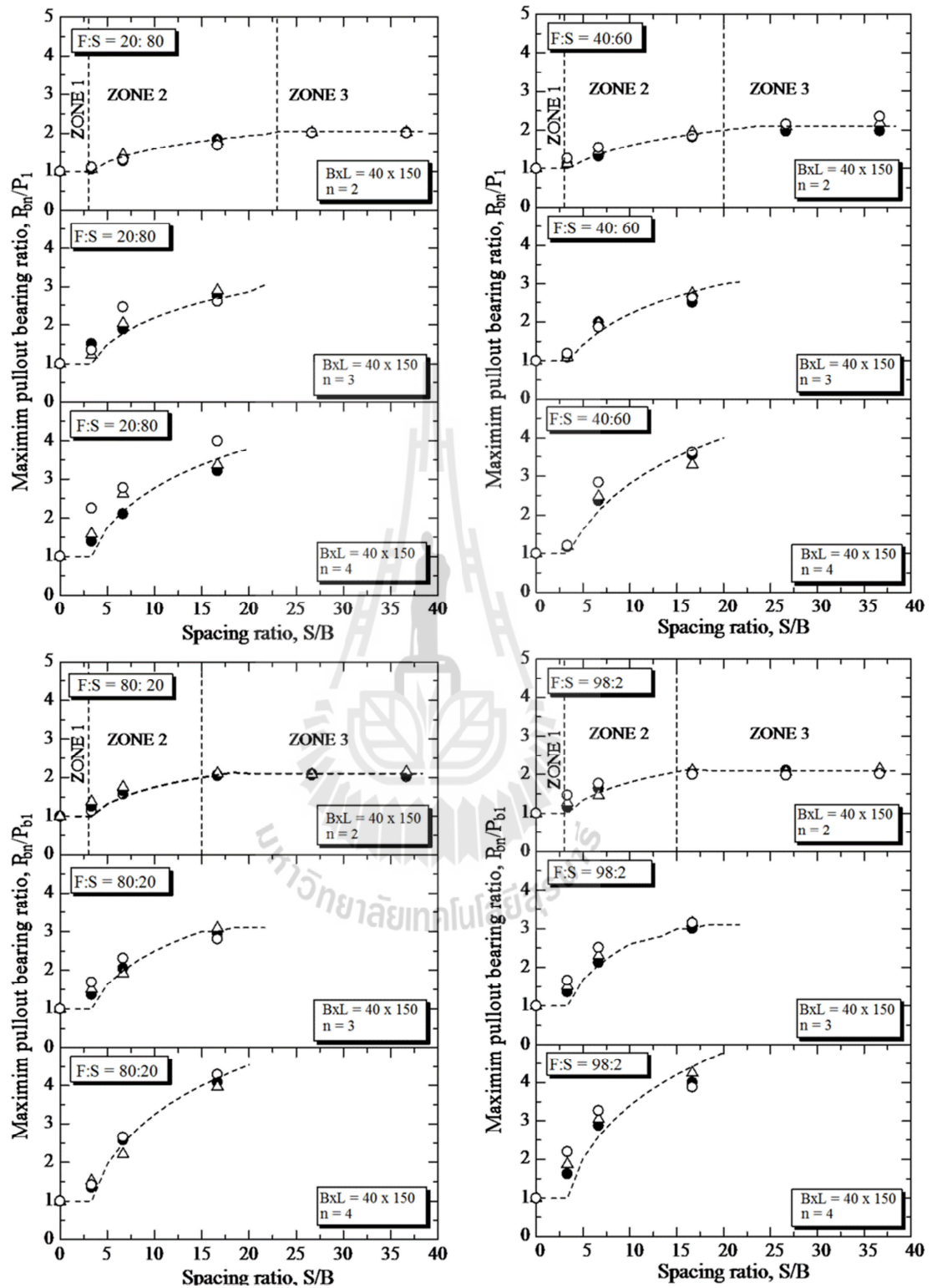
$$S_2 / B = -0.121F + 25.16 \quad (3.8)$$

Table 3.2 presents an example of the predicted maximum pullout force,  $P_t$ , of bearing reinforcement with 40x150 mm transverse member and 2.6 m length of longitudinal member for  $n = 1, 2, 3$  and 4 with different  $S/B$ .  $P_t$  is the sum of  $P_f$ , and  $P_{bn}$ . In this prediction,  $P_f$  was calculated using Eq. (1) and  $P_{bn}$  was calculated using Eqs. (9) to (12), where the  $\alpha_r$  and  $\beta$  values were determined from the fine contents. The predicted and the measured values are in very good agreement, which verifies the applicability of the proposed pullout resistance equations.



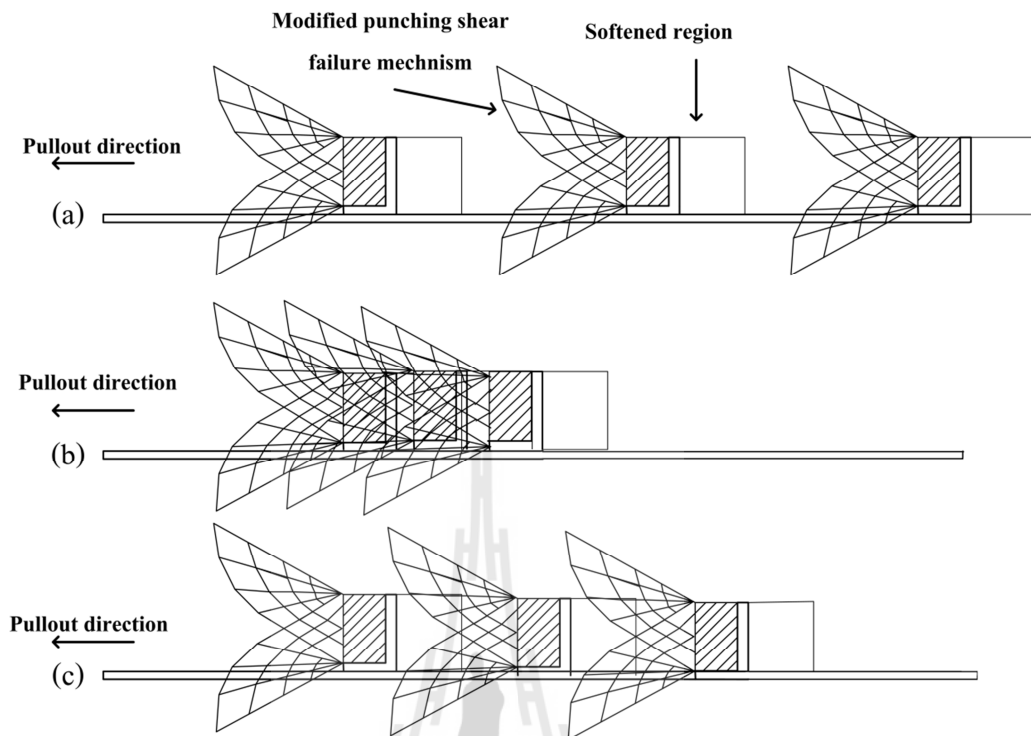
**Table 3.2** Predicted and measured pullout resistance of bearing reinforcement with 40x150 mm transverse member  
for  $n = 1, 2, 3$ , and 4 and F:S = 20:80.

Fine content	$C$ (kPa)	$\phi$ (Deg)	$\sigma_n$ (kPa)	n	S/B	F	Prediction					Measured
							$\alpha$	$P_f$ (kPa)	$\beta$ (Rad.)	$P_b$ (kPa)	$P_t$ (kPa)	$P_t$ (kPa)
20	20	35	30	1	-	1	0.564	3.02	1.574	7.40	10.43	8.98
			50				0.564	4.05	1.574	10.09	14.15	12.35
			90				0.564	6.11	1.574	15.47	21.59	21.08
			30	2	6.25	0.658	0.564	3.02	1.574	9.73	12.76	11.25
			50				0.564	4.05	1.574	13.27	17.33	16.81
			90				0.564	6.11	1.574	20.35	26.48	28.05
			30		16.25	0.910	0.564	3.02	1.574	13.47	16.50	16.85
			50				0.564	4.05	1.574	18.37	22.43	23.45
			90				0.564	6.12	1.574	28.16	34.29	37.51
			30	3	6.25	0.541	0.564	3.02	1.574	12.02	15.04	14.03
			50				0.564	4.05	1.574	16.38	20.44	20.05
			90				0.564	6.12	1.574	25.12	31.25	34.22
			30		16.25	0.877	0.564	3.02	1.574	19.46	22.49	23.62
			50				0.564	4.05	1.574	26.54	30.60	32.41
			90				0.564	6.12	1.574	40.69	46.82	55.21
			30	4	6.25	0.485	0.564	3.02	1.574	14.35	17.38	18.53
			50				0.564	4.05	1.574	19.57	23.63	22.52
			90				0.564	6.12	1.574	30.01	36.13	38.21
			30		16.25	0.862	0.564	3.02	1.574	25.53	28.56	30.71
			50				0.564	4.05	1.574	34.81	38.87	42.10
			90				0.564	6.12	1.574	53.37	59.50	62.52



**Figure 3.10** Measured and predicted and relationships

for 40 x 150 mm transverse members.



**Figure 3.11** Transverse member interference.

### 3.4 Conclusions

This chapter of study presents the effects of fine content on the pullout mechanism of the bearing reinforcement embedded in cohesive-frictional soils with different fine contents of 20, 40, 80, and 98% by weight. The following conclusions can be drawn from this study:

1. The pullout resistance of the bearing reinforcement is the sum of pullout friction and pullout bearing resistances. The pullout friction resistances ( $P_{f,max}$  and  $P_{f,residual}$ ) are dependent upon soil shear strength and soil-reinforcement interaction factor  $\alpha$ . The  $\alpha$  value can be approximated in term of fine content using a proposed linear function.

2. The modified punching shear solution is considered as the generalized expression for different failure mechanisms. The general shear and modified punching shear failure mechanisms are approached when the failure plane  $\beta$  values are  $\pi/1.65$  and  $\pi/3$ , respectively. Using the modified punching shear solution, the maximum pullout bearing stresses for various cohesive-frictional soils are predicted satisfactorily where the  $\beta$  value decreases as the fine content increases. In other words, the failure mechanism approaches punching shear as the fine content increases. The relationship between  $\beta$  and fine content is represented by a polynomial function. The  $\beta$  value of  $\pi/2$  is recommended for  $F < 45\%$ .
3. The transverse member interference is essentially dependent upon  $S/B$ , which is strongly controlled by fine content. The transverse member interference zones are classified into three zones. Zone 1 ( $S/B \leq 3.75$ ) is block failure where all transverse members act like a rough block. Zone 2 ( $3.75 < S/B < S_2/B$ ) is member interference failure. Zone 3 ( $S/B > S_2/B$ ) is individual failure. The  $S_2/B$  value decreases linearly with an increase in fine content, indicating that the larger soft region develops with the smaller fine content.
4. The proposed pullout resistance equations are useful for examination of the internal stability against pullout failure of the BRE wall. The equations required only shear strength parameters, fine content and dimension of bearing reinforcement. The application of the equations are presented and verified in this paper.



### 3.5 References

- Al-Shayea, N.A., 2001. **The combined effect of clay and moisture content on the behavior of remolded unsaturated soils.** Engineering Geology 62, 679-698.
- Alforo, M.C., Hayashi, S., Miura, N., Watanabe, K., 1995. **Pullout interaction mechanism of geogrid strip reinforcement.** Geosynthetics International 2, 679-698.
- ASTM D6706-01, 2013. **Standard Test Method for Measuring Geosynthetic Pullout Resistance in Soil.** Annual book of ASTM standards 04.13.
- Bakeer, R.M., Sayed, S.M., Cates, P., Subramanian, R., 1998. **Pullout and shear tests on geogrid reinforcement.** Geosynthetics International 2, 679-698.
- Bergado, D.T., Chai, J.C., Marui, H., 1996. **Prediction of pullout resistance and pullout force displacement relationship for inextensible grid reinforcements.** Soils and Foundations 36, 11-22.
- Cazzuffu, D., Picarelli, L., Ricciuti, A., Rimold, P., 1993. **Laboratory investigation on the shear strength of geogrid reinforced soils.** ASTM Spec, Tech. Publ 1190.
- Horpibulsuk, S., Niramitkronburee, A., 2010. **Pullout resistance of bearing reinforcement embedded in sand.** Soils and Foundations 50.
- Lallejo, L.E., Mawby, R., 2000. **Porosity influence on the shear strength of granular material clay mixtures.** Engineering Geology 58, 125-136.
- Palmeira, E.M., 2004. **Bearing force mobilisation in pull-out tests in geogrids.** Geosynthetics International 22, 481-509.
- Palmeira, E.M., Milligan, G.W.E., 1990. **Scale and other factors affecting the results of pull-out tests of grids buried in sand.** Geotechnique V39, N3,

- Sept 1989, P511–524. International Journal of Rock Mechanics and Mining Sciences & Geomechanics Abstracts 27, A103.
- Suksiripattanapong, C., Chinkulkijniwat, A., Horpibulsuk, S., Rujikiatkamjorn, C., Tangsutthinon, T., 2012. **Numerical analysis of bearing reinforcement earth (BRE) wall.** Geotextiles and Geomembranes 32, 28-37.
- Suksiripattanapong, C., Horpibulsuk, S., Chinkulkijniwat, A., Chai, J.C., 2013. **Pullout resistance of bearing reinforcement embedded in coarse-grained soils.** Geotextiles and Geomembranes 36, 44-54.
- Tanchaisawat, T., Bergado, D.T., Vootipruex, P., Shehzad, K., 2010. **Interaction between geogrid reinforcement and tire chip-sand lightweight backfill.** Geotextiles and Geomembranes 28.
- Tatliso, N., Edil, T.B., Benson, C.H., 1998. **Interaction between reinforcing geosynthetics and soil-tire chip mixtures.** Journal of Geotechnical and Geoenvironmental Engineering 124.
- Tiwari, B., Marui, H., 2005. **A new method for the correlation of residual shear strength of soil with mineralogical composition.** Journal of Geotechnical and Geoenvironmental Engineering 65.
- Wang, S., Chan, D., Lam, K.C., 2009. **Experimental study of the effect of fines content on dynamic compaction grouting decomposed granite of Hong Kong.** Construction and Building Materials 23, 1249-1264.

# **CHAPTER IV**

## **PULLOUT RESISTANCE OF BEARING**

### **REINFORCEMENT EMBEDDED IN MARGINAL**

### **LATERITIC SOIL AT MOLDING WATER CONTENTS**

#### **4.1 Statement of problem**

When coarse-grained soils are not locally available within the construction site, the construction cost is largely dependent on the haulage cost. The haulage cost between a borrow source and the construction site is often exorbitant. A potential means to reduce the construction cost is to use locally available soils as backfill materials. The use of locally available marginal soils (e.g. low quality soils with more than 15% fine content) as a backfill could reduce the cost of fill material by as much as 60% compared to using high-quality offside soils and reduce the air pollution from the transportation (Esmaili et al., 2014; Keller, 1995). To ensure the usage of fine-grained material as a backfill material, Sukmak et al. (2015) investigated the pullout mechanism of the bearing reinforcements embedded in cohesive-frictional soils at various fine contents. The bearing pullout mechanism was found to be dominant by the fine content and approaches punching shear failure when the fine content increases.

The previous work was however limited to the compacted cohesive-frictional soils at optimum point (optimum water content and maximum dry unit weight) while the field compaction is generally specified at  $w_{owc} \pm 2.5\%$  according the Department

of Highways, Thailand, where  $w_{owc}$  is the optimum water content. The effect of molding water contents (on dry and wet sides of optimum water content) on the pullout resistance mechanism of bearing reinforcement embedded in a marginal lateritic soil has not been previously investigated and is the focus of this paper. Pullout tests were undertaken on marginal lateritic soil at various molding water contents ( $w_{owc} \pm 2.5\%$ ), which are generally specified for the field compaction. This study is based on the total strength parameters, widely accepted in practice for compacted unsaturated soils (Abdi and Arjomand, 2011; Bergado et al., 1996; Bergado et al., 1993; Liu et al., 2009; Sukmak et al., 2015). The pullout resistance equations at various molding water contents are proposed in term of direct shear strength parameters, normal stress, and dimension of bearing reinforcement. The proposed equation is useful for examination of BRE wall in the short-term condition (during construction and at the end of construction).

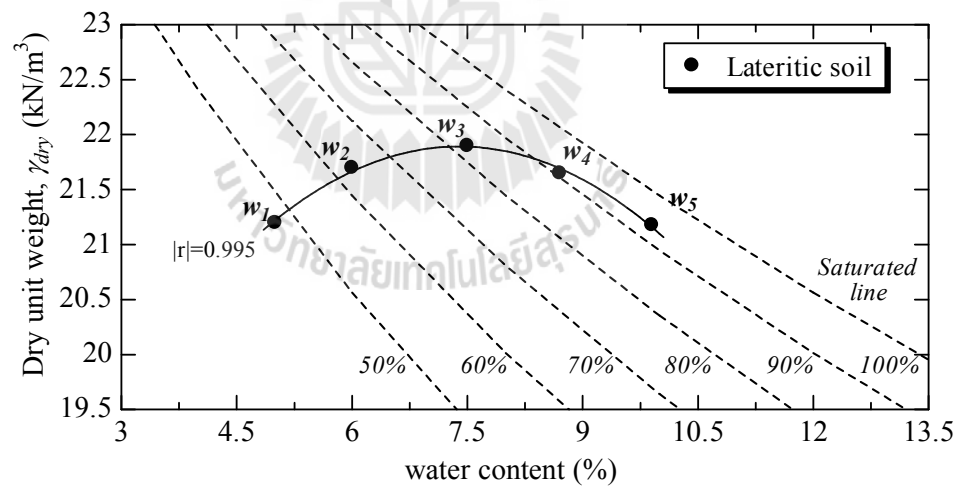
## 4.2 Laboratory investigation

### 4.2.1 Soil samples

The tested soil was collected from Nakhon Ratchasima province, Thailand. The soil was air-dried, pulverized using a rubber mallet, and passed through a 25 mm sieve. The soil has a specific gravity of 2.73 and liquid and plastic limits of approximately 28% and 8%, respectively. The lateritic soil consists of 23% gravel, 56.2% sand, and 20.8% fine particles (silt and clay) and is classified as clayey sand (SC) with gravel according to the Unified Soil Classification System (USCS). The average grain size,  $D_{50}$  of the lateritic soil is 1.07 mm. California Bearing Ratio, CBR of this tested soil at 95% maximum dry unit weight is 14%, which does not meet the

specification for subbase (required CBR > 25%) of Department of Highways, Thailand. It is moreover noted that the fine content of the tested soil is greater than the limitation of 15%, specified by ASSHTO and Department of Highways, Thailand. Consequently, the tested soil is considered as a marginal lateritic soil.

The water contents of the tested soil were adjusted by spraying water droplets into the air-dried soil. The moist soil specimens were then transferred to plastic bags and placed without agitation for about 48 hours to have uniform moisture before compaction testing (i.e. direct and pullout tests). The maximum dry unit weight and  $w_{OWC}$  of the tested soils compacted under the standard Proctor energy (ASTM D698-91, 1995) are 22.0 kN/m<sup>3</sup> and 7.5%, respectively. A relationship between dry unit weight and water content of the tested soil is shown in Figure 4.1.



**Figure 4.1** Compaction curve.

#### 4.2.2 Large scale direct shear tests

Direct shear tests were conducted on the lateritic soil at five different molding water contents. The tested water contents were on the dry side of optimum

( $w_1 = 5.0\%$  and  $w_2 = 6.0\%$ ), at  $w_{OWC}$  ( $w_3 = 7.5\%$ ), and on the wet side of optimum ( $w_4 = 9.0\%$  and  $w_5 = 10.0\%$ ) (*vide* Figure 4.1). The degrees of saturation,  $S_r$ , corresponding to  $w_1$ ,  $w_2$ ,  $w_3$ ,  $w_4$  and  $w_5$  are 48, 63, 85, 92 and 95%, respectively. The water content ratios,  $w/w_{OWC}$  for all the samples are shown in Table 1. The dry unit weight is not sensitive to the water content; i.e., it varies within a small range of 21.2-22.0 kN/m<sup>3</sup>.

Total strength parameters of the tested soils were obtained from a large direct shear device with a dimension of 305 mm x 305 mm x 240 mm depth. The details of the test can be referenced to Sukmak et al. (2015). The soil specimens were prepared at the required molding water contents (obtained from laboratory compaction tests) and transferred to the large direct shear box. The applied normal stresses were 30, 50 and 90 kPa, respectively. The test commenced with no time allowed for the specimen to consolidate during the applied normal stress and shearing. The shear force was applied at a constant shearing rate of 1 mm/min till the specimen was sheared to 40 mm. The soil specimens were sheared at a fast rate to ensure minimal changes in matric suction during the shearing processes (Fleming et al., 2006; Oloo and Fredlund, 1996). After completed shearing test, the soil specimens at failure plane were collected in order to determine final water content. It was found that the difference of initial and final molding water contents of tested soils is very low (= 0.15-0.25%), which confirms the undrained condition.

The two main normal shear strength parameters: apparent cohesion and internal friction angle were determined to illustrate the effect of water content and are summarized in Table 4.1. The internal friction angle decreases rapidly with increasing

water content on the dry side of optimum and then is insensitive to water content being approximately 24 degrees. The maximum cohesion value is obtained at about  $w_{OWC}$  and equals to 52 kPa. The cohesion on the dry and wet sides of optimum decreases as the reduction and increment of molding water content, respectively.

**Table 4.1:** Physical and engineering properties of tested soils.

Properties of tested soils	$w_1$	$w_2$	$w_3$	$w_4$	$w_5$
Dry density, $\gamma_{dry}$ (kN/m <sup>3</sup> )	21.20	21.70	21.90	21.65	21.18
Water content (%)	5.0	6.0	7.5	9.0	10.0
Degree of saturation, $S_r$ (%)	48	63	85	92	95
Relative degree of compaction (%)	96.36	98.63	100	98.63	96.36
Water content ratio	0.67	0.80	1	1.2	1.33
Angle of internal friction, $\phi$	36	33	28	25	24
Cohesion, $c$ (kPa)	42	48	52	41	32

#### 4.2.3 Bearing reinforcement

The pullout tests on the bearing reinforcements with different dimensions, spacing and number of transverse members embedded in the tested lateritic soils were conducted under different applied normal stresses of 30, 50 and 90 kPa. The diameter and length of the longitudinal member were 16 mm and 2600 mm, respectively. The leg lengths,  $B$  of the tested transverse members (steel equal angles) were 25, 40 and 50 mm, which are generally used for BRE walls. The lengths of the tested transverse member,  $L$  were 100, 150 and 200 mm. The spacing between the transverse members,  $S$ , varies from 100 to 1200 mm, depending upon the number of transverses members,  $n$ . In this study,  $n$  was 1 to 4.

#### 4.2.4 Pullout tests

Pullout tests were conducted in the laboratory using a rigid pullout box. It was fabricated with rolled steel plates, angles, channels, and H-sections welded or bolted together to give inside dimensions of 2.60 m in length, 0.60 m in width and 0.8 m in height. The details and sketch of the pullout apparatus are referenced to Horpibulsuk and Niramitkronburee (2010). Normal stresses of 30, 50, and 90 kPa were applied to the upper layer of soil above the bearing reinforcement with a pressurized air bag. The pullout force was applied at a rate of 1 mm/min. The maximum applied pullout displacement at the end of a test was 40 mm.

### 4.3 TEST RESULTS AND DISCUSSION

#### 4.3.1 Pullout friction resistance

The pullout friction resistance of bearing reinforcement (without transverse member) is investigated on the longitudinal member with a diameter of 16 mm and length of 2.6 m. The friction resistance,  $P_f$ , develops between the tested soil and the friction surface of the longitudinal member, and depends on both the soil-reinforcement interaction and the normal stress. The influence of molding water content on pullout friction resistance, and the maximum and residual pullout friction forces ( $P_{f,max}$  and  $P_{f,residual}$ ) are determined and analyzed by using Eq. (4.1). In Eq.(4.1),  $A$  is equal to  $\pi DL$ , in which  $D$  and  $L$  are the diameter and length of the longitudinal members, respectively.

$$P_f = A\alpha(c + \sigma_n \tan \phi) \quad (4.1)$$



Where  $A$  is the total surface area of the longitudinal member,

$\alpha$  is the interaction factor,

$c$  and  $\phi$  are the soil strength parameters and,

$\sigma_n$  is the applied normal stress.

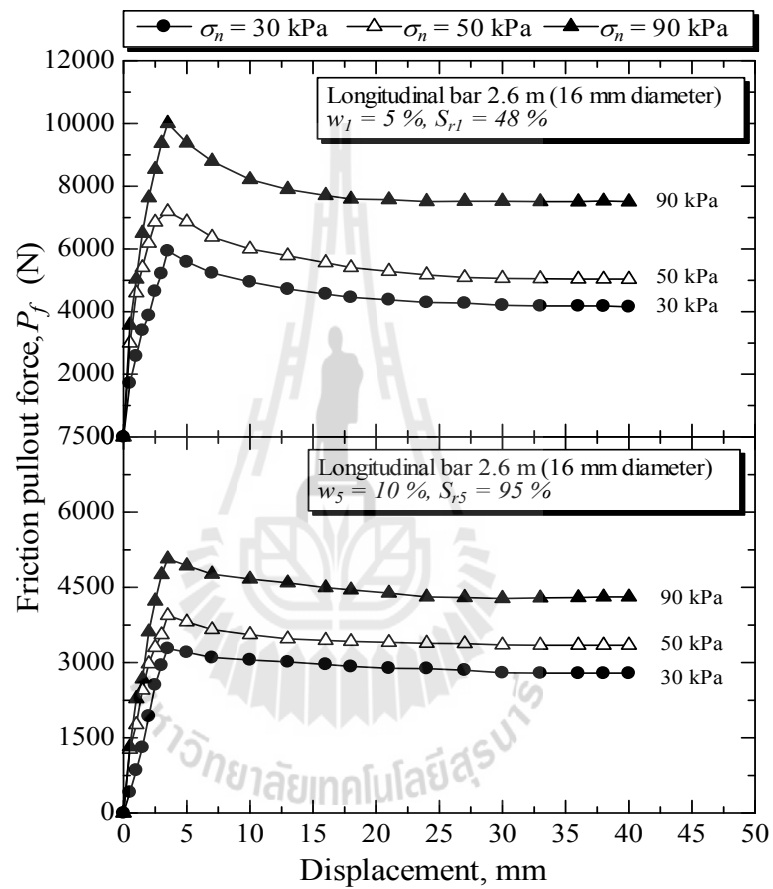
The results of the pullout friction test at various water contents are shown in the Figure 4.2. The relationship between friction pullout force and displacement is similar for all the water contents tested. The friction force increases rapidly with increasing the pullout displacement until  $P_{f,max}$  is reached at approximately 3-5 mm and then levels off at a large displacement of 40 mm (end of test). The values of  $P_{f,max}$  and  $P_{f,residual}$  increase with an increase of the normal stress and are dependent upon the water content. The lower water content results in the higher  $P_{f,max}$  and  $P_{f,residual}$  values because of the higher shear strength of the tested soil. It is expected that this relationship is similar to that of the strip reinforcement because their pullout resistances are mainly governed by friction component.

The difference in  $P_{f,max}$  and  $P_{f,residual}$  indicates the interlocking effect.

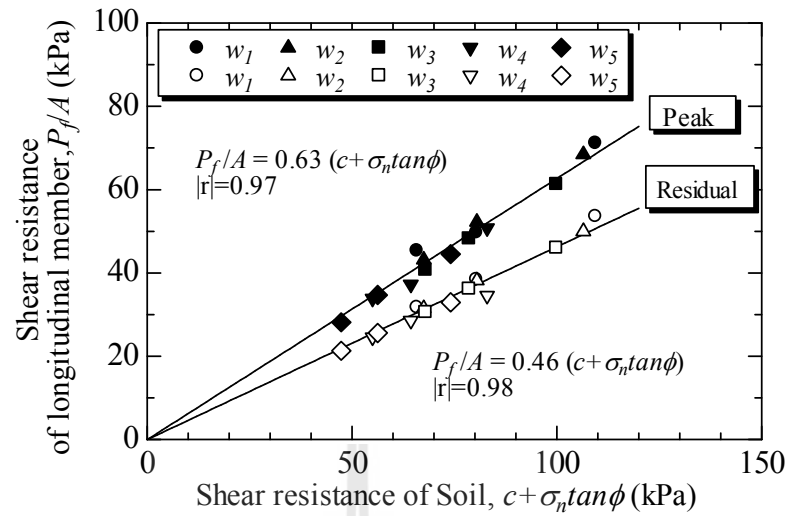
The higher interlocking effect results in the higher  $P_{f,max}$  and is associated with the higher  $P_{f,max} / P_{f,residual}$  ratio. The lower water content soil on the dry side of optimum exhibits higher  $P_{f,max}$  and  $P_{f,max} / P_{f,residual}$  values, which are possibly because the compacted soil particles are more aggregated.

Figure 4.3 shows the interface shear strength envelopes of the longitudinal member, which was analyzed using Mohr-Coulomb theory. From a linear regression analysis, the peak and residual interaction factors ( $\alpha_p$  and  $\alpha_r$ ) (in Eq. 4.1)

are irrespective of molding water contents tested and are approximately 0.63 and 0.46, respectively. This indicates the pullout friction resistance is mainly dependent upon soil's shear strength. The high  $\alpha_p$  of greater than 0.5 indicates the strong bonds between soil and reinforcement (Tatlisoiz et al., 1998).



**Figure 4.2** Pullout test results of a longitudinal member under different normal stresses.



**Figure 4.3** Relationship between soil-soil and soil-longitudinal interfaces of all tested soils.

#### 4.3.2 Pullout bearing resistance of a single isolated transverse member (n = 1)

Figure 4.4 shows the typical total pullout force and displacement relationships for the bearing reinforcement with a 2.6 m longitudinal member and a 40x150 (BxL) mm transverse members in the lateritic soil, at various molding water contents. The pullout force increases with increasing applied normal stresses for all molding water contents. The pullout force increases sharply before the pullout displacement reaches about 3 mm in which the friction pullout resistance is fully developed. Subsequently, the pullout force gradually increases until the end of the test at a large displacement of approximately 40 mm. It is noted that the bearing pullout resistance significantly reduces even with a small increase in water content; especially, on the dry side of optimum. For example, the bearing pullout resistances at normal stress of 90 kPa are 50, 30, 21, 13, 12.2 kN for water contents of 5%, 6%,

7.5% ( $w_{owc}$ ), 9% and 10%, respectively. The bearing pullout resistance does not linearly decrease with decreasing shear strength, unlike the friction pullout resistance. In other words, besides the shear strength, the failure mode (general shear, modified punching shear and punching shear) controls the bearing pullout resistance.

The maximum bearing resistance of a single isolated transverse member,  $\sigma_{b\max}$ , in cohesive-frictional soil can be evaluated by the modified punching mechanism (Sukmak et al., 2015). The  $\sigma_{b\max}$  in cohesive-frictional soil can be approximated using the following equations:

$$\sigma_{b\max} = cN_c + \sigma_n N_q \quad (4.2)$$

$$N_q = \frac{1}{\cos \phi} \exp[2\beta \tan \phi] \tan\left(\frac{\pi}{4} + \frac{\phi}{2}\right) \quad (4.3)$$

$$N_c = \frac{1}{\sin \phi} \exp[2\beta \tan \phi] \tan\left(\frac{\pi}{4} + \frac{\phi}{2}\right) - \cot \phi \quad (4.4)$$

Where  $N_q$  and  $N_c$  are the bearing capacity factors and,

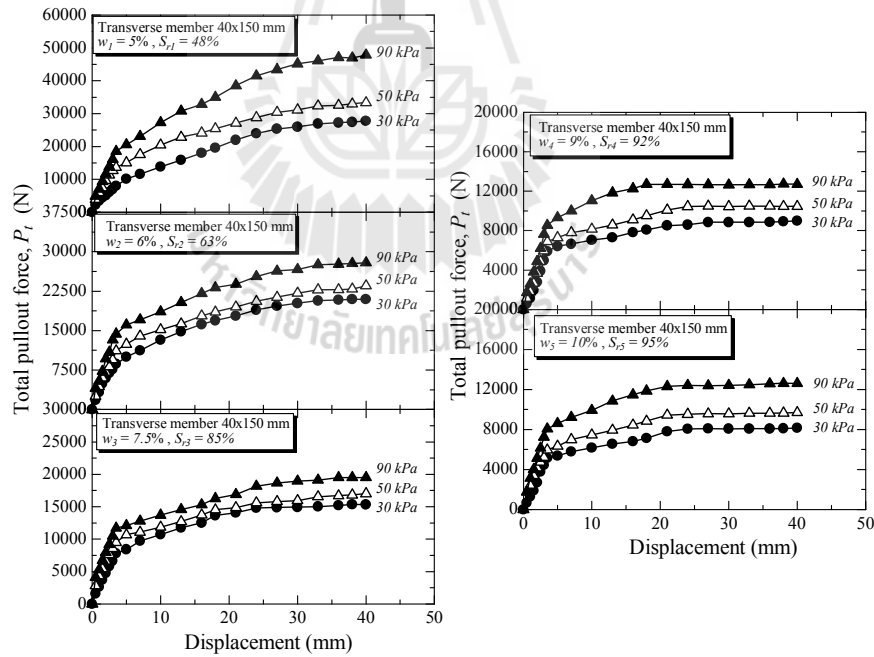
$\beta$  is the angle of transformation, varying with fine content.

The failure modes at various water contents are investigated and shown in Figure 4.5. The test results show that the  $\beta$  values of various dimensions ( $B \times L$ ) for different molding water contents are between  $\pi/1.61$  and  $\pi/3$ . The  $\beta$  value decreases with increasing molding water content; i.e., the failure mechanism approaches the punching shear failure when the molding water content increases due to the decrease in degree of aggregation. With the shift of failure modes approaching the punching shear mechanism and the reduction in shear strength, the bearing pullout resistance significantly decreases with increasing water content

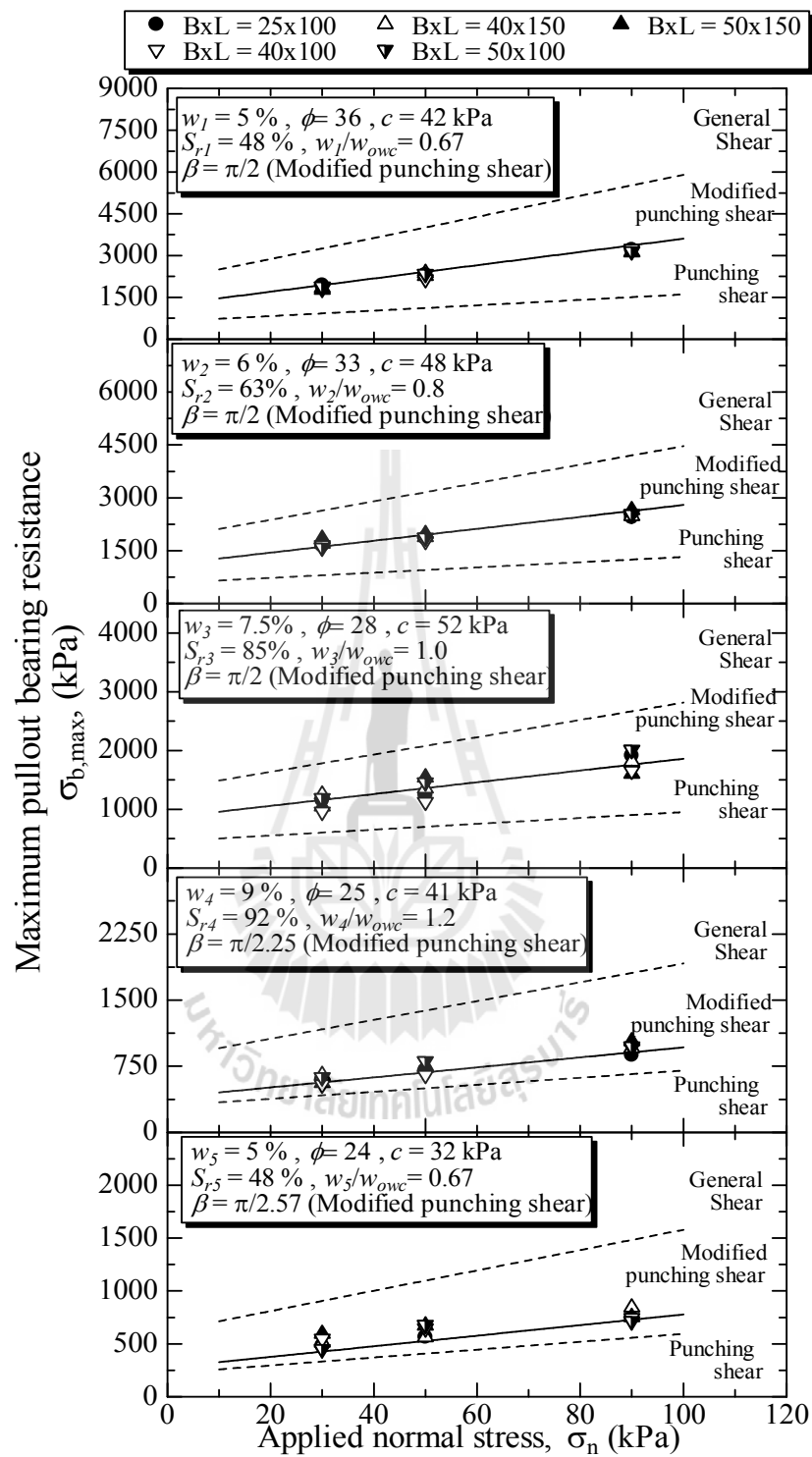
The relationship between  $\beta$  and  $w/w_{OWC}$  is shown in Figure 4.6. The  $\beta$  values of the compacted soil on the dry side of optimum and at  $w_{OWC}$  are essentially constant and equal to  $\pi/2$ . On the wet side of optimum, the  $\beta$  value decreases polynomial with an increase in molding water content. The relationship between  $\beta$  and  $w/w_{OWC}$  is represented in the form:

$$\beta_{(rad)} = \pi/2 \quad \text{for } 0.67 \leq w/w_{owc} \leq 1.0 \quad (4.5)$$

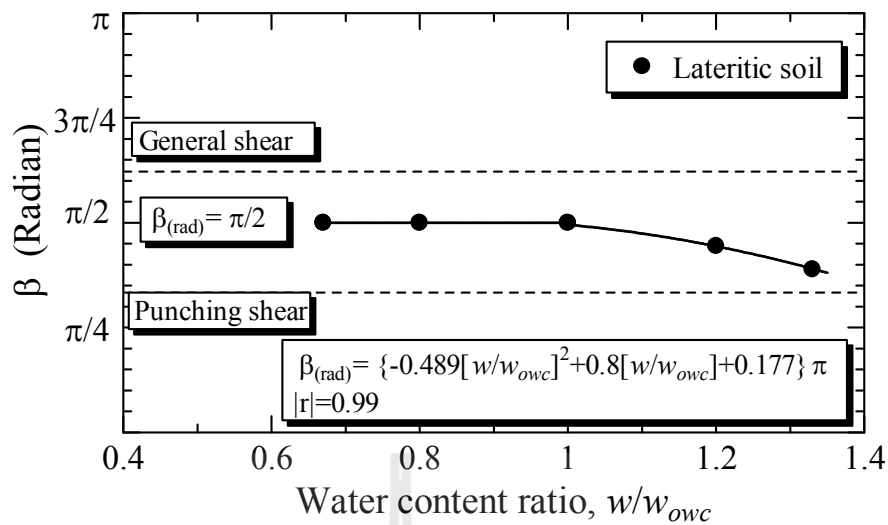
$$\beta_{(rad)} = \left\{ -0.489[w/w_{owc}]^2 + 0.8[w/w_{owc}] + 0.177 \right\} \pi \quad \text{for } 1.0 < w/w_{owc} < 1.33 \quad (4.6)$$



**Figure 4.4** Typical pullout test of the bearing reinforcement in tested soils.



**Figure 4.5** Maximum pullout bearing resistance of a single isolated transverse member for all tested soils.



**Figure 4.6** Relationship between  $\beta$  and water content ratio.

#### 4.3.3 Pullout resistance of the bearing reinforcement ( $n > 1$ )

The bearing reinforcement has several transverse members at regular intervals. The pullout resistance of bearing reinforcement is controlled by the interference between transverse members. During the pullout of the bearing reinforcement from compacted soil, the transverse members can interfere with each other and the interference is dependent upon the spacing between transverse members. A dimensionless parameter, transverse member spacing ratio,  $S/B$ , was originally proposed by Bergado et al. (1996) in order to express the influence of center-to-center spacing,  $S$ , and dimension ( $B$ ) of transverse member on the pullout resistance. This parameter was subsequently used to investigate the transverse member interference of compacted soils at  $w_{owc}$  by Horpibulsuk and Niramitkronburee (2010) and Suksiripattanapong et al. (2013) for cohesionless soils and by Sukmak et al. (2015) for cohesive-frictional soils.

Palmeira (2004) suggested two mechanisms for the transverse member interference during pullout. The first is the increase in the magnitude of stresses and the rotation of principal stresses ahead of the members due to the mobilization of soil passive resistance. The second mechanism takes place behind each transverse member where a low stress region is formed and results in the softened region caused by the movement of a transverse member (Dyer, 1985). It was revealed that the failure mechanism of the bearing reinforcement was classified into three failure characteristics: block failure, interference failure, and individual failure, depending upon the  $S/B$  value (Bergado et al., 1993; Horpibulsuk and Niramitkronburee, 2010; Suksiripattanapong et al., 2013). The  $S_1/B$  is defined as the spacing ratio, which separates the block failure and interference failure zones and the  $S_2/B$  is defined as the spacing ratio, which separates the interference failure and individual failure zones

Figure 4.7 shows a typical relationship between the maximum pullout bearing force ratio and  $S/B$  for 40 x 150 mm transverse members ( $n = 2$  to 4) under various applied normal stresses. The maximum pullout bearing force ratio is defined as a ratio of the maximum pullout bearing force of  $n$  transverse members,  $P_{bn}$ , to the maximum pullout bearing force of a single isolated transverse member,  $P_{b1}$ . It is found that the  $P_{bn}/P_{b1}$  ratio is controlled by the  $S/B$  value. For  $S/B \leq S_1/B$  (block failure), the shear surface caused by each transverse member joins together and forms a rough shear surface and only the first transverse member provide bearing resistance. For  $S_1/B < S/B < S_2/B$  (member interference failure), the interference degree decreases as the increase of  $S/B$ . For  $S/B > S_2/B$  (individual failure), the soil in front of each transverse member fails individually.



Figure 4.7 illustrates that the  $S_1/B$  value is the same for all the molding water contents tested and equals 3.75. The  $S_2/B$  value of the compacted soil is essentially the same for the soil compacted on the dry side of optimum and at  $w_{OWC}$  and equals 25. These two values are the same as those reported by Horpibulsuk and Niramitkronburee (2010) and Suksiripattanapong et al. (2013) for coarse-grained soils, which were compacted at  $w_{OWC}$ . It is however evident that the  $S_2/B$  value of the lateritic soil compacted on the wet side of optimum varies with molding water content and smaller than 25.

The increase of water content (decrease in shear strength) affects the stress region and failure plane in front of the transverse member. Based on the analysis of this study (Figure 4.8), the relationship between  $S_2/B$  and  $w/w_{owc}$  is expressed as follows:

$$S_2/B = 25 \quad \text{for } 0.67 \leq w/w_{owc} \leq 1.0 \quad (4.7)$$

$$S_2/B = -30.7[w/w_{owc}] + 55.45 \quad \text{for } 1.0 < w/w_{owc} \leq 1.33 \quad (4.8)$$

The ratio between  $P_{bn}$  to  $nP_{b1}$  is defined as the interference factor,  $IF$ . Based on the analysis of the present test data and previous works (Horpibulsuk and Niramitkronburee, 2010; Suksiripattanapong et al., 2013), the interference factor is mainly dependent upon  $S/B$  and  $n$  for a particular soil, and irrespective of applied normal stress:

$$IF = \frac{P_{bn}}{nP_{b1}} = a + b \ln\left(\frac{S}{B}\right) \quad (4.9)$$

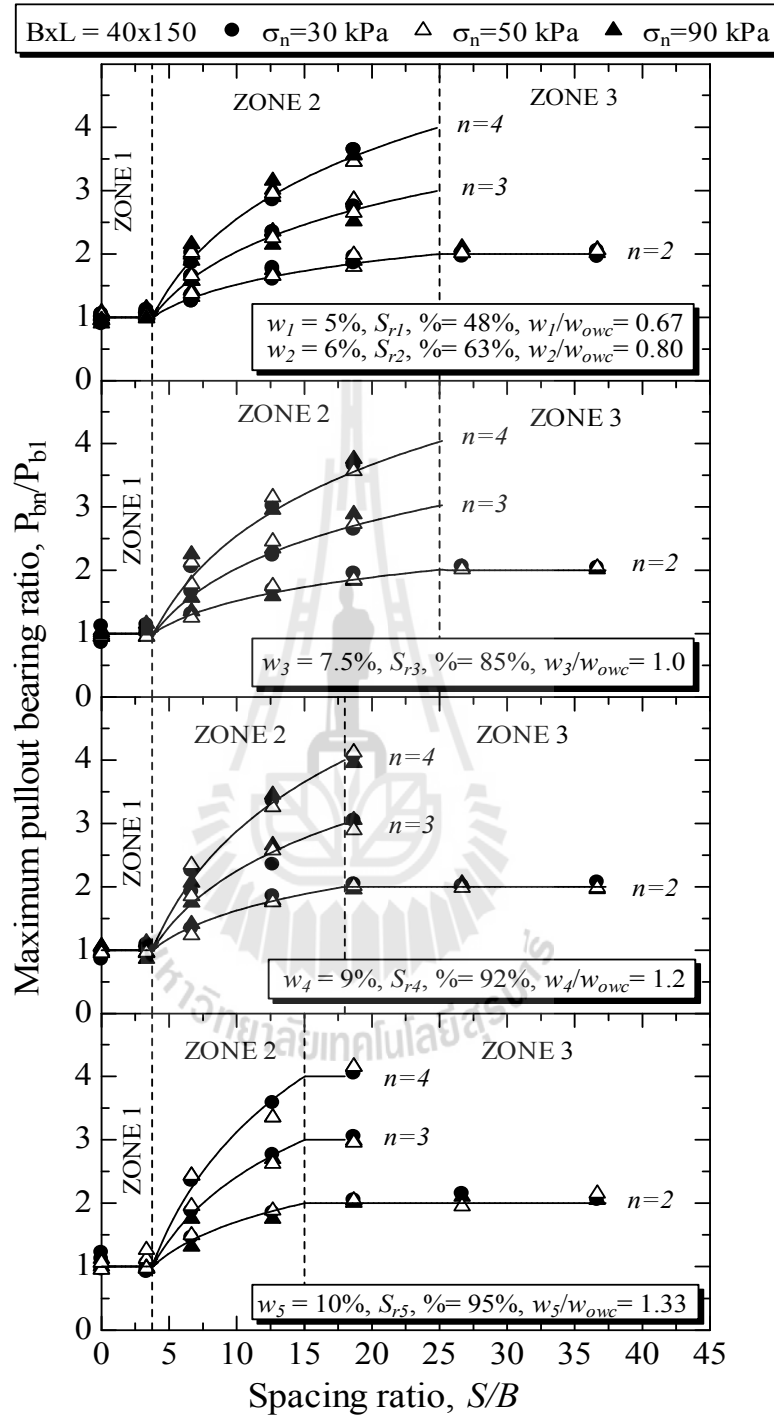
Where  $a$  and  $b$  are constants, depending upon  $n$  and water content.

These two constants can be obtained under two physical conditions: (1) when  $S/B$  equals 3.75,  $IF$  equals  $1/n$  because  $P_{bn}$  and  $P_{b1}$  are essentially the same, and (2) when  $S/B$  equals  $S_2/B$ ,  $IF$  equals unity. These two conditions define the lower and upper values of  $IF$  at the corresponding values of  $S/B = S_1/B$  and  $S/B = S_2/B$ , respectively. From these two conditions, the constants  $a$  and  $b$  can be determined by the following equations:

$$b = \frac{\left[1 - \frac{1}{n}\right]}{\left[\ln\left(\frac{S_2}{B}\right) - \ln\left(\frac{S_1}{B}\right)\right]} = \frac{\left[1 - \frac{1}{n}\right]}{\left[\ln\left(\frac{S_2}{B}\right) - 1.322\right]} \quad (4.10)$$

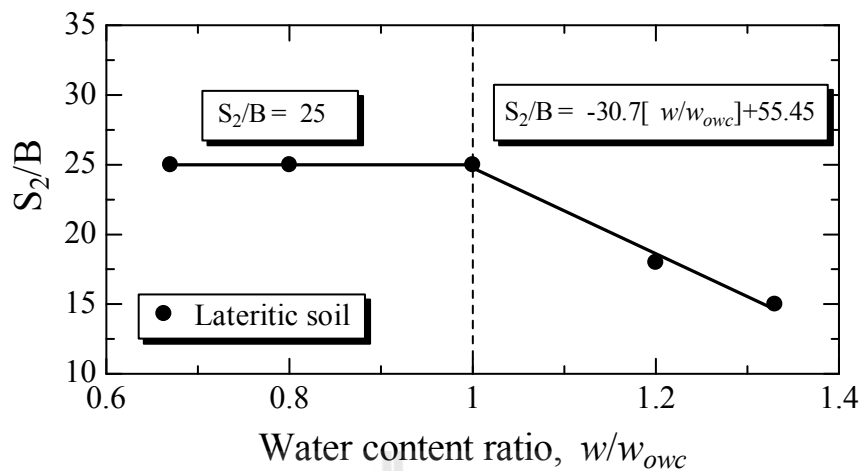
$$a = 1 - b \ln\left(\frac{S_2}{B}\right) \quad (4.11)$$

Table 4.2 presents an example of the predicted maximum pullout force,  $P_t$ , of bearing reinforcement with 40x150 mm transverse member and 2.6 m length of longitudinal member for  $n = 1, 2, 3$  and 4 with different  $S/B$  values.  $P_t$  is the sum of  $P_f$ , and  $P_{bn}$ . In this prediction,  $P_f$  was calculated using Eq. (1) and  $P_{bn}$  was calculated using Eqs. (2) to (11), where  $\alpha_r$  was taken as 0.46 and  $\beta$  and  $S_2/B$  values were determined from  $w/w_{OWC}$  using Eqs. (5) and (6), and Eqs. (7) and (8), respectively. The predicted and the measured values are in very good agreement, which verifies the applicability of the proposed pullout resistance equations.



**Figure 4.7** Measured and predicted  $P_{bn}/P_{b1}$  and  $S/B$  relationship

for 40x150 mm transverse members.



**Figure 4.8** Effect of water content ratio on  $S_2/B$  .

#### 4.4. CONCLUSIONS

This paper investigates effect of molding water content on the pullout resistance mechanism of bearing reinforcement embedded in the marginal lateritic soil. The critical analysis of test results leads to the development of pullout resistance equations in term of total strength parameters and  $w/w_{owc}$  of compacted soil and dimension of bearing reinforcement. The following conclusions can be drawn from this study:

1. The pullout friction resistances ( $P_{f,max}$  and  $P_{f,residual}$ ) are dependent upon soil shear strength and soil-reinforcement interaction factor,  $\alpha$ . The peak and residual interaction factors ( $\alpha_p$  and  $\alpha_r$ ) are irrespective of molding water contents tested and are approximately 0.63 and 0.46, respectively.
2. The modified punching shear solution with various  $\beta$  values is valid as a generalized expression to approximate pullout bearing resistances of a single transverse member at various molding water contents. The  $\beta$  value

decreases with increasing water content. The  $\beta$  value of the compacted soil at  $0.67 \leq w/w_{owc} \leq 1.0$  is essentially constant and equal to  $\pi/2$ . For  $1.0 < w/w_{owc} \leq 1.33$ , the  $\beta$  value decreases polynomial with an increase in water content ratio.

3. The failure mechanism of bearing reinforcement with  $n$  transverse members is essentially dependent upon spacing ratio  $S/B$ , which is strongly controlled by  $w/w_{owc}$ . The failure mechanism is the block failure when  $S/B \leq 3.75$ , the member interference failure when  $3.75 < S/B < S_2/B$  and the individual failure when  $S/B > S_2/B$ .  $w/w_{owc}$  affects the stress region and failure plane in front of transverse members. The  $S_2/B$  value increases linearly with a decrease in  $w/w_{owc}$  when  $w > w_{owc}$  and essentially constant when  $w < w_{owc}$ .
4. The proposed pullout resistance equations are derived based from the total strength parameters of the compacted marginal lateritic soil at  $w = w_{owc} \pm 2.5\%$ , which is typically specified for the field compaction. The proposed equations required only shear strength parameters, water content ratio, and dimension of bearing reinforcement. The applicability of the proposed equations is verified and presented in this paper. The proposed equations are useful for an examination of the internal stability against pullout failure of the BRE wall during construction and at the end of construction.

**Table 4.2** Predicted and measured pullout resistance of bearing reinforcement with 40x150 mm transverse member  
for  $n = 1, 2, 3$ , and 4 and  $w_4/w_{owc} = 1.20$ .

Water content ratio	$C$ (kPa)	$\phi$ (Deg)	$\sigma_n$ (kPa)	n	$S/B$	$IF$	Predicted					Measured
							$\alpha_r$	$P_f$ (kPa)	$\beta$ (Rad.)	$P_b$ (kPa)	$P_t$ (kPa)	$P_t$ (kPa)
1.20	41	25	30	1	-	1	0.46	3.76	1.395	3.87	7.63	7.21
			50				0.46	4.40	1.395	4.64	9.04	8.12
			90				0.46	5.67	1.395	6.17	11.84	12.01
			30	2	6.66	0.682	0.46	3.76	1.395	5.28	9.04	8.84
			50				0.46	4.40	1.395	6.32	10.72	10.53
			90				0.46	5.67	1.395	9.02	14.69	14.22
			30		12.66	0.890	0.46	3.76	1.395	6.89	10.65	10.45
			50				0.46	4.40	1.395	8.25	12.65	11.77
			90				0.46	5.67	1.395	11.77	17.44	16.76
			30	3	6.66	0.574	0.46	3.76	1.395	6.69	10.45	10.25
			50				0.46	4.40	1.395	7.99	12.39	13.05
			90				0.46	5.67	1.395	11.39	17.06	19.12
			30		12.66	0.851	0.46	3.76	1.395	9.88	13.64	12.89
			50				0.46	4.40	1.395	11.83	16.23	16.21
			90				0.46	5.67	1.395	16.88	22.55	22.81
			30	4	6.66	0.521	0.46	3.76	1.395	8.07	11.83	12.79
			50				0.46	4.40	1.395	9.66	14.06	16.65
			90				0.46	5.67	1.395	13.79	19.46	21.71
			30		12.66	0.832	0.46	3.76	1.395	12.89	16.65	16.29
			50				0.46	4.40	1.395	15.44	19.84	20.16
			90				0.46	5.67	1.395	22.02	27.69	25.45

## 4.5 References

- Abdi, M.R., Arjomand, M.A., 2011. **Pullout tests conducted on clay reinforced with geogrid encapsulated in thin layers of sand.** Geotextiles and Geomembranes 29, 588-595.
- ASTM D698-91, 1995. **Test method for laboratory compaction characteristics of soil using standard effort (12,400 ft-lbf/ft<sup>3</sup> (600 kN-m/m<sup>3</sup>).** Annual book of ASTM standards 04.08, 69-76.
- Bergado, D.T., Chai, J.C., Marui, H., 1996. **Prediction of pullout resistance and pullout force displacement relationship for inextensible grid reinforcements.** Soils and Foundations 36, 11-22.
- Bergado, D.T., Macatol, K.C., Amin, N.U., Alraro, M.C., 1993. **Interaction of lateritic soil and steel grid reinforcement.** Can. Geotech. J 30, 376-384.
- Dyer, M.R., 1985. **Observation of the stress distribution in crushed glass with applications to soil reinforcement.** PhD. Thesis, University of Oxford, UK.
- Esmaili, D., Hatami, K., Miller, G.A., 2014. **Influence of matric suction on geotextile reinforcement-marginal soil interface strength.** Geotextiles and Geomembranes 42, 139-153.
- Fleming, I.R., Sharma, J.S., Jogi, M.B., 2006. **Shear strength of geomembrane-soil interface under unsaturated conditions.** Geotextiles and Geomembranes 24, 274-284.
- Horpibulsuk, S., Niramitkronburee, A., 2010. **Pullout resistance of bearing reinforcement embedded in sand.** Soils and Foundations 50, 215-226.
- Keller, G.R., 1995. **Experiences with mechanically stabilized structures and native soil backfill.** Transportation Research Record 1474, 30-38.

- Abdi, M.R., Arjomand, M.A., 2011. **Pullout tests conducted on clay reinforced with geogrid encapsulated in thin layers of sand.** Geotextiles and Geomembranes 29, 588-595.
- ASTM D698-91, 1995. **Test method for laboratory compaction characteristics of soil using standard effort (12,400 ft-lbf/ft<sup>3</sup> (600 kN-m/m<sup>3</sup>).** Annual book of ASTM standards 04.08, 69-76.
- Bergado, D.T., Chai, J.C., Marui, H., 1996. **Prediction of pullout resistance and pullout force displacement relationship for inextensible grid reinforcements.** Soils and Foundations 36, 11-22.
- Bergado, D.T., Macatol, K.C., Amin, N.U., Alraro, M.C., 1993. **Interaction of lateritic soil and steel grid reinforcement.** Can. Geotech. J 30, 376-384.
- Dyer, M.R., 1985. **Observation of the stress distribution in crushed glass with applications to soil reinforcement.** PhD. Thesis, University of Oxford, UK.
- Esmaili, D., Hatami, K., Miller, G.A., 2014. **Influence of matric suction on geotextile reinforcement-marginal soil interface strength.** Geotextiles and Geomembranes 42, 139-153.
- Fleming, I.R., Sharma, J.S., Jogi, M.B., 2006. **Shear strength of geomembrane-soil interface under unsaturated conditions.** Geotextiles and Geomembranes 24, 274-284.
- Horpibulsuk, S., Niramitkronburee, A., 2010. **Pullout resistance of bearing reinforcement embedded in sand.** Soils and Foundations 50, 215-226.
- Keller, G.R., 1995. **Experiences with mechanically stabilized structures and native soil backfill.** Transportation Research Record 1474, 30-38.



- Liu, C.N., Ho, Y.H., Huang, J.W., 2009. **Large scale direct shear tests of soil/PET-yarn geogrid interfaces.** Geotextiles and Geomembranes 27, 19-30.
- Oloo, S.Y., Fredlund, D.G., 1996. **A method for determination of  $\phi_b$  for statically compacted soils.** Canadian Geotechnical Journal 33, 272-280.
- Palmeira, E.M., 2004. **Bearing force mobilisation in pull-out tests in geofrids.** Geosynthetics International 22, 481-509.
- Sukmak, K., Sukmak, P., Suksun, H., Han, J., Shen, S.L., Arulrajah, A., 2015. **Effect of fine content on the pullout resistance mechanism of bearing reinforcement embedded in cohesive-frictional soils.** Geotextiles and Geomembranes 43, 107-117.
- Suksiripattanapong, C., Horpibulsuk, S., Chinkulkijniwat, A., Chai, J.C., 2013. **Pullout resistance of bearing reinforcement embedded in coarse-grained soils.** Geotextiles and Geomembranes 36, 44-54.
- Tatliso, N., Edil, T.B., Benson, C.H., 1998. **Interaction between reinforcing geosynthetics and soil-tire chip mixtures.** Journal of Geotechnical and Geoenvironmental Engineering 124.

# **CHAPTER V**

## **NUMERICAL PARAMETRIC STUDY ON BEHAVIOR OF BEARING REINFORCEMENT EARTH (BRE) WALLS WITH DIFFERENT BACKFILL MATERIAL PROPERTIES**

### **5.1 Statement of problem**

MSE walls are often designed based on internal and external stability analyses using limit equilibrium methods. Limit equilibrium method can be used to predict a failure surface location and to assess the system stability in term of factors of safety (FS). For internal stability, reinforcement should be designed against potential rupture and pullout. The pullout resistance of the reinforcement depends on the geometry and properties of the reinforcement and the soil properties and is often determined by pullout tests. The major limitation of the limit equilibrium method is not able to calculate lateral deformation, settlement, and stress distribution in MSE walls (Han and Leshchinsky, 2004; Ho and Rowe, 1994; Rowe and Ho, 1998).

According to many researchers (Abdelouhab et al., 2011; Abdi and Zandieh, 2014; Bergado and Teerawattanasuk, 2008; Damians et al., 2015; Golam et al., 2014; Hegde and Sitharam, 2015; Ho and Rowe, 1994; Reddy and Navarrete, 2008; Suksiripattanapong et al., 2012; Wang et al., 2014; Youwai and Bergado, 2004), numerical methods (i.e. finite difference and finite element methods) have been

widely used for design and analysis of MSE structures. Numerical methods can model structural components, material properties, construction sequence and compute deformations, forces, strains, and stress distribution at any location of interest in a reinforced soil structure (Mohamed et al., 2014). In addition, they can be used for design, parametric studies, and simulation of the behavior of the earth structures (Collin, 1986).

However, the suitability of a numerical method for modeling MSE structures requires calibration and validation between calculated and observed behavior of laboratory and full-scale tests in order to produce convincing results. Hence, a numerical method validated with experimental test results should be used to investigate the behavior and performance of MSE structures. The PLAXIS program has been proved as a powerful and accurate tool to predict the performance of the MSE wall and pullout test results (Bergado et al., 2003; Khedkar and Mandal, 2009; Suksiripattanapong et al., 2012). Thus, the finite element code incorporated in PLAXIS 2D was used in this study.

In this study, finite element models with material properties were first calibrated according to laboratory large-scale pullout tests reported by Horpibulsuk and Niramitkornburee (2010) and Sukmak et al. (2015) and the full-scale bearing reinforced earth wall reported by Horpibulsuk et al. (2011). The calibrated models were then adopted in this study to investigate the behavior and performance of BRE walls with different backfill material properties.

The primary objective of this paper was to improve the understanding of bearing stress, settlement, lateral earth pressure, and horizontal wall movement of BRE walls with different backfill materials during and at the end of construction.

Horizontal wall deformations are especially important for serviceability of MSE structures. They can be induced by the deformations in reinforced and unreinforced zones, due to foundation lateral movement and settlement, and post-construction deformation. The post-construction deformation of the earth wall is mainly contributed by creep of the reinforcement. The creep of the reinforcement is usually assumed to result in a decrease in stiffness of reinforcement (Rowe and Ho, 1998). Therefore, the deformation of the wall due to post-construction can be assessed by examining the effect of reducing the reinforcement stiffness.

The second objective of this study was to evaluate the effects of various soil-structure interactions, foundations, and stiffness of reinforcements on horizontal wall deformations. This objective was achieved by a parametric study. The knowledge gained from this study provides useful information for further analysis and design of other BRE walls with different types of backfills, ground conditions, and features of bearing reinforcement.

## **5.2 Full-scale test earth wall for reference numerical model**

### **5.2.1 Foundation and backfill**

The construction of a bearing reinforcement earth (BRE) wall was completed on the campus of the Suranaree University of Technology (SUT) in Thailand on 20 July 2009. The foundation consisted of a 1.5-m thick weathered crust layer of silty sand, which was underlain by a medium dense silty sand layer down to about 6 m deep and then a very dense silty sand layer. Soil samples were obtained from a borehole at the construction site down to 8 m deep. The ground water was not detected during boring. The backfill for the earth wall was clean sand, which is

classified as poorly-graded sand (SP), according to the Unified Soil Classification System (USCS). The details of the foundation and the backfill can be found in Horpibulsuk et al. (2011).

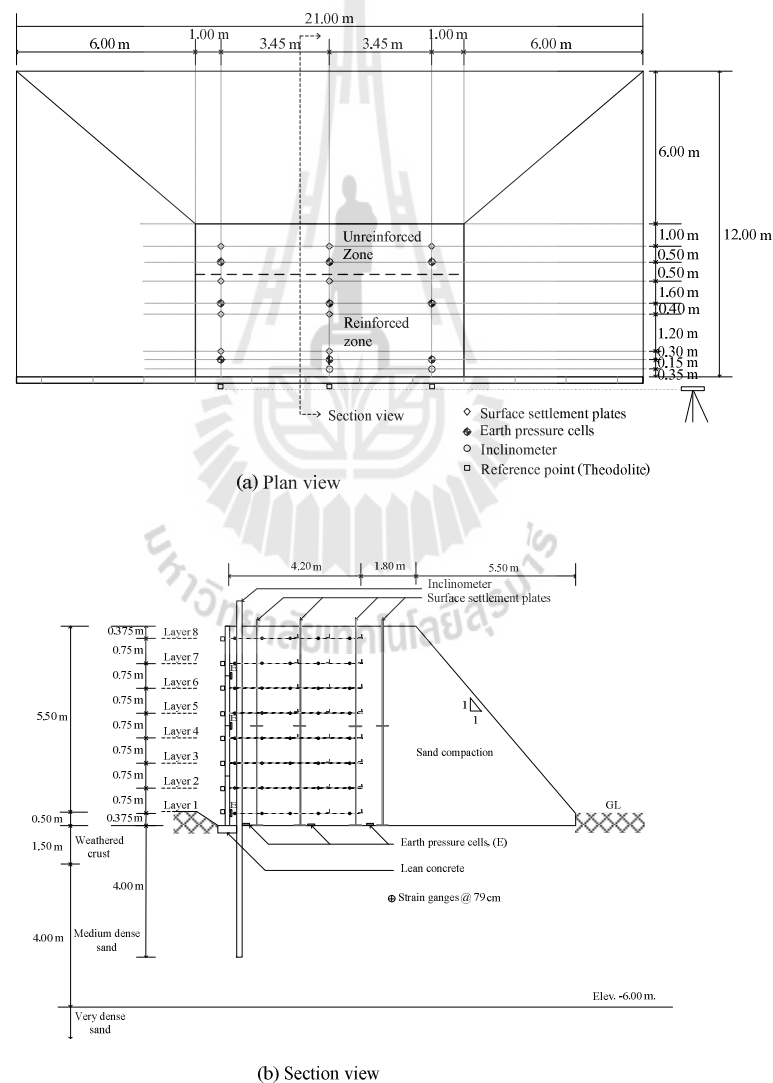
### 5.2.2 Construction and instrumentation of the test wall

The test wall was 6 m high, 9 m wide, 6 m long at the top, and 21 m wide at the base, as illustrated in Figure 5.1. The side and back slopes were 1:1. The wall facing panels made of segmental concrete panels (1.50 x 1.50 x 0.14) were placed on a lean concrete leveling pad (0.15 m wide and 0.15 thick) at two days after curing. During the construction, four facing panels were installed in the middle portion of the wall width ( $9 \times 6 \times 6 \text{ m}^3$ ) with eight reinforcement levels. The longitudinal reinforcement members for all layers were 12 mm diameter and 4.2 m long. The transverse members were equal steel angles that had 25 mm leg length ( $B$ ) and 180 mm length ( $L$ ). The transverse member was spaced at 750 mm for all transverse members. The vertical spacing between each reinforcement level was 750 mm. Their horizontal spacing was 750 mm for levels 4-8 and 0.5 m for levels 1-3. The details of the bearing reinforcement for each layer are summarized in Table 5.1.

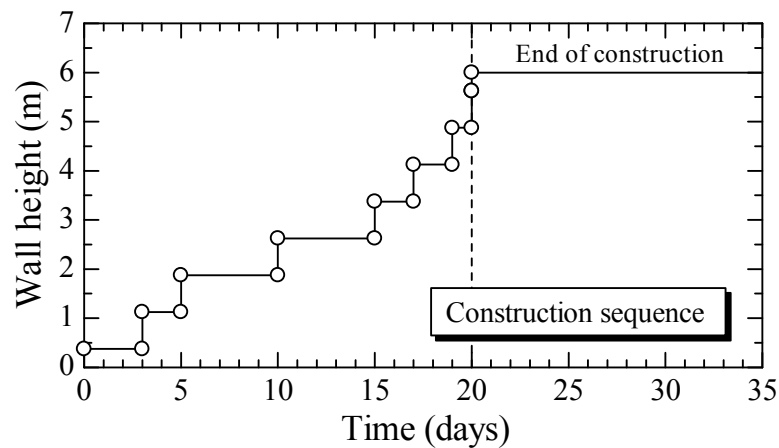
The backfill was compacted in layers of about 0.15 m lift thickness to a density of higher than 90% the standard Proctor maximum density. The total time spent for the construction of the wall was 20 days. The construction sequence is shown in Figure 5.2.

The BRE wall was extensively instrumented both in the subsoil and within the wall itself as shown in Figure 5.1. The ground water table observation well and piezometer were not used in this investigation because the ground water was deeper than 8 m (i.e., the bottom of boring). Lateral movement of each segmental

panel during construction was recorded by a theodolite with reference to the benchmark. The lateral movements after the end of construction were measured using digital inclinometers. The inclinometer casing was installed from top of wall down to the medium dense sand about 4 m below the wall base. The earth pressure cells were installed behind the facing panels and on the subsoil. The settlement plates were installed in the subsoil foundation and the backfill.



**Figure 5.1** Schematic diagram of the test wall instrumentation.



**Figure 5.2** Construction sequence.

**Table 5.1** Reinforcement details for the test wall.

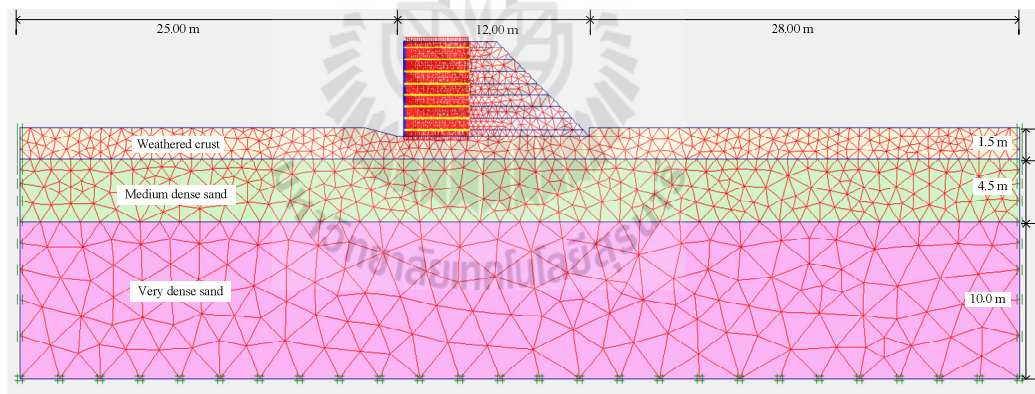
(Horpibulsuk and Niramitkornburee, 2010).

Facing panel	Reinforcement layer	Spacing between longitudinal members (mm)	Number
1	1 (bottom)	500	2
	2	500	2
2	3	500	2
	4	750	3
3	5	750	3
	6	750	3
4	7	750	3
	8 (Top)	750	3

### 5.3 Material constitutive models and parameters

The 2D Plaxis Finite Element (FE) program was used to simulate the construction of the wall. The BRE wall was modeled as a plane strain problem. The FE mesh and boundary condition are shown in Figure 5.3. The nodal points at the bottom

boundary were fixed in both directions and those on the side boundaries were fixed only in the horizontal direction. The soil elements were modeled using 15-noded triangular elements (totally 28,631 nodes of 3,190 elements). Local element size factor, which controls the mesh coarseness around the geometry line, of wall facing and reinforcements was 0.1 and soil-reinforcement thickness factor was 0.05. The simulation was performed under a drained condition because the ground water was not detected during the test. Properties of the compacted soil were determined from conventional laboratory tests that did not consider the time-dependent behavior, such as creep of soil. The creep model is beyond the scope of this study because it aimed to simulate the wall behavior with simple and well-known soil models for practical design.



**Figure 5.3** Numerical model and mesh details for 2D FE

model simulation of BRE wall.



### 5.3.1 Backfill and Foundation

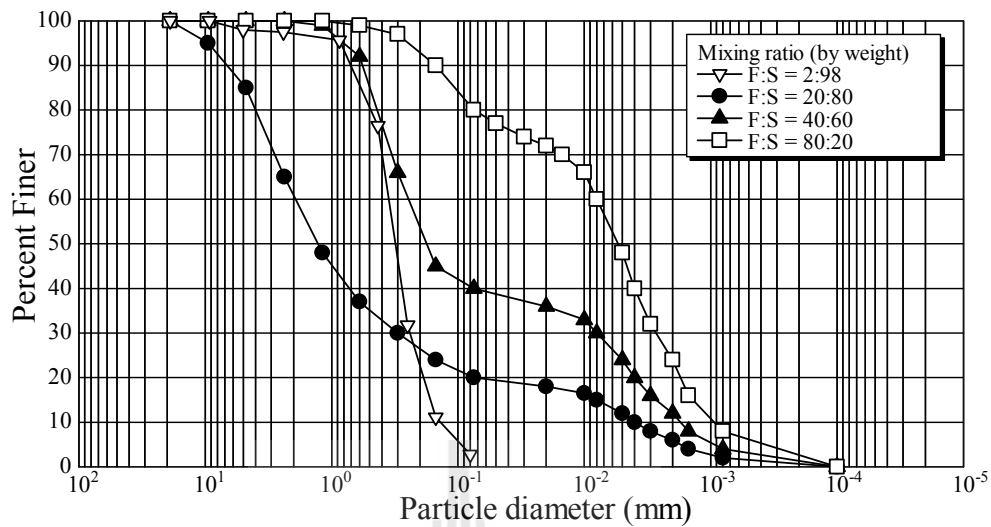
#### 5.3.1.1 Backfill

The backfill materials used in this study consisted of four types of soils, which were mixtures of silty clay and sand at different fine contents. The grain size distribution curves of the samples are shown in Figure 5.4. The four backfill materials were poorly-graded sand (F:S=2:98), clayey sand (F:S=20:80), clayey sand (F:S=40:60), and high-plasticity clay (F:S=80:20), in which F stands for percentage of fines and S stands for percentage of sand. Considering the average normal stress at the mid-height of the backfill (3 m high), the average normal stress was calculated to be about 60 kPa, which was used to select the backfill properties of the BRE wall. The material properties used for simulation were determined according to the laboratory large-scale direct shear tests reported by Horpibulsuk and Niramitkornburee (2010) and Sukmak et al. (2015). All backfill materials were modeled as linearly elastic-perfectly plastic materials with the Mohr-Coulomb (MC) failure criteria, which had five input parameters: elasticity modulus ( $E$ ), Poisson's ratio ( $\nu$ ), cohesion ( $c$ ), internal friction angle ( $\phi$ ), and dilatancy angle ( $\psi$ ).

The apparent cohesion and the friction angle were determined using a large direct shear apparatus with the diameter of 350 mm. The soil samples were prepared at the optimum water content (obtained from laboratory compaction tests) and transferred to the large direct shear box. For poorly-graded sand (F:S=2:98), the apparent cohesion and the friction angle were determined under a drained condition and equal to  $c' = 3$  kPa and  $\phi' = 40^\circ$ . However, for clayey sands and high-plasticity clay, the test commenced with no time allowed for the sample to consolidate

during the applied normal stress and shearing. The shear force was then applied at a constant shearing rate of 1 mm/min until the sample was sheared to 40 mm. The direct shear test was conducted to simulate the shear condition of the soil under a short-term condition (during construction and at the end of construction of the BRE wall) and to obtain the total strength parameters. The apparent cohesion and the friction angle were determined under an undrained condition. The cohesive-frictional soils were compacted and sheared at the optimum water content, at which the degree of saturation was between 78% and 87% (unsaturated soil). Therefore, consolidation and drainage are not an issue for this kind of soil. For an unsaturated soil, total strength parameters are more appropriate to describe the soil behavior than undrained or drained parameters (Sukmak et al., 2015). The total strength parameters of backfill compacted at a saturation degree of about 70% under an unconsolidated undrained condition have been used for analysis and simulation of the stability of reinforced embankments (Bergado et al., 1995; Chai et al., 1994).

According to the total stress analysis suggested in the Plaxis manual, the properties of all soil parameters used in this study were considered as a drained condition. Barkan (1962) proposed that the ranges of Poisson's ratio for sand and unsaturated clay were 0.30-0.35 and 0.35-0.40, respectively. Therefore, Poisson's ratio of poorly-graded sand was taken as 0.33 and Poisson's ratio of unsaturated clayey sands and clay of high plasticity was 0.40. The tested soils were compacted at optimum water contents, which were in an unsaturated state. The material properties of the backfill used for the FE simulation are shown in Table 5.2.



**Figure 5.4** Grain size distributions.

### 5.3.1.2 Foundation

A linearly elastic, perfectly plastic Mohr-Coulomb model was used to simulate the behavior of all foundation soils. The material properties used for the FE simulations are shown in Table 5.2.

Suksiripattanapong et al. (2012) used the 2D PLAXIS program to simulate the BRE wall model with a poorly-graded sand backfill. The simulated lateral wall movement from this model did not agree with that from the full-scale test. The measured lateral movement was smaller than the simulated lateral movement. The authors speculated that the elastic modulus ( $E = 1,875 \text{ kN/m}^3$ ) of the weathered crust foundation layer used in this model obtained from undisturbed sample was a lower field value. Thus, this paper attempts to eliminate the casing and foundation parameter effect by refining all mesh elements and increasing the elastic modulus of the weathered crust foundation layer in the reference numerical model. The elastic modulus ( $E = 6,250 \text{ kN/m}^3$ ) was selected by trial and error to match the predicted

lateral wall movement, lateral earth pressure, settlement, and bearing stress on the foundation with those measured during and at end of construction with poorly-graded sand backfill. The elastic modulus of the weathered crust layer falls within the range for a medium dense silty sand ( $E = 6,000\text{-}10,000 \text{ kN/m}^3$ ) reported by Bowles (1996) and Kezdi (1974).

### **5.3.2 Wall Facing and Reinforcement**

#### **5.3.2.1 Wall facing**

The wall face was made of segmental concrete panels, which were  $1.50 \times 1.50 \times 0.14 \text{ m}$  thick in dimension. The facing panel was modeled as beam (plate) elements. The input parameters for strength and modulus of elasticity are shown in Table 5.3. Linearly elastic material was used to simulate behavior of wall facing. The soil-facing panel interface coefficient,  $R$ , was taken as 0.9, which is generally used for interaction between soil and concrete (Bathurst, 1993).

#### **5.3.2.2 Reinforcement**

The bearing reinforcement was modeled as continuous sheet elements (called geotextile elements) in the Plaxis manual. The geotextile elements were assigned a constant axial stiffness ( $EA$ ) based on the elastic modulus ( $E$ ) of reinforcement and its cross-sectional area ( $A$ ). Linearly elastic material was used to simulate behavior of reinforcement. The input parameters of reinforcement are shown in Table 5.3.

**Table 5.2** Model parameters for backfills and foundations.

Types of soil	Backfill				Foundation		
	Poorly-graded sand	Clayey sand (F:S =20:80)	Clayey sand (F:S =40:60)	High plasticity clay (F:S =80:20)	Weathered crust	Medium dense sand	Very dense sand
Material model	Mohr Coulomb	Mohr Coulomb	Mohr Coulomb	Mohr Coulomb	Mohr Coulomb	Mohr Coulomb	Mohr Coulomb
$\gamma_{dry} (kN / m^3)$	17.0	20.1	18.9	16.1	17.0	17.15	18
$\gamma_{sat} (kN / m^3)$	18.15	22.0	20.8	18	18.0	18.15	19.0
$k_x (m / sec)$	1	$10^{-6}$	$10^{-7}$	$10^{-8}$	1	1	1
$k_y (m / sec)$	1	$10^{-6}$	$10^{-7}$	$10^{-8}$	1	1	1
$E_{ref} (kN / m^3)$	35,000	10,000	5,000	1,500	6,250	40,000	50,000
$\nu$	0.33	0.40	0.40	0.40	0.3	0.25	0.25
$c$	3	20	25	38	20	1	1
$\phi$	40	35	32	14	26	35	38
$\psi$	8	0	0	0	0	3	8

**Table 5.3** Model parameters for reinforcement and concrete facing.

	Bearing reinforcement (Geotextile)			Concrete facing (Plate element)
Material model	Elastic			Elastic
EA ( $kN / m$ )	4.5 E+4			3.556 E+6
EI ( $kN.m^2 / m$ )	-			5,808
w ( $kN / m / m$ )	-			3.36
$\nu'$	-			0.15
$R_{int}$	Poorly-graded sand	n=2	0.65	-
		n=3	0.75	
	Clayey sand (F:S =20:80)	n=2	0.60	
		n=3	0.70	
	Clayey sand (F:S =40:60)	n=2	0.55	
		n=3	0.65	
	High plasticity clay (F:S =80:20)	n=2	0.38	
		n=3	0.40	

### 5.3.2.3 Soil-reinforcement interaction

The soil-reinforcement interaction ratio,  $R_{inter}$  is defined as the ratio of the shear strength of soil-reinforcement interface to the shear strength of the surrounding soil (Vermeer and Brinkgreve, 1995 ). The soil-reinforcement interaction ratio in the numerical model was determined by simulating large-scale laboratory pullout test results. The geotextile elements, which cannot resist the bending moment, were employed to model the bearing reinforcement with longitudinal and transverse (bearing) members. The contribution of both friction and bearing resistances was converted to the equivalent frictional resistance. This method was used by Bergado et al. (2003), Khedkar and Mandal (2009), Abdelouhab et al. (2011), and Suksiripattanapong et al. (2012). The equivalent frictional resistance is

represented by the soil-structure interaction ratio,  $R_{inter}$ . The linearly elastic-perfectly plastic model was used to simulate the interaction between soil and bearing reinforcement.

### 5.3.3 Staged construction

In order to model the actual construction stages, the reinforced backfill and the retained backfill were modeled in eight layers. Each layer was constructed in the following stages:

- Stage 1: the first concrete panel (plate element) was set up, the first soil layer was placed and compacted into a layer thickness of 0.375 m, and then the first bearing reinforcement (geotextile element) was placed on the first compacted soil layer.
- Stage 2: the second soil layer was placed and compacted into a lift thickness of 0.75 m and then the second bearing reinforcement was placed on the second soil layer.
- Stage 3: the second concrete panel was set up, the third soil layer was placed and compacted into a layer thickness of 0.75 m, and then the third bearing reinforcement (geotextile element) was placed on the third compacted soil layer.
- These stages were repeated up to the wall height of 6 m.

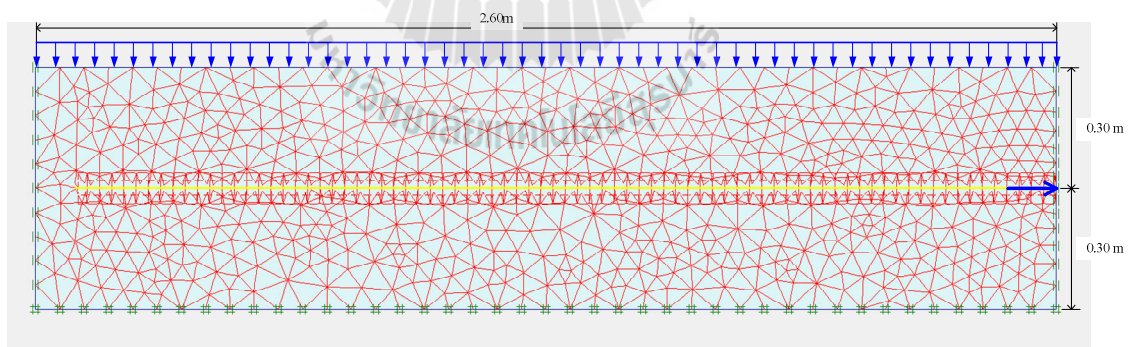
The backfill compaction during construction of the BRE wall model was simulated by applying a uniform vertical stress equal to 8 kPa to the entire surface of each newly placed soil layer in both reinforced and unreinforced zones. This vertical stress was removed before the placement of the next soil layer. This

intensity of the vertical stress was used to simulate compaction effects (Hatami and Bathurst, 2006; Hatami and Bathurst, 2005).

## 5.4 Finite element analysis

### 5.4.1 Soil-structure interaction ratio, $R_{inter}$

Several laboratory pullout tests were carried out in a metallic box of 2.6 m x 0.6 m x 0.6 m high. The longitudinal member of the reinforcement was 12 mm in diameter and 2.6 m long. The width of the transverse member was 150 mm. The number of transverse members,  $n$  used in this study were  $n = 2$  and 3. The  $R_{inter}$  value is dependent on the number of transverse members and soil properties. The laboratory pullout test was modeled as a plane strain problem as shown in Figure 5.5. The nodal points at the bottom boundary were fixed in both directions and those on the side boundaries were only fixed in the horizontal direction.



**Figure 5.5** Finite element model for pullout tests.

The soil-bearing reinforcement interaction ratio was back-calculated from the laboratory pullout tests by Horpibulsuk and Niramitkornburee (2010) for poorly-graded sand (F:S = 2:98) and by Sukmak et al. (2015) for clayey sands



(F:S = 20:80), clayey sand (F:S = 40:60), and high-plasticity clay (F:S = 80:20). Several pullout tests at different applied normal stresses were modeled ( $\sigma_n = 30, 50$ , and 90 kPa) in order to simulate the reinforcement at different depths in the wall. The input parameters for soils and reinforcement were provided in Tables 2 and 3.

Figures 5.6a and 5.6b show the measured and simulated total pullout force and displacement relationships of the bearing reinforcement with 2 and 3 transverse members ( $n = 2$  and 3), respectively embedded in clayey sand (F:S = 20:80). The  $R_{inter}$  value was varied until the modeled curves coincided with the laboratory curves. The numerical curves well reproduced the curves of laboratory tests as a function of the applied pullout force. The numerical simulation captured the behavior of bearing reinforcement, in which the total pullout resistance increased with an increase in the applied normal stress for all tested soils.

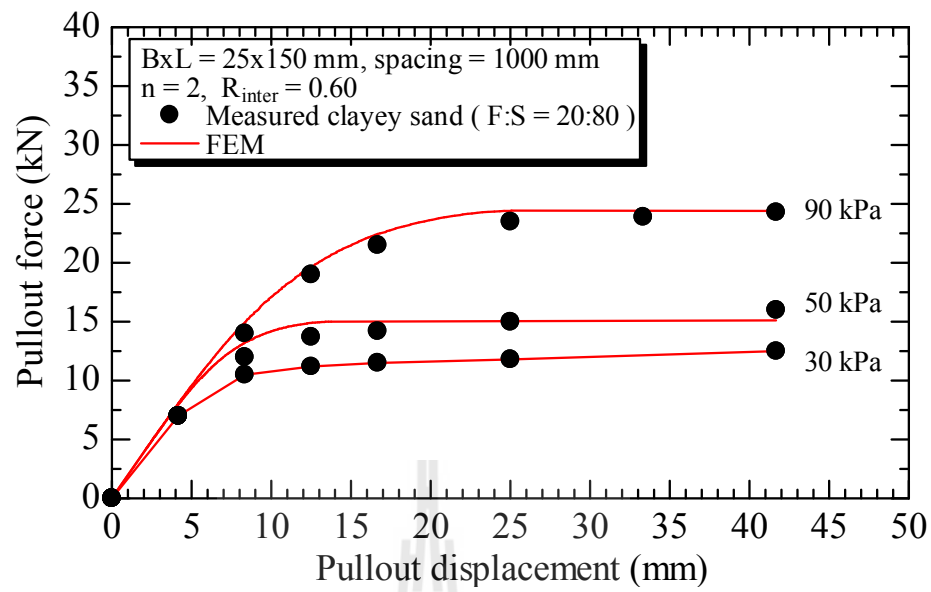
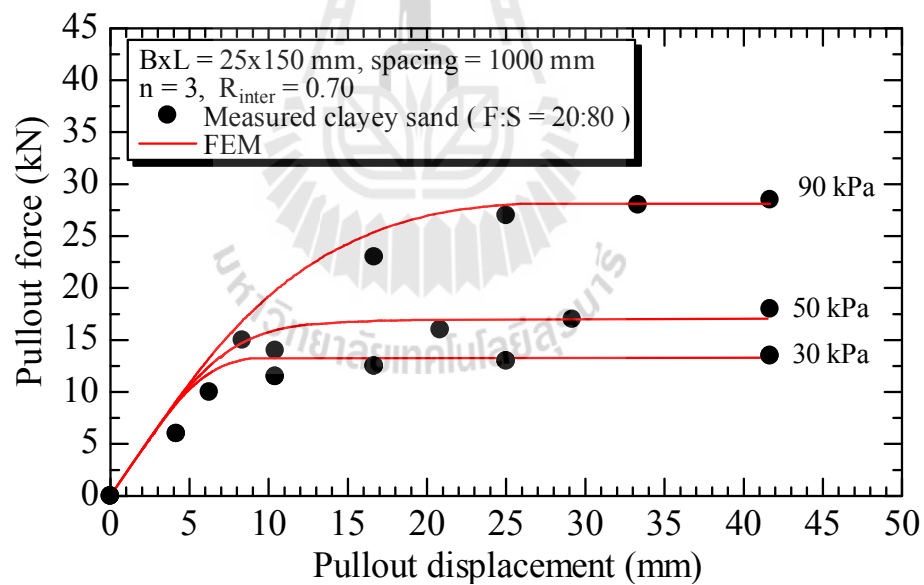
The relationships between the soil-structure interaction and the fine content for  $n = 2$  and 3 are shown in Figure 5.7. The  $R_{inter}$  values decreased with an increase in fine content, which also reduced the interface stiffness as well as the shear strength. The soil-structure interactions varied as an increase of fine content in the ranges of 0.65-0.38 and 0.75-0.40 for  $n = 2$  and 3, respectively. The relationships between  $R_{inter}$  and the fine content for  $n = 2$  and 3 are represented by polynomial functions in the following forms:

$$R_{inter} = -(4 \times 10^{-5})F^2 - (6 \times 10^{-4})F + 0.65$$

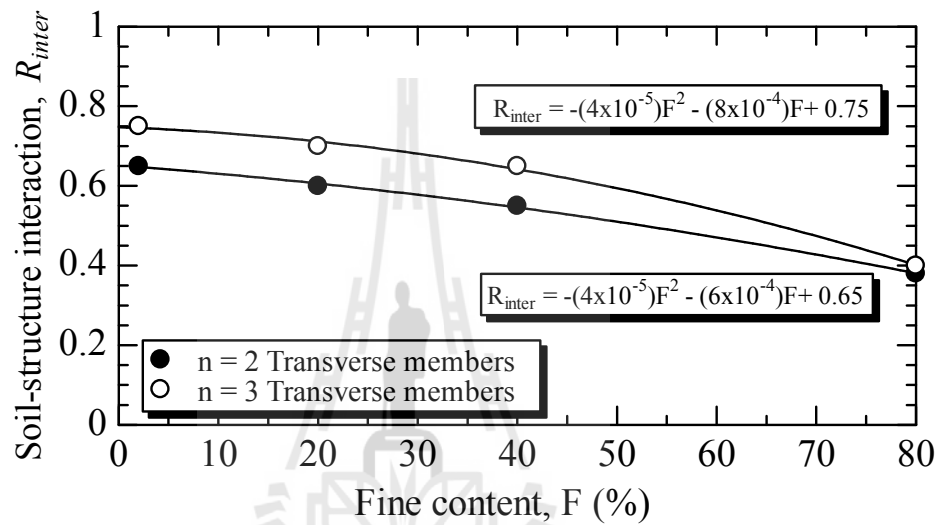
$$\text{for } 2 < F < 80\% ; n = 2 \quad (5.1)$$

$$R_{inter} = -(4 \times 10^{-5})F^2 - (8 \times 10^{-4})F + 0.75$$

$$\text{for } 2 < F < 80\% ; n = 3 \quad (5.2)$$

(a) number of transverse members,  $n = 2$ ,(b) number of transverse members,  $n = 3$ **Figure 5.6** Simulated and measured pullout test results of the bearing reinforcement.

The  $R_{inter}$  values at  $n = 2$  and  $3$  for high-plasticity clayey soil (F:S = 80:20) were nearly same due to the development in the bearing pullout resistance was comparatively low for  $F > 80\%$  (Sukmak et al., 2015). The  $R_{inter}$  values summarized in Table 5.3 were used to simulate the field performance of the BRE wall.



**Figure 5.7** Relationship between soil-structure interaction and fine content.

#### 5.4.2 Behavior of BRE wall with different types of soil

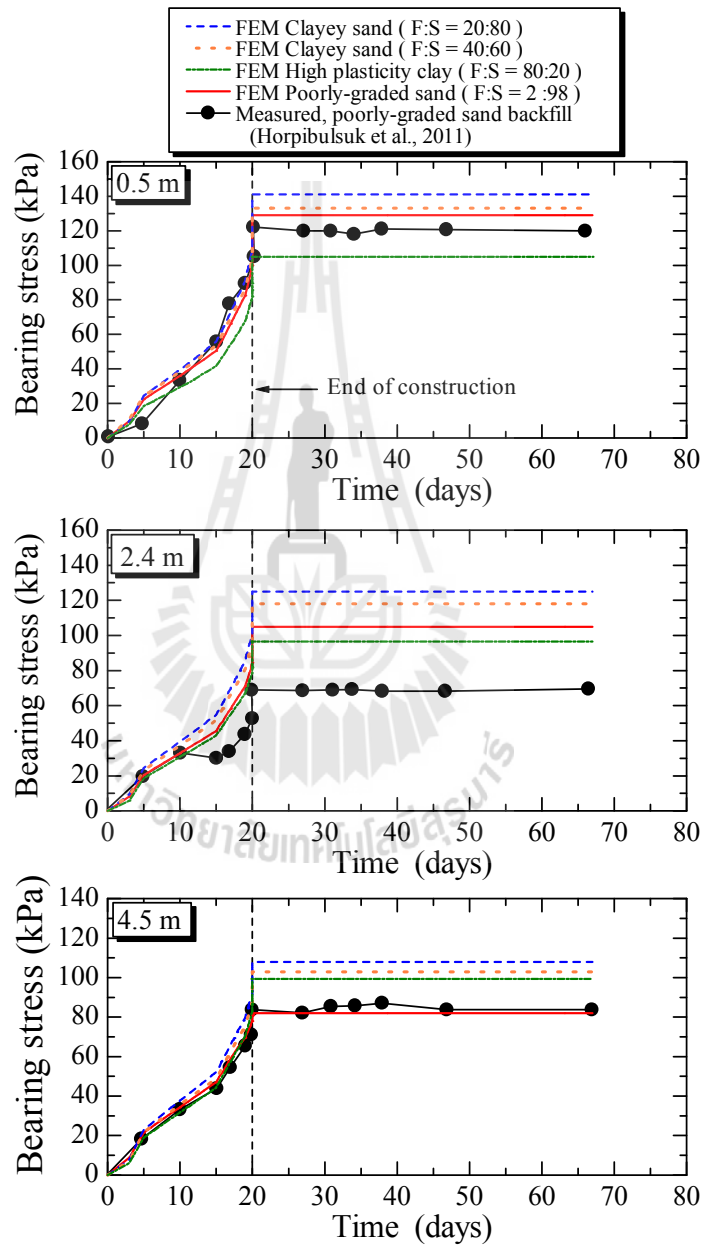
##### 5.4.2.1 Bearing stress

The relationships between bearing stress and construction in both the reinforced zone (0.5 and 2.4 m from the wall facing) and the unreinforced zone (4.5 m from the wall facing) for poorly-graded sand (F:S = 2:98), clayey sand (F:S = 20:80) and (F:S = 40:60), and high-plasticity clay (F:S = 80:20) are shown in Figure 5.8. The bearing stresses at the bottom of the earth wall with backfill soils increased during construction due to the backfill placement. After the completion of construction, the bearing stress changed insignificantly with time. For the poorly-

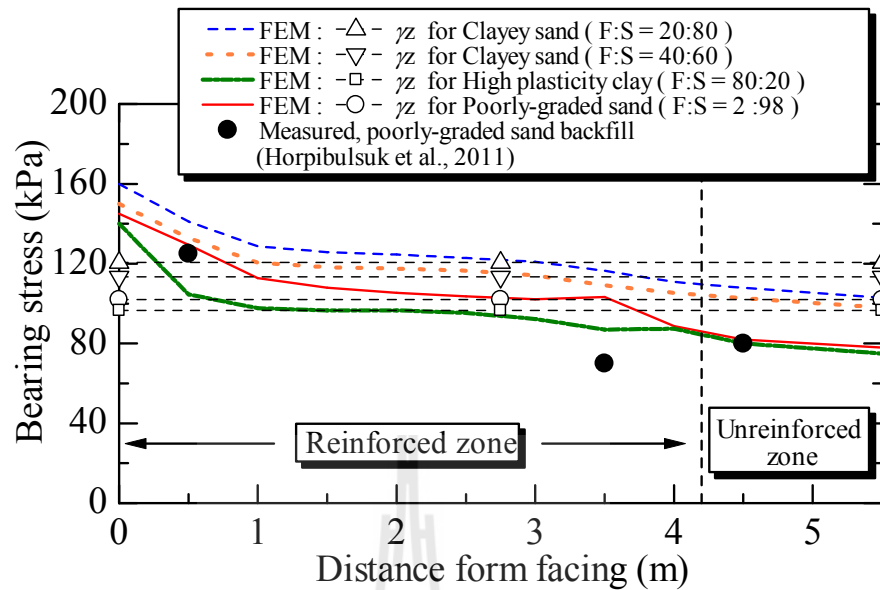
graded sand backfill, the simulated bearing stresses for both reinforced and unreinforced zones are in good agreement with the measured ones. At 2.4 m away from the wall face, the measured bearing stress was lower than the simulated one due to the non-uniformity of compaction at this particular location; therefore, the earth pressure cell sank into the ground at the vertical pressure of 32 kPa (the 2<sup>nd</sup> loading) (Suksiripattanapong et al., 2012). The bearing stress with the clayey sand (F:S = 20:80) was the highest the overburden stress of the backfill due to its highest maximum dry density. In other words, the bearing stress decreased as the maximum dry density decreased. It clearly shows that the bearing stress depended on the density of backfill.

Figure 5.9 shows the distributions of the measured and simulated bearing stresses and the calculated overburden stress ( $\sigma_v = \gamma z$ ) at the end of construction. The measured and simulated bearing stresses show a consistent reduction from the wall facing. A similar behavior of the bearing stresses decreasing with the distance from the wall facing was observed in the instrumented concrete facing reinforcement walls built on rigid foundations (Damians et al., 2014; Huang et al., 2009). The simulated bearing stress in the reinforced zone decreased from the front to the back because the BRE wall behaved as a rigid body built on the relatively firm foundation retaining the unreinforced backfill. The maximum bearing stress at the toe of the wall facing resulted from the eccentric load caused by the lateral thrust from the unreinforced backfill and the vertical load from the weight of segmental concrete panels. These simulated results were in agreement with the measured toe loads recorded from the instrumented field wall. Damians et al. (2012) concluded that the vertical toe loads were higher than the self-weight of the facing units. At 2.75 m

away from the wall facing, the simulated bearing stresses under all the backfills were close to the calculated overburden stress. The bearing stress in the unreinforced zone insignificantly decreased.



**Figure 5.8** Comparison between the simulated and measured settlements with construction time for different backfill.



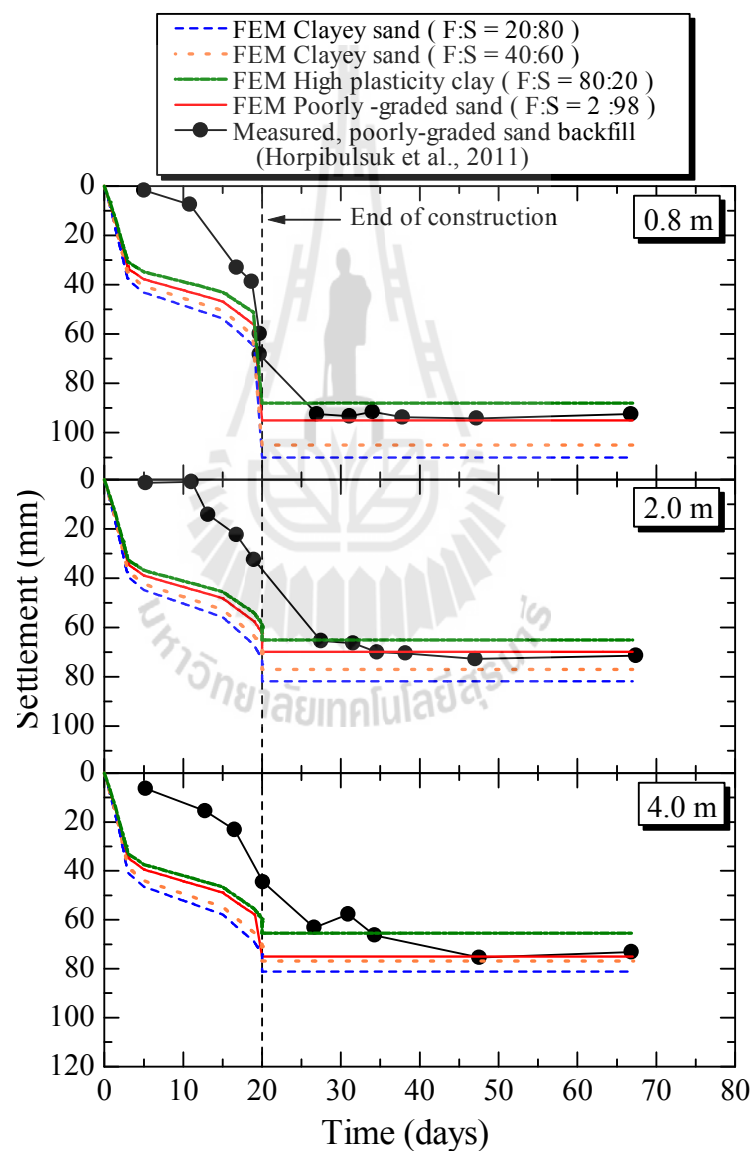
**Figure 5.9** Measured and simulated bearing stresses and calculated overburden stresses for different backfill.

#### 5.4.2.2 Settlement

The measured and simulated settlements of the BRE wall with different backfills are shown in Figure 5.10. The measured settlements from three settlement plates (at 0.8, 2.0, and 4.0 m from the wall facing) under the BRE wall with poorly-graded sand backfill were compared with the simulation. The base settled fast during the construction. The simulated settlements at the end of construction with the poorly-graded sand backfill were much closer to the measured ones. After the completion of the construction (at 20 days), the settlement increased insignificantly. Because the wall was founded on the relatively dry and firm stratum, the immediate settlement was dominated (i.e., insignificant consolidation settlement).

The settlements of the walls with the backfills having  $F: S = 20:80$  and  $F: S = 80:20$  were the largest and smallest due to the highest and lowest

bearing stresses on the base of the wall (Figure 5.9), respectively. The settlement decreased from the facing of the wall to the unreinforced zone. The settlement was highest at the toe of the wall because a portion of the self-weight of the backfill was transferred from the reinforcement to the facing of the wall and the wall also slightly rotated thus increasing the pressure at the toe (Rowe and Skinner, 2001).



**Figure 5.10** Measured and simulated settlements with construction time  
for different backfill

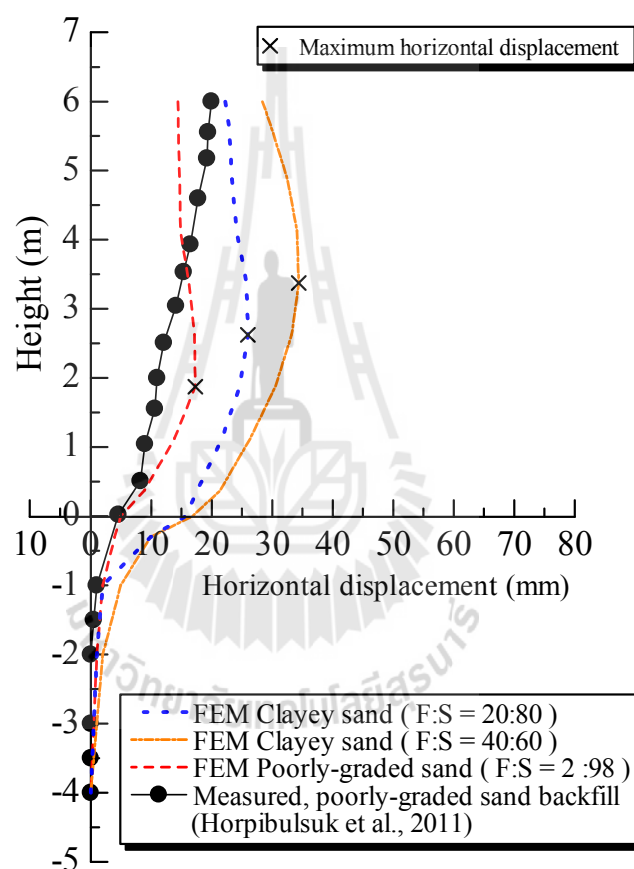
### 5.4.2.3 Horizontal wall movement

The simulated and measured horizontal wall movements with different backfills are compared and shown in Figure 5.11. The simulated result of the wall with the fill of F:S = 80:20 is not included because of its excessive horizontal wall movement. The comparison between the measured and simulated horizontal wall movements with the backfill of F:S = 2:98 is considered to be reasonable. The horizontal wall movements were the sum of the horizontal movement during construction (caused by the lateral movement of reinforced and unreinforced soil zones) and the foundation wall movement and settlement. The horizontal wall movements increased as the fine content increased due to the decrease in shear strengths of the backfills. The increase of the fine content changed the location of the maximum wall movement higher up from 2.0 m for F:S = 2:98 to 6.0 m (the top of the wall) for F:S = 80:20.

Figure 5.12 shows the simulated horizontal movement of the unreinforced soil zone at 4.5 m away from the facing of the wall. The simulated horizontal movement of the unreinforced soil zone increased as the increase of fine content due to the performance of the reinforced zone decreased. The performance of the reinforced zone was represented by the horizontal movement ratio ( $U_{x(\text{unreinforced})}/U_{x(\text{max wall})}$ ) of the maximum horizontal movement of the unreinforced zone to the maximum horizontal movement of the wall facing. This ratio indicated the ability of the reinforced zone to resist the horizontal movement (pressure) of the unreinforced zone. When this ratio is low, the BRE wall has better performance due to its increased stability. At the locations of the maximum wall movement with each backfill, the horizontal movement ratios are 0.36, 0.46, 0.56, and 0.84 for F:S = 2:98,



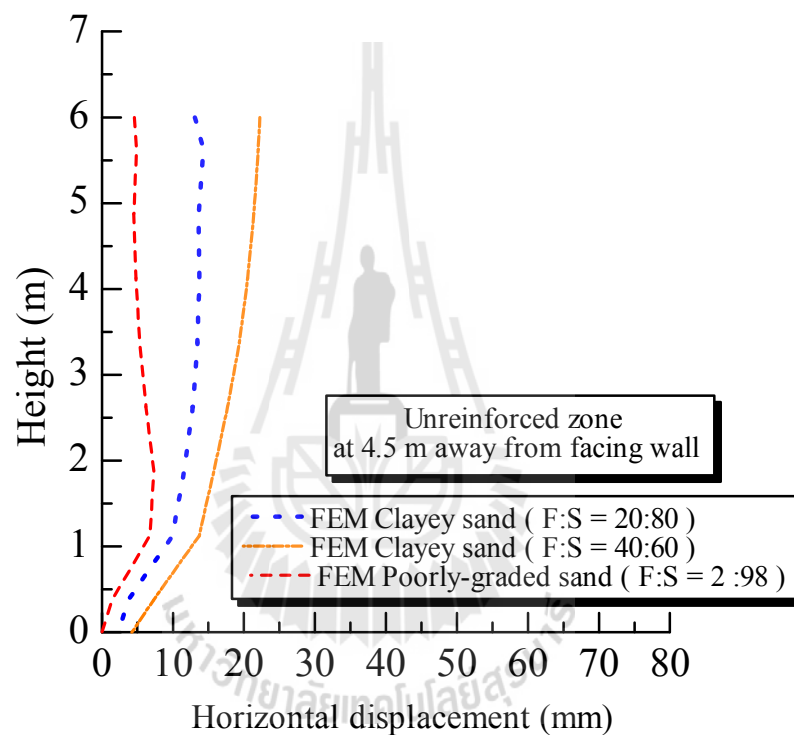
20:80; 40:60, and 80:20, respectively. The high horizontal movement ratio for  $F:S = 80:20$  shows that the BRE wall could not resist the horizontal movement (pressure) of the unreinforced zone. In addition, the maximum horizontal movement occurred at the top of the wall (6 m high). This characteristic implies that the BRE wall tends to rotate around the toe.



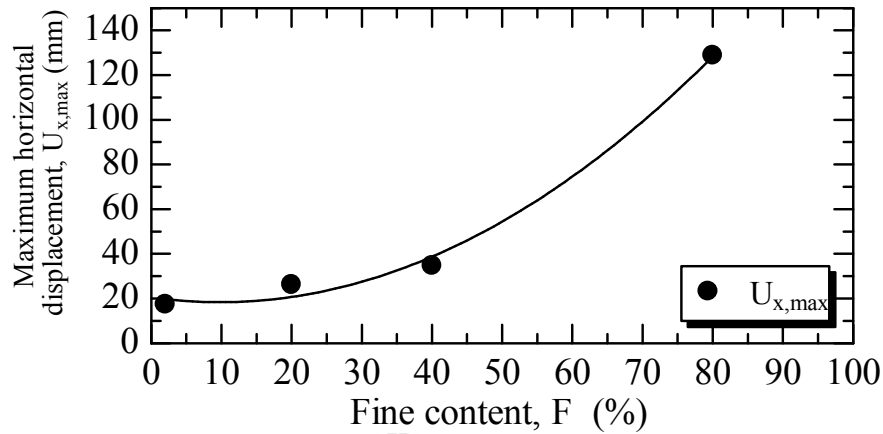
**Figure 5.11** Comparison between the measured and simulated horizontal wall movement for different soil embankments.

Figure 5.13 shows the relationship between the maximum horizontal wall movement and the fine content. This relationship can be expressed by a polynomial function. The maximum horizontal wall movement significantly

increased with the fine content especially for  $F > 45\%$ . Thus, the selected soil that can minimize horizontal movement should not contain fine contents higher than 45%. The large horizontal displacement for  $F:S = 80:20$  may result from the low shear strength of the backfill and the low bearing resistance due to the failure mode approaching to the punching shear (Sukmak et al., 2015).



**Figure 5.12** Simulation horizontal movement of unreinforced zone at 4.5 m away from facing wall for different soil embankments.



**Figure 5.13** Relationship between maximum horizontal wall movement and fine content.

#### 5.4.2.4 Lateral earth pressure

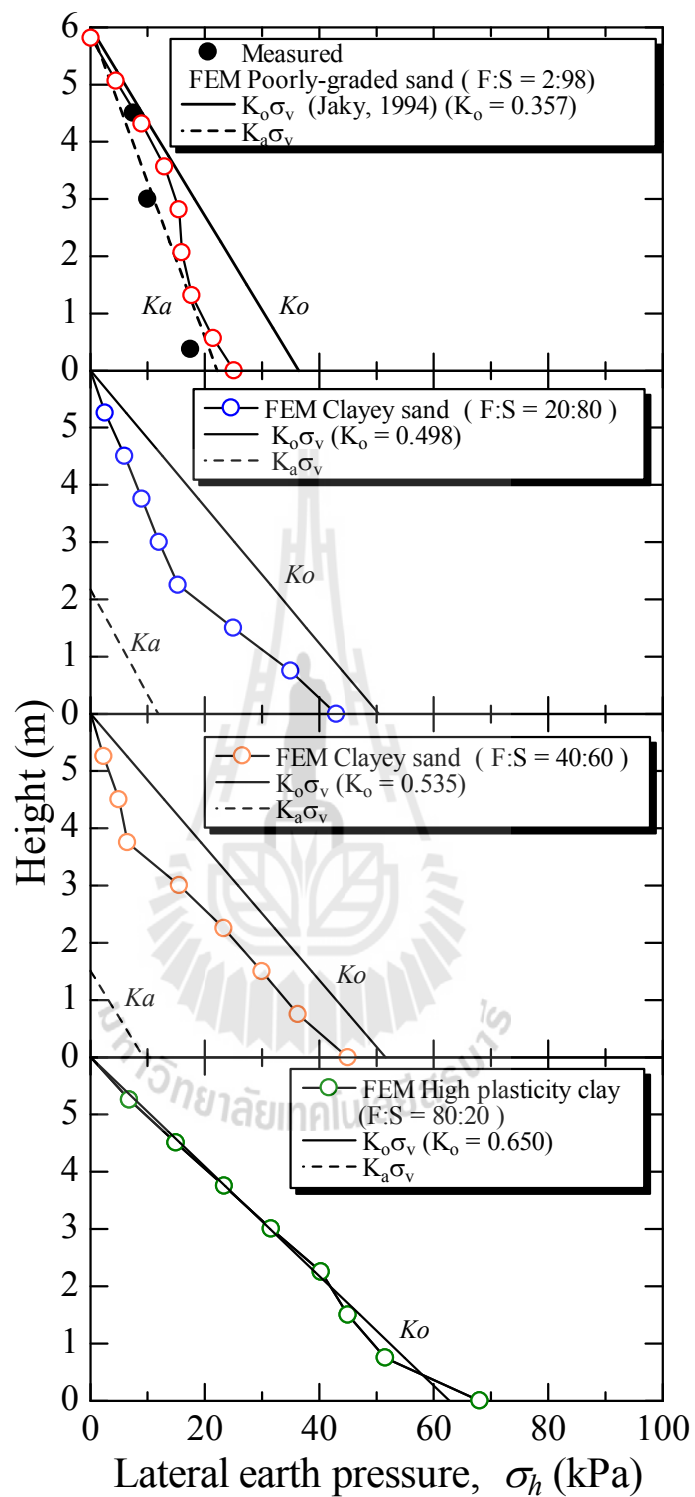
Figure 5.14 shows the measured and simulated lateral earth pressures,  $\sigma_h$  for different backfills.  $\sigma_h$  is the ratio of maximum tensile force to vertical spacing. For the coarse-grained soil with F:S = 2:98, the coefficient of at-rest earth pressure,  $K_o$  can be estimated by using the empirical relationship (Jaky, 1944) as shown in Eq. (3). For the fine-grained soils with F:S = 20:80, 40:60, and 80:20, the values of  $K_o$  were obtained from the  $K_o$ -consolidated simulation in the PLAXIS program. The coefficient of Rankine's active earth pressure is given in Eq. (4), which was used for all soil backfills.

$$K_o = 1 - \sin \phi \quad \text{For F:S} = 2:98 \quad (5.3)$$

$$K_a = \tan^2\left(45 - \frac{\phi}{2}\right) \quad \text{For F:S} = 2:98, 20:80, 40:60, \text{ and } 80:20 \quad (5.4)$$

From the simulated results, the maximum tension plane occurred at the connections between the reinforcement and the wall facing due to the bearing reinforcement embedded in backfill were stretched to resist the horizontal movement of the wall facing. Figure 5.14 clearly shows that the lateral earth pressure in each reinforcement approached to the at-rest earth pressure as the fine content increased. For F:S = 2:98, the comparison between the measured and simulated lateral earth pressures is considered to be reasonable. The calculated  $\sigma_h$  was close to the at-rest-earth pressure when the wall height was greater than 3 m. Below this height, the calculated  $\sigma_h$  approached to the Rankine active earth pressure ( $\sigma_h = \sigma_v K_a$ ), which is in agreement with the recommendation by AASHTO (2002). However, for F:S = 20:80 and 40:60, the simulated lateral earth pressures are between the calculated active earth pressure ( $\sigma_h = \sigma_v K_a - 2c\sqrt{K_a}$ ) and at-rest earth pressure ( $\sigma_h = K_o \sigma_v$ ). Moreover, for F:S = 80:20, the simulated lateral earth pressure was essentially the same as the calculated at-rest earth pressure. This result is similar to that obtained by Chai (1992), in which he studied the interaction behavior between steel grid reinforcements and lateritic backfill soil.

The overall results from the numerical analysis, including bearing stress, settlement, horizontal wall movement, and lateral earth pressure in this study can provide a preliminary guideline in predicting the behavior of the bearing reinforced earth wall using cohesive-frictional mixture soils as backfill. However, to confirm the results from the numerical analysis, full-scale tests of BRE walls with cohesive-frictional backfill are needed.



**Figure 5.14** Measured and simulated lateral earth pressure distributions for different backfill.

### 5.4.3 Parametric study on horizontal wall displacement

The influence of soil-structure interaction, foundation, and stiffness of reinforcement on the horizontal wall displacement was studied for different types of backfill. Horizontal wall deformations are especially important for serviceability of MSE structures. This parametric study was conducted based on the reference numerical BRE wall model discussed above and their parameters are defined and given in Figure 5.1, Table 5.1, Table 5.2, and Table 5.3, including geometry, foundation, backfill, and structural elements. These parameters were adopted for all analyses unless otherwise indicated. This study was conducted by varying one parameter of soil-structure interaction, foundation, or stiffness of reinforcement at a time while all other parameters were kept constant.

#### 5.4.3.1 Influence of soil-structure interaction ratio, $R_{inter}$

Figure 5.15 shows the relationship between the maximum horizontal displacement and the soil-structure interaction ratio. The maximum horizontal displacement rapidly decreased with an increase of the soil-structure interaction ratio and then became insensitive to the soil-structure interaction ratio after the ratio was approximately 0.67 for all backfill materials. When the soil-structure interaction ratio was less than 0.67, the large displacement is due to slip failure between reinforcement and soil. Rowe and Ho (1998) indicated that the variation in the horizontal displacement was insignificant when the interface coefficient decreased from 1.0 to 0.67. The present results furthermore illustrated that the transitional  $R_{inter}$  that separates low and high horizontal movement was essentially the same and equal to 0.67, irrespective of the fine content.

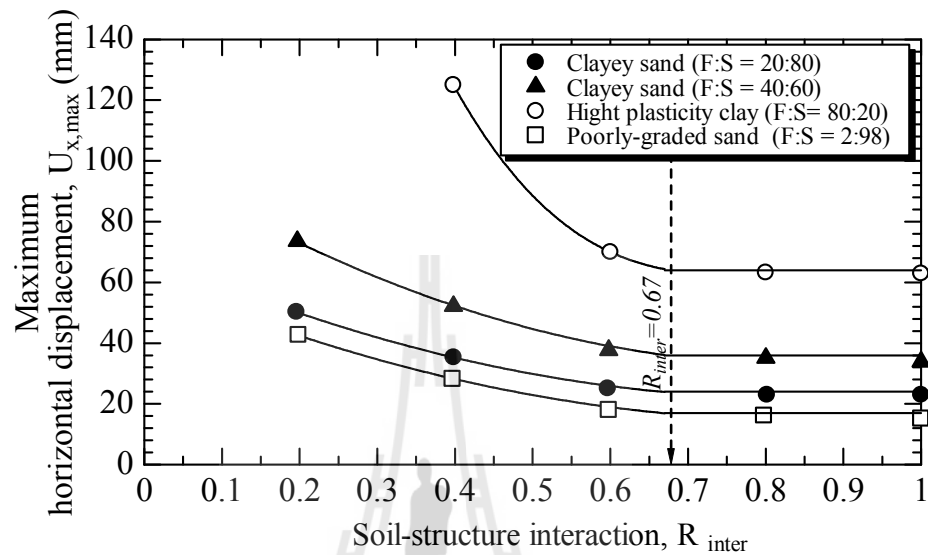
According to Figure 5.7, for F:S = 2:98, 20:80, and 40:60, the  $R_{inter}$  of  $n = 3$  was equal to 0.75, 0.70, and 0.65, respectively, which were close to or higher than 0.67. This implies that the bearing reinforcements with at least three transverse members when used in BRE wall will provide small horizontal wall movement for  $F < 40\%$ . It is evident that the change in  $U_{x,max}$  when  $R_{inter} < 0.67$  is significant for F:S = 80:20, compared to other F:S ratios.

#### 5.4.3.2 Influence of reinforcement stiffness, EA

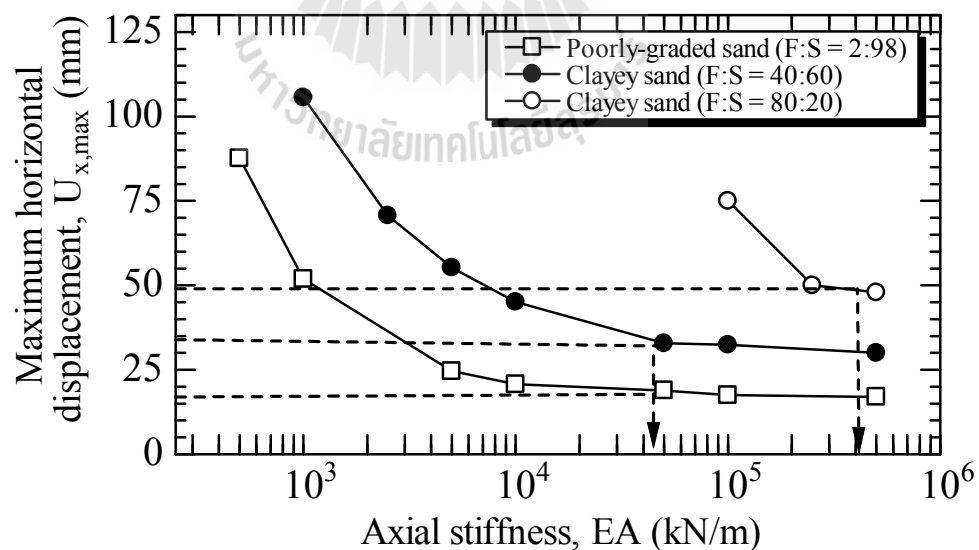
The variations of the maximum horizontal displacement with the axial stiffness of reinforcement are shown in Figure 5.16. These results were obtained by varying the reinforcement stiffness, EA in the range of 500-500,000 kN/m with all other parameters kept the same. The axial stiffness values were presented in a logarithmic scale. Figure 5.16 shows that the tendency of the horizontal displacement increased with the decrease in the axial stiffness. These results are similar to those from the parametric studies investigated by Rowe and Ho (1997), Bergado et al. (2000), and Youwai and Bergado (2004).

The horizontal wall displacement increased significantly at the stiffness lower than 45,000 kN/m (referred to as transitional stiffness) for F:S = 2:98, 40:60, but the change in the horizontal displacement was not significant at higher stiffness. Whereas the transitional stiffness was 400,000 kN/m for F:S = 80:20, which is almost ten times that for F:S = 2:98, 40:60. In other words, more EA is required for a higher fine content for the same reinforcement dimension to attain the same horizontal displacement. Rowe and Ho (1998) stated that the strain (deformation) development within the reinforced zone was restricted considering that the strain

compatibility existed between the reinforcement and the soil. Thus, higher axial stiffness resulted in the smaller horizontal displacement (smaller strain).



**Figure 5.15** Relationship between maximum horizontal displacement and soil-structure interaction ratio for different backfill.



**Figure 5.16** Relationship between maximum horizontal displacement and axial stiffness.



### 5.4.3.3 Influence of foundation

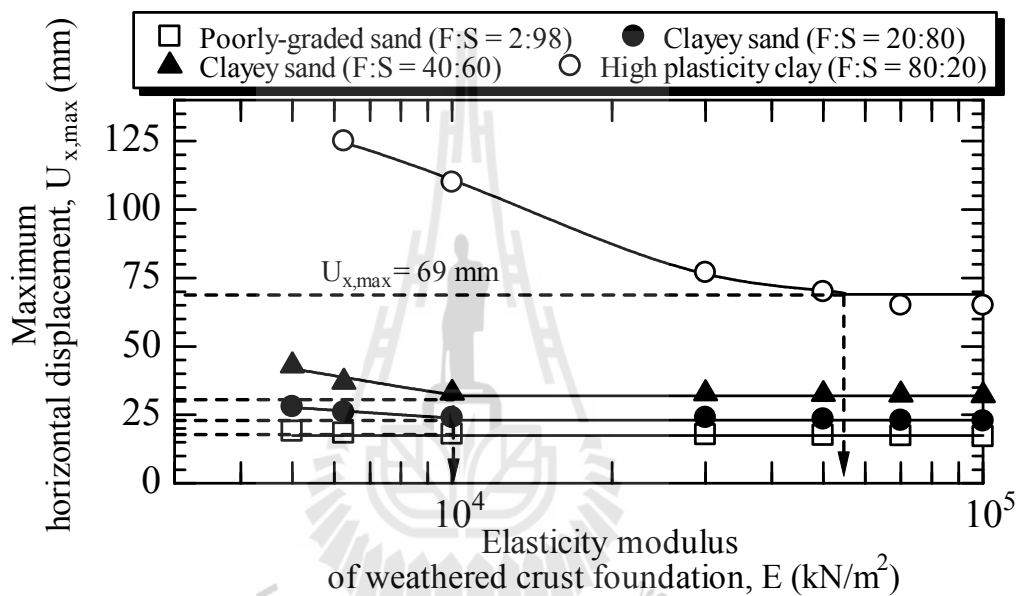
The foundation type has an influence on the overall behavior of reinforced soil structures; hence, it is worth considering the horizontal displacement of the wall supported either on a firm foundation or on a soft foundation. The influence of the foundation was investigated by varying elasticity modulus ( $E$ ) of the weathered crust layer while the thickness of this layer was kept constant as shown in Figure 5.17. The range of elasticity modulus was 5,000-100,000  $\text{kN/m}^2$ , which was simulated for loose soil to dense soil foundation according to Bowles (1996) and Kezdi (1974).

Figure 5.17 shows that the maximum horizontal wall displacement changed insignificantly when the elasticity modulus of the weathered crust foundation was higher than 10,000  $\text{kN/m}^2$  for F:S = 2:98, 20:80, and 40:60 and 45,000  $\text{kN/m}^2$  for F:S = 80:20.

The horizontal displacement of the wall increased as the elasticity modulus of the foundation decreased because of the increase in lateral and vertical (settlement) movements of the foundation. The small horizontal displacement occurred at the toe of the wall facing when it was supported on the firm foundation with an elastic modulus higher than (10,000  $\text{kN/m}^2$ ) for F:S = 2:98 and 20:80 and higher than 45,000  $\text{kN/m}^2$  for F:S = 80:20 and the maximum horizontal movement was found at about the mid of the wall height.

For a soft (loose) foundation ( $E < 5,000 \text{ kN/m}^2$ ), the maximum lateral movement occurred at the top of the wall for F:S = 20:80 40:60, and 80:20. This characteristic implies that the BRE wall tended to rotate forward around the toe

of the wall due to the combined effects of the movement of the foundation and the active lateral earth pressure from the unreinforced backfill. This finding is consistent with the test data of the MSE wall on soft Bangkok clay reported by Bergado et al. (1995). The foundation type significantly affected the pattern of lateral wall movement.



**Figure 5.17** Influence of Elasticity modulus of foundation.

## 5.5 Conclusions

This paper presents a numerical parametric study on behavior of bearing reinforcement earth (BRE) walls with different backfill properties using the numerical software PLAXIS 2D. The backfill materials consisted of four types of soils, which were mixtures of silty clay and sand at different fine contents of 2, 20, 40, and 80% by weight. Moreover, the influence of several parameters (soil-structure interaction, foundation, and stiffness of reinforcement) on the horizontal wall deformations was

studied. The overall results from the numerical analysis in this study can provide a preliminary guideline in predicting the behavior of BRE walls. The following conclusions can be drawn from this study:

1. The geotextile elements were used to model the bearing reinforcements by converting the contribution of friction and bearing resistances to the equivalent friction resistance. The equivalent friction resistance was represented by the soil-bearing reinforcement interaction ratio,  $R_{inter}$ , which was back-calculated from the laboratory pullout test. The  $R_{inter}$  values decreased following a polynomial function with an increase in the fine content. The soil-structure interactions varied as an increase of the fine content in the ranges of 0.65-0.38 and 0.75-0.40 for  $n=2$  and 3, respectively.
2. Overall, the behavior of bearing stresses, settlements, lateral earth pressures, and horizontal wall movement of the BRE wall with different backfill materials during and at the end of construction was simulated satisfactorily and agreed well with the prediction. The simulated bearing stress in the reinforced zone decreased from the front to the back because the BRE wall behaved as a rigid body built on the relatively firm foundation retaining the unreinforced backfill. The bearing stress depended on the density of backfill. The foundation settlement decreased from the facing of the wall to the unreinforced zone for all backfills due to the slight rotation of the wall. The relationship between the maximum horizontal wall movement and the fine content can be expressed by a polynomial function. The maximum horizontal wall movement

significantly increased as the fine content was more than 45% ( $F > 45\%$ ). The increase of the fine content changed the location of the maximum wall movement higher up from the mid to top of the wall. The simulated lateral earth pressure coefficient of the BRE wall tended to approach to the at-rest earth pressure coefficient ( $K_o$ ) when the fine content increased.

3. Soil-structure interaction, stiffness of reinforcement, and foundation affected the horizontal wall deformation, which is especially important for serviceability of the BRE wall. For all backfill materials, the maximum horizontal displacement rapidly decreased with an increase of the soil-structure interaction ratio and then became insensitive to the soil-structure interaction ratio after the ratio was approximately 0.67. The horizontal displacement of the BRE wall increased significantly at the stiffness lower than 45,000 kN/m when the backfill contained the fine content less than 45%, but the change in the horizontal displacement was not significant at the higher stiffness. For designing BRE wall, the stiffness of bearing reinforcement should be added to 400,000 kN/m for the backfill material contained a fine content higher than 80%. The horizontal displacement of the wall changed insignificantly when the foundation modulus was higher than 10,000 kN/m<sup>2</sup>. Moreover, for F:S = 80:20, the maximum horizontal displacement increased significantly when the elastic modulus of the weathered crust foundation was lower than 45,000 kN/m<sup>2</sup>.
4. The simulation approach presented in this paper successfully investigated the performance of the BRE wall in Thailand. However, to confirm the

results from the numerical analysis, full-scale tests of BRE walls with cohesive-frictional backfill are needed.

## 5.6 References

- AASHTO, 2002. **Standard Specifications for Highway Bridges**, seventeenth ed. American Association of State Highway and Transportation Officials, Washington, DC, USA.
- Abdelouhab, A., Dias, D., Freitag, N., 2011. **Numerical analysis of the behaviour of mechanically stabilized earth walls reinforced with different types of strips**. *Geotextiles and Geomembranes* 29, 116-129.
- Abdi, M.R., Zandieh, A.R., 2014, 2014. **Experimental and numerical analysis of large scale pull out tests conducted on clays reinforced with geogrids encapsulated with coarse material**. *geotextiles and Geomembranes* 42, 495-504.
- Barkan, D.D., 1962. **Dynamics of Bases and Foundations**. McGraw Hill Book Co. New York.
- Bathurst, R.J., 1993. **Investigation of footing resistant on stability of large-scale reinforcement soil wall tests**. *Proceedings of 46th Canadian Geotechnical Conference*, 389-398.
- Bergado, D., Chai, J., Miura, N., 1995. **FE analysis of grid reinforced embankment system on soft Bangkok clay**. *Computers and Geotechnics* 17, 447-471.
- Bergado, D.T., Teerawattanasuk, C., 2008. **2D and 3D numerical simulations of reinforced embankments on soft ground**. *Geotextiles and Geomembranes* 26, 39-55.

- Bergado, D.T., Teerawattanasuk, C., Youwai, S., Voottipruex, P., 2000. **Finite element modeling of hexagonal wire reinforced embankment on soft clay.** Canadian Geotechnical Journal 37, 1209-1226.
- Bergado, D.T., Youwai, S., Teerawattanasuk, C., Visudmedanukul, P., 2003. **The interaction mechanism and behavior of hexagonal wire mesh reinforced embankment with silty sand backfill on soft clay.** Computers and Geotechnics 30, 517-534.
- Bowles, J.E., 1996. Foundation analysis and design. 5th Ed., McGraw Hill, New York.
- Chai, J., 1992. **Interaction behavior between grid reinforcements and cohesive frictional soils and performance of reinforced wall/embankment on soft ground.** Doctoral dissertation GT 91-1, Aisan Institute of Technology, Bangkok, Thailand.
- Chai, J., Saiichai, S., Norihiko, M., 1994. **Stability analysis of embankment on soft ground (a case study).** soils and Foundations 34, 107-114.
- Collin, J.G., 1986. **Earth wall design.** Ph.D. dissertation, Univ. California, Berkeley, CA.
- Damians, I., Bathurst, R., Josa, A., Lloret, A., 2014. **Numerical Analysis of an Instrumented Steel-Reinforced Soil Wall.** International Journal of Geomechanics 15, 04014037.
- Damians, I., Bathurst, R., Josa, A., Lloret, A., Albuquerque, P., 2012. **Vertical-Facing Loads in Steel-Reinforced Soil Walls.** Journal of Geotechnical and Geoenvironmental Engineering 139, 1419-1432.

- Damians, I., Bathurst, R.J., A., J., Lloret, A., 2015. **Numerical Analysis of an Instrumented Steel-Reinforced Soil Wall.** International Journal of Geomechanics 15, 04014037.
- Golam, K., Sahadat, H., Mohammad, S.K., 2014. **Influence of Soil Reinforcement on Horizontal Displacement of MSE Wall.** International Journal of Geomechanics 14, 130-141.
- Han, J., Leshchinsky, D., 2004. **Limit equilibrium and continuum mechanics-based numerical methods for analyzing stability of MSE walls.** Proc., 17th ASCE Engineering Mechanics Conf., ASCE, Reston, VA.
- Hatami, K., Bathurst, R., 2006. **Numerical Model for Reinforced Soil Segmental Walls under Surcharge Loading.** Journal of Geotechnical and Geoenvironmental Engineering 132, 673-684.
- Hatami, K., Bathurst, R.J., 2005. **Development and verification of a numerical model for the analysis of geosynthetic-reinforced soil segmental walls under working stress conditions.** Canadian Geotechnical Journal 42, 1066-1085.
- Hegde, A., Sitharam, T.G., 2015. **3-Dimensional numerical modelling of geocell reinforced sand beds.** Geotextiles and Geomembranes 43, 171-181.
- Ho, S.K., Rowe, R.K., 1994. **Predicted Behavior of Two Centrifugal Model Soil Walls.** Journal of Geotechnical Engineering 120, 1845-1873.
- Horpibulsuk, S., Niramitkornburee, A., 2010. **Pullout resistance of bearing reinforcement embedded in sand.** Soils Found 50, 215-226.

- Horpibulsuk, S., Suksiripattanapong, C., Niramitkornburee, A., Chinkulkijniwat, A., Tangsutthinon, T., 2011. **Performance of an earth wall stabilized with bearing reinforcements**. *Geotextiles and Geomembranes* 29, 514-524.
- Huang, B., Bathurst, R., Hatami, K., 2009. **Numerical Study of Reinforced Soil Segmental Walls Using Three Different Constitutive Soil Models**. *Journal of Geotechnical and Geoenvironmental Engineering* 135, 1486-1498.
- Jaky, J., 1944. **The coefficient of earth pressure at rest**. *Journal of the Society of Hungarian Architects and Engineers* 7, 355-358.
- Kezdi, A., 1974. **Handbook of Soil Mechanics**. Elsevier, Amsterdam.
- Khedkar, M.S., Mandal, J.N., 2009. **Pullout behaviour of cellular reinforcements**. *Geotextiles and Geomembranes* 27, 262-271.
- Mohamed, S.B.A., Yang, K.-H., Hung, W.-Y., 2014. **Finite element analyses of two-tier geosynthetic-reinforced soil walls: Comparison involving centrifuge tests and limit equilibrium results**. *Computers and Geotechnics* 61, 67-84.
- Reddy, D.V., Navarrete, F., 2008. **Experimental and Analytical Investigation of Geogrid MSE Walls**, *From Research to Practice in Geotechnical Engineering*, pp. 277-291.
- Rowe, R., Ho, S., 1997. **Continuous Panel Reinforced Soil Walls on Rigid Foundations**. *Journal of Geotechnical and Geoenvironmental Engineering* 123, 912-920.
- Rowe, R.K., Ho, S.K., 1998. **Horizontal deformation in reinforced soil walls**. *Canadian Geotechnical Journal* 35, 312-327.



- Rowe, R.K., Skinner, G.D., 2001. **Nuerical analysis of geosynthetic reinforced retaining wall constructed on a layered soil foundation**. Geotextiles and Geomembranes 19, 387-412.
- Sukmak, K., Sukmak, P., Horpibulsuk, S., Han, J., Shen, S.-L., Arulrajah, A., 2015. **Effect of fine content on the pullout resistance mechanism of bearing reinforcement embedded in cohesive–frictional soils**. Geotextiles and Geomembranes 43, 107-117.
- Suksiripattanapong, C., Chinkulkijniwat, A., Horpibulsuk, S., Rujikiatkamjorn, C., Tanhsutthinon, T., 2012. **Numerical analysis of bearing reinforcement earth (BRE) wall**. Geotextiles and Geomembranes 32, 28-37.
- Vermeer, P.A., Brinkgreve, R.B.J., 1995 **Finite Element Code for soil and rock analsis**. A.A. Balkema, Rotterdam (Netherlands).
- Wang, Z., Jacobs, F., Ziegler, M., 2014. **Visualization of load transfer behaviour between geogrid and sand using PFC2D**. Geotextiles and Geomembranes 42, 83-90.
- Youwai, S., Bergado, D.T., 2004. **Numerical analysis of reinforced wall using rubber tire chips–sand mixtures as backfill material**. Computers and Geotechnics 31, 103-114.

## **CHAPTER VI**

### **CONCLUSIONS AND RECOMMENDATIONS**

#### **6.1 Summary and conclusions**

This thesis consists of three main objectives. The first objective is to investigate the effect of fine content on the pullout resistance mechanism of bearing reinforcement embedded in cohesive-frictional soils. The tested soils were a mixture of silty clay and sand at various ratios. The second objective is to understand the role of molding water content on the pullout resistance mechanism of bearing reinforcement embedded in cohesive-frictional soil. The tests were conducted on the lateritic soil at five different molding water contents. The last objective is to investigate the role of fine content on the performance of Bearing Reinforcement Earth (BRE) wall via the numerical parametric study. The PLAXIS program, a powerful and accurate tool, was used to predict the performance of the MSE wall. The conclusions can be drawn as follows:

##### **6.1.1 Effect of fine content on the pullout resistance mechanism**

The effects of fine content on the pullout mechanism of the bearing reinforcement embedded in cohesive-frictional soils with different fine contents of 20, 40, 80, and 98% by weight is summarized as follows:

###### **6.1.1.1 Pullout friction resistance**

The pullout resistance of the bearing reinforcement is the sum of pullout friction and pullout bearing resistances. The pullout friction resistances

( $P_{f,\max}$  and  $P_{f,\text{residual}}$ ) are dependent upon soil shear strength and soil-reinforcement interaction factor  $\alpha$ . The  $\alpha$  value can be approximated in term of fine content using a proposed linear function.

#### 6.1.1.2 Pullout bearing mechanism

The modified punching shear solution can be used as the generalized expression for different failure mechanisms. The general shear and modified punching shear failure mechanisms are approached when the failure plane  $\beta$  values are  $\pi/1.65$  and  $\pi/3$ , respectively. Using the modified punching shear solution, the maximum pullout bearing stresses for various cohesive-frictional soils are predicted satisfactorily where the  $\beta$  value decreases as the fine content increases. In other words, the failure mechanism approaches punching shear as the fine content increases. The relationship between  $\beta$  and fine content is represented by a polynomial function. The  $\beta$  value of  $\pi/2$  is recommended for  $F < 45\%$ .

The transverse member interference is essentially dependent upon  $S/B$ , which is strongly controlled by fine content. The transverse member interference zones are classified into three zones. Zone 1 ( $S/B \leq 3.75$ ) is block failure where all transverse members act like a rough block. Zone 2 ( $3.75 < S/B < S_2/B$ ) is member interference failure. Zone 3 ( $S/B > S_2/B$ ) is individual failure. The  $S_2/B$  value decreases linearly with an increase in fine content, indicating that the larger soft region develops with the smaller fine content.

### 6.1.2 Effect of molding water content on the pullout resistance mechanism

The effect of molding water content on the pullout resistance mechanism of bearing reinforcement embedded in the marginal lateritic soil was studied. The critical analysis of test results leads to the development of pullout resistance equations in term of total strength parameters and  $w/w_{OWC}$  of compacted soil and dimension of bearing reinforcement.

#### 6.1.2.1 Pullout friction resistance

The pullout friction resistances at peak and residual states ( $P_{f,max}$  and  $P_{f,residual}$ ) are dependent upon soil shear strength and soil-reinforcement interaction factor,  $\alpha$ . The peak and residual interaction factors ( $\alpha_p$  and  $\alpha_r$ ) are irrespective of molding water contents tested and are approximately 0.63 and 0.46, respectively.

#### 6.1.2.2 Pullout bearing mechanism

The modified punching shear solution with various  $\beta$  values is valid as a generalized expression to approximate pullout bearing resistances of a single transverse member at various molding water contents. The  $\beta$  value decreases with increasing water content. The  $\beta$  value of the compacted soil at  $0.67 \leq w/w_{OWC} \leq 1.0$  is essentially constant and equal to  $\pi/2$ . For  $1.0 < w/w_{OWC} \leq 1.33$ , the  $\beta$  value decreases polynomial with an increase in water content ratio.

The failure mechanism of bearing reinforcement with  $n$  transverse members is essentially dependent upon spacing ratio  $S/B$ , which is

strongly controlled by  $w/w_{OWC}$ . The failure mechanism is the block failure when  $S/B \leq 3.75$ , the member interference failure when  $3.75 < S/B < S_2/B$  and the individual failure when  $S/B > S_2/B$ .  $w/w_{OWC}$  affects the stress region and failure plane in front of transverse members. The  $S_2/B$  value increases linearly with a decrease in  $w/w_{OWC}$  when  $w > w_{owc}$  and essentially constant when  $w < w_{owc}$ .

### **6.1.3 Numerical parametric study on behavior of bearing reinforcement earth (BRE) walls with different backfill material properties**

The numerical parametric study on behavior of the bearing reinforcement earth (BRE) wall with different backfill properties by PLAXIS 2D is investigated. The backfill materials consist of four types of soils, which are mixtures of silty clay and sand at different fine contents of 2, 20, 40, and 80% by weight. Moreover, the influence of several parameters (soil-structure interaction, foundation, and stiffness of reinforcement) on the horizontal wall deformation is studied. The overall results from the numerical analysis in this study provide the preliminary guideline in predicting the behavior of BRE wall.

#### **6.1.3.1 Behavior of BRE wall with different types of soil**

The geotextile elements are used to model the bearing reinforcements by converting the contribution of friction and bearing resistances to the equivalent friction resistance. The equivalent friction resistance is represented by the soil-bearing reinforcement interaction ratio,  $R_{inter}$ , which is back-calculated from the laboratory pullout test. The  $R_{inter}$  values polynomial decreases with an increase in fine content. The soil-structure interactions vary as an increase of fine content in the ranges of 0.65-0.38 and 0.75-0.40 for  $n = 2$  and 3, respectively.

Overall, the behavior of bearing stresses, settlements, lateral earth pressures, and horizontal wall movement of the BRE wall with different backfill materials during and at the end of construction is simulated satisfactorily and agrees well with prediction. The simulated bearing stress in the reinforced zone decreases from the front to the back because the BRE wall behaves as a rigid body built on the rigid foundation retaining the unreinforced backfill. The bearing stress depends on the density of backfill. The foundation settlement decreases from the facing of the wall to the unreinforced zone for all backfills due to the wall slightly rotated. The relationship between the maximum horizontal wall movement and the fine content can be expressed by a polynomial function. The maximum horizontal wall movement significantly increases as the fine content is more than 45% ( $F > 45\%$ ). The increase of the fine content moves the location of the maximum wall movement higher up from mid to top of the wall. The simulated lateral earth pressure coefficient of the BRE wall tends to approach to the at-rest earth pressure coefficient ( $K_o$ ) when the fine content increases

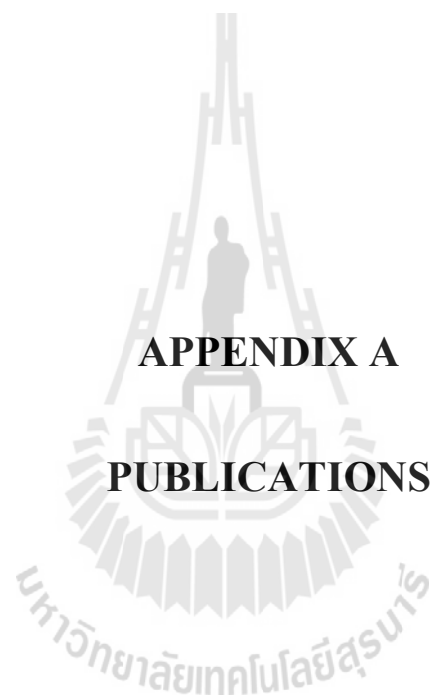
#### **6.1.3.2 Parametric study on horizontal wall displacement**

Soil-structure interaction, stiffness of reinforcement, and foundation affect the horizontal wall deformation, which is especially important for serviceability of the BRE wall. For all backfill material, the maximum horizontal displacement rapidly decreases with an increase of the soil-structure interaction ratio and then becomes insensitive to the soil-structure interaction ratio after the ratio is approximately 0.67. The horizontal displacement of the BRE wall increases significantly at stiffness lower than 45,000 kN/m when the backfill contains fine content less than 45%, but the change in the horizontal displacement is not significant

at higher stiffness. For designing BRE wall, the stiffness of bearing reinforcement should be 400,000 kN/m for the backfill material containing fine content higher than 80%. The horizontal displacement of the wall changes insignificantly when the foundation modulus is higher than 10,000 kN/m<sup>2</sup>. Moreover, for F:S = 80:20, the maximum horizontal displacement increases significantly when the elasticity modulus of weathered crust foundation is less than 45,000 kN/m<sup>2</sup>.

## 6.2 Recommendations for future work

- The finite element analysis of the BRE wall in this study was performed in 2-D plain strain condition. The simulation approach presented was successfully applied to investigate the performance of the BRE wall in Thailand. However, to confirm the results from the numerical analysis, full-scale tests of BRE walls with cohesive-frictional backfill are needed. Moreover, the horizontal spacing and shape of bearing reinforcement (3-D direction) affect the performance of the BRE wall. Consequently, the 3-D finite element analysis of the BRE wall should be performed and compare with the 2-D one.



## **APPENDIX A**

## **PUBLICATIONS**

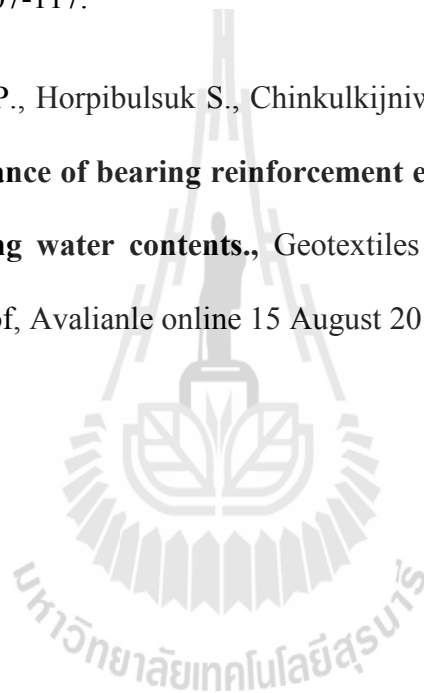


## List of Publications

### INTERNATIONAL JOURNAL PAPERS

Sukmak K., Sukmak P., Horpibulsuk S., Han J., Shen S.L., and Arul A., **Effect of fine content on the pullout resistance mechanism of bearing reinforcement embedded in cohesive-frictional soils.**, Geotextiles and Geomembranes 43(2015) pp.107-117.

Sukmak K., Sukmak P., Horpibulsuk S., Chinkulkijniwat A., Arul A., and Shen S.L., **Pullout resistance of bearing reinforcement embedded in marginal latritic soil at molding water contents.**, Geotextiles and Geomembranes (Inpress, Corrected Proof, Available online 15 August 2015).



## **BIOGRAPHY**

Mister Gampanart Sukmak was born in December 1989 in Nakhon Ratchasima, Thailand. He obtained her Bachelor's degree in Civil Engineering from the School of Civil Engineering, Suranaree University of Technology in 2010. Then, he has been awarded a Royal Golden Jubilee (RGJ) Ph.D. Program Scholarship from the Thailand Research Fund (TRF) in 2011 for his Ph.D. study in the School of Civil Engineering, Suranaree University of Technology. During his Ph.D. study (2011-2015), he has worked as a teaching assistant for Surveying Laboratory and Applied Mechanics Laboratory. He has visited the University of Kansas, Lawrence, Kansas state, USA., for his oversea research under the supervision of Prof. Dr. Jie Han from April 4, 2015 to August 26, 2015. he has published 2 international ISI journal papers.

